

Effect of the Min system on timing of bacterial cell division

Dissertation

zur

Erlangung des Doktorgrades

der Naturwissenschaften

(Dr. rer. nat.)

dem

Fachbereich Physik

der Philipps-Universität Marburg

vorgelegt von

Shuxin Jia

aus

Shandong, China

Marburg/Lahn, 2014

Vom Fachbereich Physik der Philipps-Universität als Dissertation
angenommen am: 13.03.2014
Erstgutachter: Prof. Dr. Peter Lenz
Zweitgutachter: Prof. Dr. Wolfgang Einhäuser-Treyer
Tag der mündlichen Prüfung: 25.03.2013
Hochschulkennziffer 1180

Zusammenfassung

In dieser Arbeit wird der Effekt des Min Systems hinsichtlich der zeitlichen Abläufe der Zellteilung untersucht. Zur quantitativen Untersuchung wurde die Wartezeit zwischen der Fertigstellung der Segregation der Chromosome nach der Replikation und der Zellteilung von Wildtype und *minB*⁻ Mutant verglichen. Wir haben eine Reihe von theoretischen Modellen entwickelt um diesen Effekt zu erklären. Zur Verbesserung dieser Modelle haben wir die Vorhersagen der Modelle mit Experimentellen Daten verglichen, was zu einem Modell führte, welches alle relevanten experimentellen Beobachtungen erklären kann. Es zeigt sich, dass die Polregionen und die zentralen Regionen für die Positionierung der Zellteilung potentiell gleichwertig sind, außerdem ist der Anteil von im Z-Ring gebundenem FtsZ in *minB*⁻ Mutanten nur etwa halb so hoch wie im Wildtyp. Diese Ergebnisse sind in Einklang mit früheren Studien und lassen sich mit unserem Modell erklären. Daneben konnten wir zeigen, dass das Verhältnis der intrazellulären Konzentrationen von MinD und Min E die Zeit zwischen zwei Zellteilungen festlegt und dabei selbst von der Frequenz der Oszillation des Min-Systems abhängt.

Abstract

In this work, we analyze the effect of the Min protein system on timing of cell division. We do this in a quantitative way by comparing the cell division waiting time of wild type and *minB*⁻ cells and by analyzing the Z-ring existing time. We develop a series of theoretical models to explain this effect. Direct comparison between experimental data and predictions of the theoretical models is used to improve the models. The final model is able to explain all relevant experimental observations. It also shows that polar and non-polar sites in *minB*⁻ cells are equivalent for cell division. Furthermore, we find that in *minB*⁻ cells the fraction of FtsZ protein bound in the Z-ring structure is about two fold lower than that in wild type cells. This finding is in agreement with earlier studies and with predictions of the theoretical model. Finally, we demonstrate that the ratio of intracellular concentrations of MinD to MinE determines the inter-division time that itself depends on the oscillation frequency of Min system.

Contents

Contents	vii
1 Introduction	1
1.1 Hu	5
1.2 FtsZ	5
1.3 Min system	7
2 Results	11
2.1 Experimental analysis of cell growth and chromosome segregation	12
2.2 Model I	16
2.3 Parameters of model 1	18
2.3.1 Cell length increases exponentially	19
2.3.2 The doubling time and division waiting time of wild type strain	22
2.3.3 The cell length	25
2.4 Results of model 1	26
2.5 Model 1P	33
2.6 Model 2 and model 3	36
2.7 Model 4	53
2.8 The inter-division time and the ratio of MinD to MinE	60
2.9 The increased FtsZ level in model 4	63
3 Discussion	67
4 Summary and outlook	73

4.1	Summary	73
4.2	Outlook	75
A	Materials and Methods	79
A.1	Materials	79
A.2	Methods	82
A.2.1	Cultivation of <i>E.coli</i>	82
A.2.2	Storage of <i>E.coli</i>	82
A.2.3	Polymerase chain reaction (PCR)	82
A.2.4	Agarose gel electrophoresis	84
A.2.5	Restriction and ligation of DNA fragments	84
A.2.6	DNA sequencing	84
A.2.7	Preparation of chemical- and electrocompetent <i>E. coli</i> cells	85
A.2.8	Transformation of <i>E. coli</i> cells	85
A.2.9	The construction of the plasmid for homologous recombination	85
A.2.10	Homologue recombination and looping out the plasmid from the chromosome	86
A.2.11	The microscopy and measurement	86
A.3	strains and plasmids	88
A.4	Simulation	90
	List of Figures	95
	List of Tables	99
	Bibliography	101

Chapter 1

Introduction

Living in ever changing environment bacteria are frequently forced to adjust internal processes to external conditions. Molecularly this is done by signal transduction pathways that sense external or internal signals, and generate an output response from the information encoded by these signals. In many instances these pathways produce an oscillatory response in which the output varies over time in a recurrent manner. In general terms, an oscillatory system consists of three parts: an input pathway, an output pathway and an oscillator [1]. The input and output pathways establish the link between external or internal environment. The input pathway adjust the behavior of the oscillator to internal or external signals (light, temperature, nutrition status etc.). In this way it changes, e.g., the phase or the frequency of the oscillation. The oscillator itself (which is the main part of the system) uses some biochemical machinery to generate an oscillatory output. The output pathway then translates the behavior of the oscillator into a readable downstream signal [1]. The interaction between the input and output pathways and the oscillator can occur at levels, for example by regulation of transcription, translation or at post-translation level [2–4].

Generally, oscillators can be classified into two types: temporal oscillators and spatial oscillators [5]. To implement temporal oscillations the concentration of active proteins needs to be temporally varying throughout the entire cell. This requires some molecular mechanism to control of protein function, either through production and degradation of protein or through regulation of the protein activity. To implement spatial oscillations the spatial distribution of

proteins in the cell needs to be dynamically changing. The oscillation in the localization gives rise to a time-dependent spatial pattern.

Two fundamental examples of temporal oscillators in bacteria are the cell cycle and the circadian oscillator. The cell cycle oscillator ensures the correct order of fundamental processes such as chromosome replication, chromosome segregation and cell division, and couples these to cell growth. In *Caulobacter crescentus* two interlocked genetic circuits are required to achieve this task (DnaA-GcrA-CtrA-CcrM circuit and DivK-CckA-ChpT-CtrA circuit) [6–8]. A circadian oscillator, on the other hand, allows cells to adapt cellular activities to the changing conditions during the 24 h diurnal period [9, 10]. The period of the circadian oscillator of *Synechococcus elongatus* is constantly kept at 24 hours no matter how environmental light or temperature changes, but the phase can be shifted by an external light signal. The oscillator consists of three proteins (KaiA, KaiB and KaiC) that generate an output at the post-translation level. Not all temporal oscillators have a constant period like the circadian oscillator. For example the cell cycle oscillator in *C. crescentus* behaves differently in swarmer and stalked cells [6].

While temporal oscillators typically regulate the temporal order of cellular events connected to cell growth and division, spatial oscillators are often thought to be involved in molecule positioning in a cell. For example, the establishment of the correct cell polarity during A-motility in *Myxococcus xanthus* is the outcome of an spatial oscillator consisting of the proteins MglA and MglB and the Frz system [11, 12]. In *Escherichia* the DNA segregation oscillator (the parS-ParA-ParB system) pulls plasmids back and forth in this way guaranteeing that plasmids are equally distributed in the daughter cells after division [13, 14]. A similar system is responsible for chromosome segregation in *C. crescentus* [15, 16].

Among spatial oscillators the Min system is one of the best studied examples [17]. It consists of the proteins MinC, MinD and MinE. In *E.coli* these proteins oscillate from pole to pole with a period of ~ 1 -2 minutes [18–22]. As output of the spatial oscillations the Z-ring formed by FtsZ is positioned in mid-cell [23–26]. From many experimental and theoretical approaches the following picture has emerged on how these oscillations are implemented molecularly: MinC is the inhibitor of Z-ring formation by FtsZ [29, 30, 32]. Thus, the Z-ring

can only form at membrane positions with high MinC concentrations. MinC forms a complex with MinD [28, 31] and thus follows MinD during the oscillations. MinD itself only binds to the membrane in the ATP bound form [33]. MinE binds to MinD-ATP on the membrane and stimulates ATP hydrolysis by MinD leading to unbinding of MinD-ADP from the membrane [27]. While diffusing in the cytoplasm MinD-ADP is then converted back to MinD-ATP that rebinds to the cell membrane at a new location. In this way MinE chases the MinC-MinD complex giving rise to the regular oscillations. It has been demonstrated by computer simulations that these oscillations lead to higher concentration of MinC at the cell poles and lower concentration of MinC in mid-cell [34–42]. In this way Z-ring formation is inhibited at the poles and only allowed in the mid-cell position. Then the precise positioning in mid-cell depends on the nucleoid occlusion system [43–47]. The real situation is of course more interesting than this simple picture. For example, the interaction of MinE with the MinC-MinD complex is non completely random as MinE forms a dynamic ring that wanders from pole to pole [18, 48, 49]. It has also been shown that FtsZ is not just simply expelled by MinC from the cell membrane. A kind of helix structure of FtsZ on the cell membrane is observed and this helix structure also performs an oscillatory movement along the cell length in the cell, which is also affected by the Min oscillation [51].

In *minB*⁻ cells the dynamic of FtsZ assembly are different and in FRAP experiments the recovery time of Z-ring is longer than in wild type (WT) cells [50]. This indicates that the Min system has a more complicated effect on FtsZ polymerization. Of course, the biggest change in *minB*⁻ mutants is that Z-ring structures can form at any chromosome free position. In particular, *minB*⁻ mutants can position the Z-ring close to the cell poles. Cell division thus produces mini cells which contain no chromosome and are not able to grow and divide [52]. On the other hand, *minB*⁻ can form very long filament cells where positioning of division sites is highly irregular giving rise to a distribution of different cell sizes. Before it was known that the Min system performs oscillations Teather et al. were able to explain the experimentally observed size distribution of a population of *minB*⁻ cell [53]. To do so, they assumed that division at the poles effectively inhibits division in mid-cell by recruiting the division machinery away from the mid-cell positions. The good agreement between the calculated and the exper-

imentally measured distribution implies that the oscillations of the Min system would not be required if there were a different way of preventing cell division close to the cell poles. Indeed, in other bacteria, such as *Bacillus subtilis*, the Min system does not perform oscillations but is statically attached to the cell poles [54, 55].

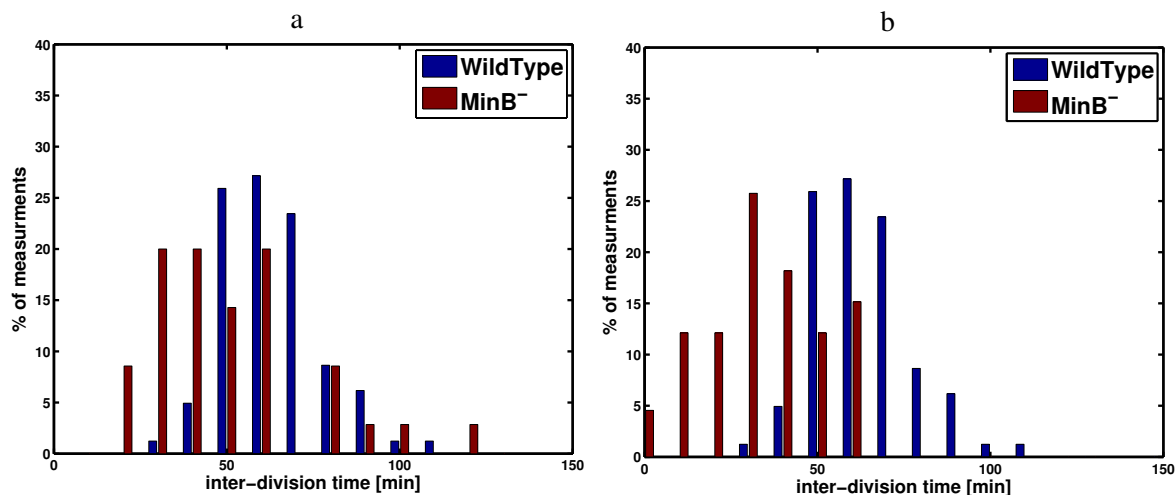


Figure 1.1 – The comparison of inter-division time between WT (blue histogram) and *minB*⁻ (red histogram) cells. (a). The inter-division time distributions of WT cells and *minB*⁻ cells with birth lengths in the same range as WT cells. (b). The inter-division time distributions of WT cells and *minB*⁻ cells with division lengths in the same range as WT cells.

Astonishingly, the effect of the Min system on timing of cell division has so far not been studied [36]. As we show here, in the absence of a functioning Min system, the time between two sequential division events (inter-division time) also becomes irregular. In order to reduce the complication caused by fluctuating cell length, we only compare the *minB*⁻ cells with birth lengths or division lengths in the same range as wild type cells. In Fig.1.1 we show the difference of inter-division times between wild type cells and *minB*⁻ mutants cells. Recently, it has been claimed that Min also has an effect on the chromosome segregation process [101, 102]. Combined with the observation mentioned above, i.e. that Min affects Z helix structure and the recovering time, it becomes apparent that the Min system operates in a more complicated fashion rather than simply blocking Z-ring formation at the cell poles. Although the Min is generally believed to be a purely spatial oscillator, the results presented here indicate that oscillations also affect the timing of cell division in this way acting also as a temporal oscillator.

1.1 Hu

Hu is a nucleoid-associated protein (NAP), which belongs to the DANBII family of DNA-binding proteins [56]. As a global regulator, Hu has many similar properties as histones do and is important for nucleoid organization [57, 58]. It is small, heat-stable and highly conserved in bacteria. Hu binds to the chromosome almost unspecifically, with a preference for A/T rich sequences. It can bind to double-stranded and single-stranded DNA, and even RNA [59].

Hu is composed of two subunits, HupA and HupB, which are encoded by two separated genes, *hupA* and *hupB* [60–62]. These two subunits can form three dimers in *E.coli* cells: HupA₂, HupB₂ and HupAB [63]. The expression of these two subunits is related to the cell culture's growth phase and regulated by CRP and FIS proteins at the transcription level [56]. In this way the composition of those dimers changes according to the growth phase of *E.coli* culture. In the early exponential phase, HupA₂ is the predominant form for Hu proteins existing in *E.coli* cells. When the culture enters to stationary phase, more and more HupAB is generated and turns to be the main forms of dimers. So it is believed that the heterodimeric form of HU, HupAB helps the cell to survive starvation [56, 63].

1.2 FtsZ

FtsZ is one of the first proteins which localizes at the division site and starts building a septum in *E.coli* [64]. It is highly conserved in a lot of bacteria and in many archaea. It is also found in some chloroplasts and a few mitochondria of eukaryotic cells [65–68]. Although it is highly conserved, FtsZ in *E.coli* can not be replaced by that from most of other species [69].

FtsZ mainly consists of four domains [68, 70]. The N-terminal segment and the spacer next to C-terminal are variable. The other two domains, a core region and the C-terminal, are highly conserved, indicating that they are important for the protein function. During the process of cell division, FtsZ first self-assembles to Z-ring structures and then recruits the other proteins which are important for septum formation. The function of self-assembly of FtsZ is achieved by the two independent parts of the core region of FtsZ, which are the Ct core and Nt core respectively. The other conserved part of FtsZ, C-terminal, is important for recruiting other

membrane-associate proteins to Z-ring for cell division [71].

In vitro, when the concentration of FtsZ is higher than a critical concentration of about $\sim 1\text{-}2\ \mu\text{M}$ [72], the proteins binding with GTP will assemble into protofilaments [73–75, 77] and then form bundles or sheets [76, 78, 79]. It is believed that this bundling process is also important and more complicated in vivo [64].

In vivo, FtsZ proteins finally assemble into Z-ring structures which are about 110 nm thick [80] and recruit over ten other membrane-associated proteins in a specific order. With those proteins, cells can form septums and finish the cell division in the end. Some of those proteins also affect the Z-ring itself. As the first two proteins which are recruited, FtsA and ZipA keep the Z-ring stable on the membrane [81, 82]. They are also important for the Z-ring to recruit other downstream proteins. Furthermore, keeping the ratio of FtsZ to FtsA around five to one is strongly required for cell division [83, 84]. There are other regulators as well, for example, ZapA and SulA, etc [85]. It is already shown experimentally and theoretically that the FtsZ structure on the cell membrane is also dynamic. It forms helical structures besides ring structures, and the assembly of Z-ring is also a dynamic process [51, 94].

So to couple the Z-ring formation to cell grow and division, there has to be some system to regulate the location and timing of Z-ring formation. In wild type *E.coli* cells, there are two negative spatial regulatory systems to guide the Z-ring to form precisely at mid-cell. They both work by preventing FtsZ from forming Z-rings at improper positions in the cells. One is the Min system, that prevents FtsZ assembling a Z-ring at the cell poles by inducing an oscillation of MinC which inhibits FtsZ. The other one is called the “NO” system (nucleoid occlusion) [43–45]. It keeps the Z-ring structure away from areas containing chromosomal DNA. This regulation in *E.coli* is mainly carried out by SlmA in *E.coli* [46, 47], which is a DNA-associated division inhibitor and interacts with FtsZ [46]. FtsZ can assemble everywhere, even on top of nucleoids, when Min system and “NO” system are both inactive. But among the several FtsZ structures in the double mutant cells, none of them can finally form a functional Z-ring [46]. This is probably because the FtsZ subunits are used out [64].

The timing of FtsZ assembly has also been studied, but to our knowledge only in wild type *E.coli* cells so far. There are three key points in the whole process of cell division, Z-ring

assembly, constriction of the Z-ring and completion of the cell division. It has been shown that the Z-ring assembles at about the same time as the chromosome finishes replication and segregation [86]. It is not very clear yet how cells regulate this timing. No direct signal has been found to start the formation of the Z-ring in *E.coli* cells yet, except for some inhibitors that work as checkpoint proteins, like Ugtp, which is sensitive to the cell size [87], or Sula which responds to DNA damage [88, 89]. Since the concentration (amount relative to total mass) of FtsZ is constant during cell growth [83], it seems that not the concentration but the total amount of FtsZ is regulating the timing of Z-ring assembly [83, 90]. Furthermore, a change of the FtsZ expression level will also affect the cell division. Over expressing FtsZ in wild type *E.coli* cells will make cells produce mini cells [91], but the Min deletion mutant in *minB*⁻ cells is somehow compensated [92]. However, too high over expression of FtsZ, like more than ten folds, will block cell division entirely [84, 91], which is not very well understood yet.

There is correlation between the time of construction of the Z-ring structure and completion of cell division, but they seem unrelated to the time of Z-ring formation [93]. However, this work did not study the timing of cell division of *minB*⁻ cells.

1.3 Min system

As mentioned in the introduction, MinD binds to the cell membrane after binding with ATP. MinE then converts MinD-ATP to MinD-ADP, which has a lower affinity for the membrane. MinD-ADP is then released from the membrane and diffuses through the cytoplasm, and switches back to MinD-ATP state by exchanging a nucleotide in the cytoplasm [27]. MinE will follow MinD after it accumulates in the other end of the cell. So these two proteins oscillate between the two cell poles. MinC is recruited by MinD to cell membrane, so it also oscillates between the cell poles. All three proteins can dimerize.

In the Min system, MinC is the effective inhibitor of FtsZ assembly in *E.coli* cells. It does not affect the oscillation of the system. MinC is only a weak inhibitor in the absence of Min, but it can be enhanced ~25-50 times by MinD [28]. MinD activates MinC by recruiting it to the cell membrane. The N-terminal of MinC is required to inhibit FtsZ assembly [29]. It

has been reported that MinC inhibits FtsZ filaments to form the structure into a solid-like gel state [30]. The C-terminal is essential for its dimerization and its interaction with MinD. Fusing an additional membrane-anchoring sequence to any end of MinC can also increase its activity as an inhibitor [95, 96]. This is similar to the way MinD works. Combining with MinD, MinC-MinD complex also targets to the septum components [31]. It has also been reported that the MinC-MinD complex maybe involved in the recruiting process of FtsA to the Z-ring [32]. Besides the MinC-MinD complex, DicB was also found to be able to recruit MinC to the septum [31]. When people wanted to track MinC in vivo, normally, they labeled MinC with fluorescent protein at its N terminal. We will follow this lead.

MinD and MinE are actually essential proteins for the oscillation of the whole system. MinD is an ATPase and its activity can be stimulated about ten folds by MinE in the presence of phospholipid vesicles [27]. Interestingly the affinity of MinD to the cell membrane depends on ATP [33]. So MinD binds to the cell's inner membrane with nucleotide, then it recruits MinE to its position. MinD also recruits MinC to the cell membrane, as mentioned above, and the binding site on MinD overlaps with that for MinE [97, 98]. But MinE possesses the priority to combine with MinD and activates it. After being activated by MinE, ATP is transformed to ADP, so MinD is released from cell membrane because the affinity is decreased. The N-terminal of MinE is important for binding and stimulating MinD, it is also required for suppressing MinC-MinD activity [27, 97, 99]. Changing this part sometimes makes MinE stimulate MinD ATPase less efficiently, and even results in different oscillation frequency [27]. Normally, people labeled MinE with fluorescent protein at the C-terminal and labeled MinD at the N-terminal in order to keep them functional.

The complicated interaction between MinD and MinE makes the system oscillate. Experiments showed that MinD forms a membrane-associated polar zone at cell ends [19, 20, 100]. The ring structure formed by MinE at the edge of MinC-MinD polar zone shrinks the zone and prevents the zone extending cross the middle area of cells [18, 48]. These two structures switch the accumulation place between the two cell poles with a phase separation, so that they show the oscillation behavior. MinC, as a passenger, also oscillates between the two cell poles and leaves the mid-cell free for FtsZ to form the Z-ring structure. Further studies show that

Min proteins actually form coiled structures in the polar zones, which indicated there are more details haven't been found out, yet [49].

In order to get more information about cell timing, we labeled Hu protein with fluorescent protein so that we can track the chromosome replication and segregation. We found that after chromosome segregation *minB*⁻ cells need to wait longer until division than wild type cells. In order to understand this behavior, we performed simulations based on different models. By comparing the cell length and timing obtained from different models and experiments, we show that more division sites delay the cell division while the presence of less available division sites in between cell poles leads to the formation of filament cells. This feature of *minB*⁻ cells shows the effect of the Min system on cell timing and cell sizes.

Chapter 2

Results

In this study we analyze the influence of Min system on timing of cell division. Our investigation was triggered by the observation that the distribution of inter-division times of wild type (WT) and *minB* deletion mutant cells (*minB*⁻) are very different (Fig.1.1). As can be seen from Fig.1.1, the distribution of inter-division times is much broader for *minB*⁻ cells than for WT. Considering that the only difference between the two strains is the existence of a functioning Min system, we assumed that the different distributions of inter-division times is due to Min system. To find the origin of this we compared cell division timing in the presence and absence of Min system.

To avoid the complication caused by the irregularity of the cell length of *minB*⁻ cells, we compared the timing among division sites, not among cells. More specifically, we measured the time interval between chromosome segregation and cell division (in the sequel referred to as **division waiting time**) for the two strains. The timing of chromosome duplication will also affect the inter-division time, but as can be seen from the density plots shown in Fig.2.1 and Fig.2.2, lacking Min system does not lead to any visible growth defect. To track the chromosome segregation, we labeled Hu proteins with green fluorescent protein (GFP) in WT (strain TB28 [103]) and *minB*⁻ cells (strain TB43 [46]) in the original frame (refter to details in Appendix A.3) and treated the first visible spatial separation of two chromosomes as a segregation event.

Because *minB*⁻ cells divide also at polar sites producing mini cells, we define the division

waiting time of polar sites as the time interval between a cell pole formed and cell division at this pole, as shown in Fig.2.3.

2.1 Experimental analysis of cell growth and chromosome segregation

In order to rule out the possibility that the different inter-division time of the two strains used is caused by different growth rates, we compared the OD curves of these two strains in different mediums at 37°C with a shaking speed of 220 rpm. We first grew the cultures in Luria-Bertani (LB) medium over night and diluted them to OD600<0.1 in different fresh liquid mediums, then after OD600 is around 1, we diluted the culture ten times into corresponding fresh mediums with the same growth condition, and start measuring OD regularly. This guarantees that every measurement cycle starts with the cultures in their exponential growth phase. The background values of mediums are deduced from corresponding measurements. As the OD plots in Fig.2.1 and doubling times in Table.2.1 show, there is no apparent difference of the growth rates between WT and *minB*⁻ cells.

This means that the irregularity of inter-division times of *minB*⁻ cells is not due to cell growth, but due to the cell division process itself. And this is why we tried to compare the division waiting times.

Table 2.1 – The average doubling times calculated from the growth curves in Fig.2.1.

Media	TB28	TB43
LB+0.2% glucose	22.8 min	24.7min
M9+0.2% glucose	67.6 min	67.3min
M9+0.5% glycerol	96.6 min	96.4min
M9+0.5% glycerol+1% CAA	43.5 min	45.1min

In order to measure the division waiting time, we need to track the chromosome segregation. As a DNA stain, DAPI is widely used for studying the conformation and segregation of the nucleoids [59]. But the problem in our work is, that we need to track cells for several generation and repeating staining the cells on the slide has a negative impact on their growth and is inconvenient. Labeling the DNA with a Hu protein can solve this problem.

2.1. Experimental analysis of cell growth and chromosome segregation

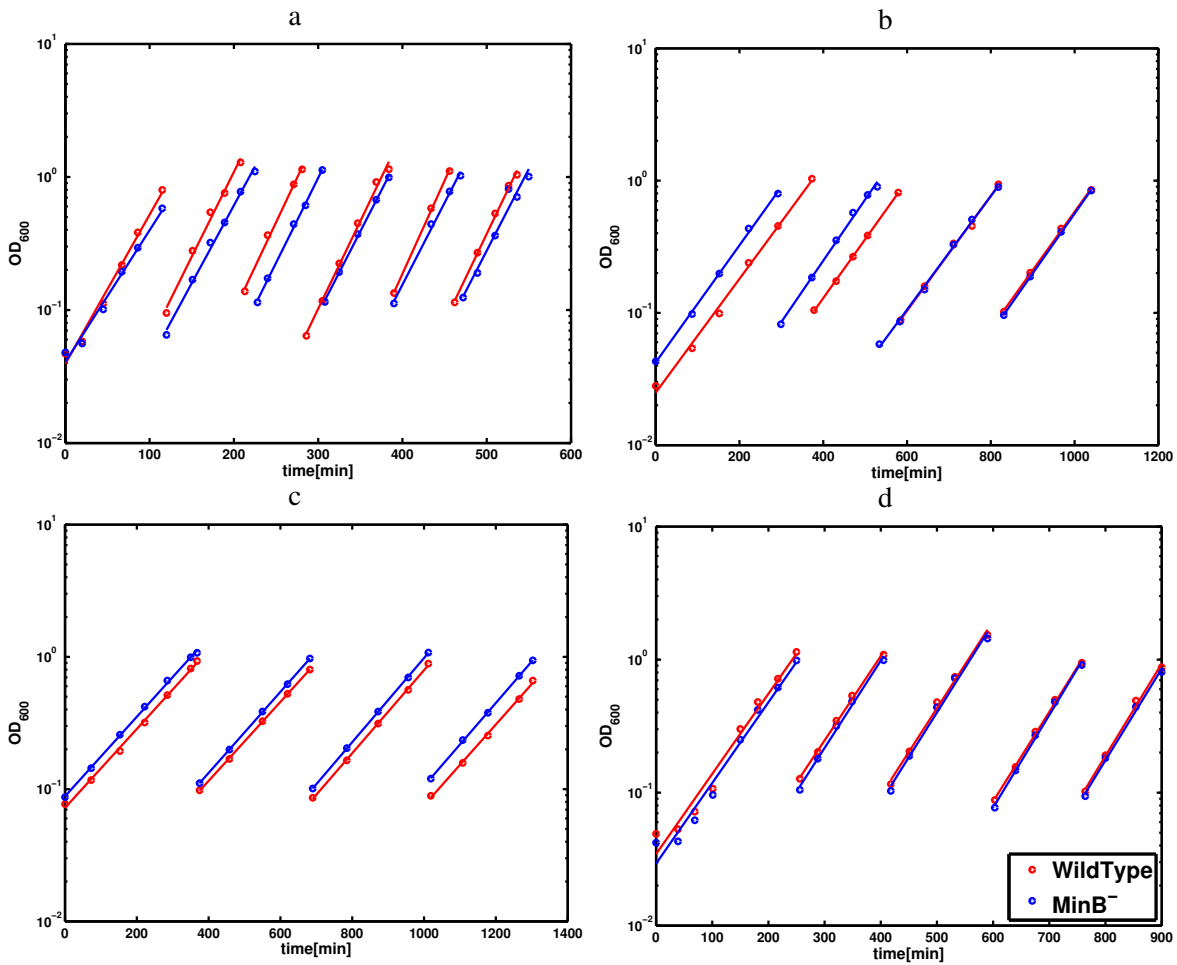


Figure 2.1 – OD plots. Cells are grown in different media: a. LB media with 0.2% glucose; b. M9 media with 0.2% glucose; c. M9 media with 0.5% glycerol; d. M9 media with 0.5% glycerol and 1% Casimino acid (CAA) in all cases $T=37^{\circ}\text{C}$ and samples were diluted to $\text{OD}_{600}=0.1$ when OD_{600} reaches 1. The corresponding doubling times are obtained by averaging over the repeated growth curves. Table.2.1 gives the obtained values.

Experimental works show that both subunits can be labeled by fluorescent protein and used for tracking the chromosome [59]. As a tool to track DNA in living cells, HU-GFP produces a fluorescent signal at the same place in the cell as DAPI does, and also indicates the same structures. The only difference is that signal from HU-GFP is stronger [59].

In this work, we only labeled the HupB subunit with GFP. We fused the GFP sequence to *hupB* on the original position on the chromosome, with a linker (see appendix) in between and the stop codon followed. The details of the experiments are shown in Appendix A.3. The phase and fluorescent photo of cells are shown in Fig.2.4. The OD curve indicates that this

2. RESULTS

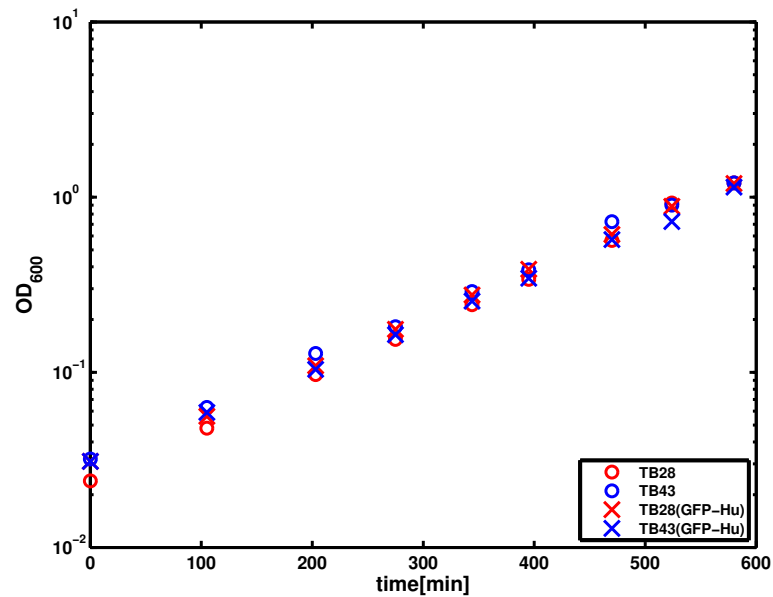


Figure 2.2 – OD plots. WT (red) and *minB*⁻ (blue) cells with (cross) and without (circle) Hu labeled by GFP. We can see that the growth curves are very similar to each other.

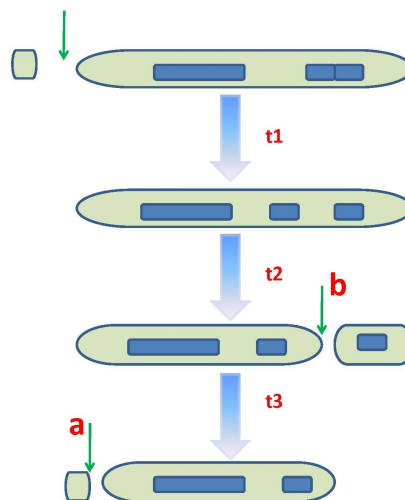


Figure 2.3 – cell division waiting time: for site b, the division waiting time is t_2 ; for site a, it is $t_1 + t_2 + t_3$. The green arrows show the cell division positions.

does not change the cell growth (as shown in Fig.2.2).

The growth curves shown in Fig.2.1 are measured with strains without labeling Hu protein with GFP, to rule out the possibility that the change of Hu protein causes the different inter-division time of the two strains, we further tested the strains with Hu labeled by GFP. As

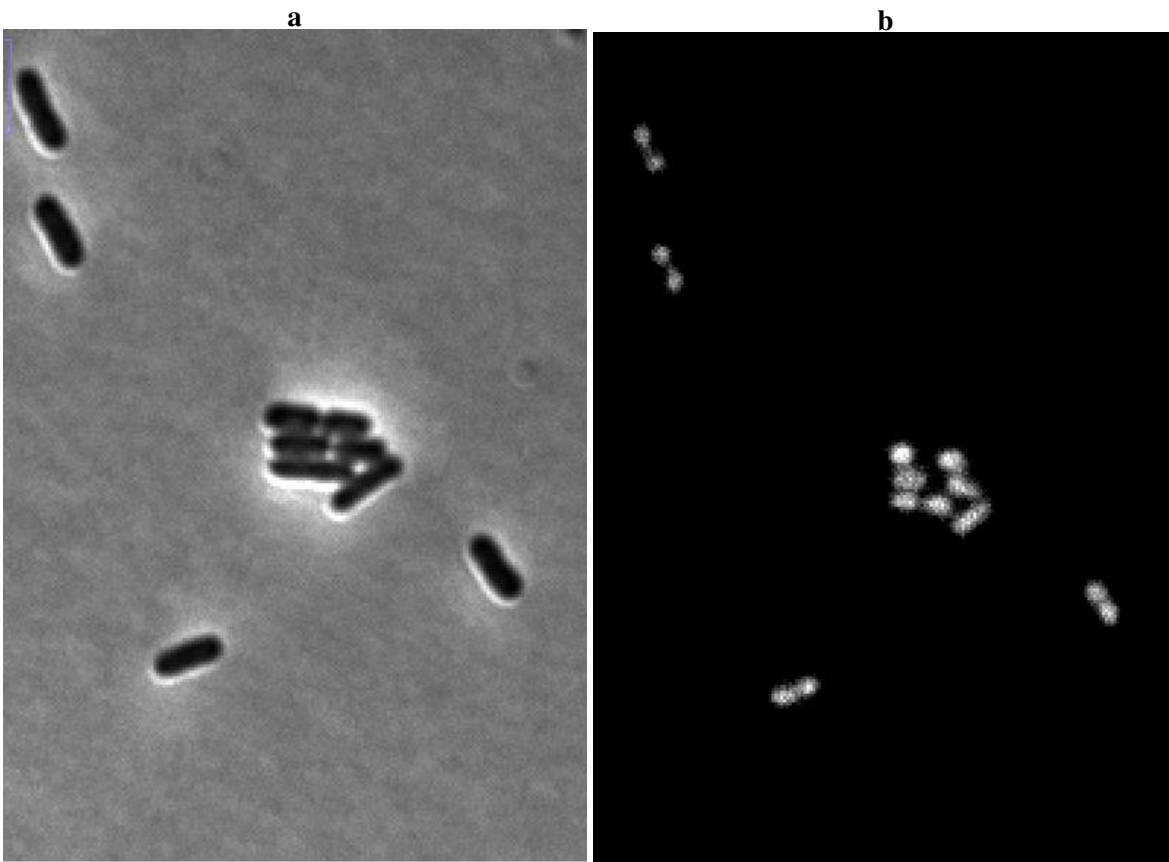


Figure 2.4 – Snapshot of growing population: a shows the phase photo of WT cells; b shows the fluorescent photo of chromosome clusters in WT cells.

shown in Fig.2.2, the growth curves of WT and *minB*⁻ cells with Hu labeled by GFP are still similar. And their growth curves are also similar to the strains where Hu is not labeled by GFP.

In order to avoid complications arising from multiple chromosomes in WT cells, we grew the cells in poor nutrition medium (M9 plus 1%CAA and 0.5%glycerol) at 30°C . We first grew the cells overnight in liquid medium, then diluted them into fresh medium and when OD was about 0.2, we transferred the cells to the slide (details are explained in Appendix, Fig.A.2 shows the photo of the slide and the stage heater). The slide in end is sealed with wax so that the agar will not shrink too fast. The stage heater keeps the temperature at about 30°C using a water bath.

Now we can track the individual cell's growth and division and we are able to measure the division waiting time. The experimental results for both strains are shown in Fig.2.5. As one can see the division waiting times of *minB*⁻ (Fig.2.5b) cells are generally longer and show

2. RESULTS

more variation than those of WT (Fig.2.5a). Furthermore for $minB^-$ cells, the division waiting times of polar sites are generally longer than that of non-polar sites. We have proven that the absence of the Min system does not lead to any measurable growth defect. Thus, the absence of the Min system not only affects positioning of division site but also timing of the division event. The difference of the division waiting times between polar and non-polar sites raises a question about the equivalency of cell division at different positions.

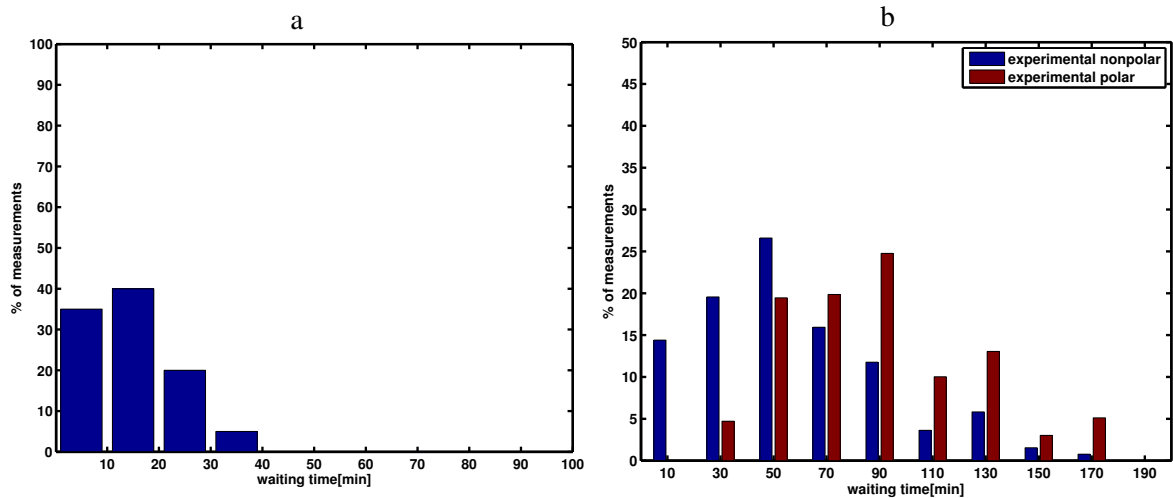


Figure 2.5 – Division waiting time distribution of WT (a) and $minB^-$ (b) cells. The x-axis is time in minute. In (b), the waiting time distributions of polar sites (red histogram) and non-polar sites (blue histogram) are also measured separately.

2.2 Model I

To understand these findings in a quantitative way, we developed a simple model for cell growth and cell division that we applied to WT and the $minB^-$ cells. We tried to first build a platform where we can implement our hypotheses and test them with numeric simulation. This requires us to get a model that captures the experimental observations of a $minB^-$ culture when we set all the parameters of cell growth and division according to the experimental measurement. The simple model (in the following referred to as model 1) is based on the following assumptions (further details are shown below):

- i. Each cell has its individual doubling time T drawn from a normal distribution ($75 \pm$

15min). As we show in the section 2.3.1 individual cells increase their length exponentially in time. Thus, every time step Δt , each cell increases its length by an amount

$$\Delta L = L_s \cdot \frac{\ln 2}{T} \cdot \exp\left(t \cdot \frac{\ln 2}{T}\right) \cdot \Delta t. \quad (2.1)$$

Here, L_s is the length of the cell at birth. Furthermore, t is the time since the last division event of the cell (which for daughter cells corresponds to their current age). This increase in length guarantees that after time T the cell length has been doubled and the mass of cell increases exponentially with time. As shown in Fig.2.6, this leads to exponential growth of the culture with a doubling time of 75 min.

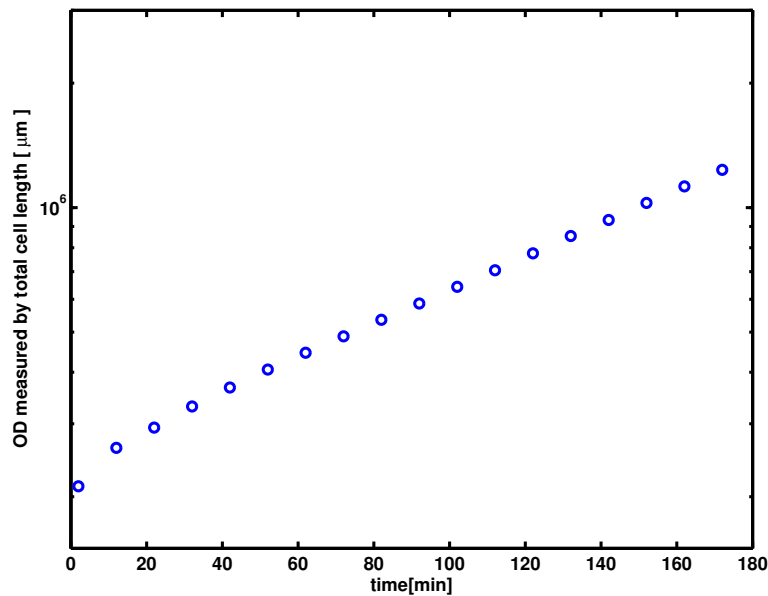


Figure 2.6 – OD curve as determined from the simulations. We take total cell length as measure of OD of the culture. This quantity is calculated every minute in the simulations. As one can see the increase in total cell length is clearly linear on a log scale and the slope corresponds to a doubling time of 75 minutes.

- ii. *minB*⁻ mutant cells might have several chromosomes. Then, each cellular compartment containing a full or partial chromosome is treated as an independent cell. Thus, for cells with several chromosomes the different compartments might have different doubling times. These growth rates are assigned to the compartments upon initiation of a new round of replication. The starting length of the new compartment is also drawn from a

normal distribution (1812 ± 181 nm). To test the validity of this assumption we performed simulations of a modified model where all cell compartments in the culture have the same doubling time. In this case we obtained very similar results with the only difference being that the simulations required more time to reach steady state. The advantage of doing this is that after a filamentous cell divides into two shorter cells, the two daughter cells will keep their own growth rate as they were parts of one mother cell with several compartments growing at different rates. Considering that the growth conditions do not change a lot before and after cell division, this is more reasonable than distribute two new random doubling times to the two daughter cells which are totally unrelated to their mother cell.

- iii. Cell growth and chromosome replication occur in synchrony. Thus, the cells (or the compartments) have doubled their length when chromosome replication and their individual division waiting time are over. For WT the division waiting time is drawn from a normal distribution with average 17.7min and standard deviation 12min. For *minB*⁻ cells each division site has its individual division waiting time drawn from the experimentally measured distribution (see section 2.3.2). Once a new pole appears it gets assigned a waiting time drawn from the experimental distribution (for polar sites).
- iv. Division site placement has a random component. For WT the daughter cells have an average size of $(2.2 \pm 0.2)\mu\text{m}$. For the *minB*⁻ cells division site placement occurs at the middle $\pm 5\%$ [47, 105, 106] between two neighboring chromosomes.

All of the above parameter values in the simulations are fixed by fitting the experimental data. To sum up, all the parameters of individual cell growth and division are set according to the statistical results from the experiments, and we try to get the properties of the whole culture, mainly for *minB*⁻ culture, from the simulations.

2.3 Parameters of model 1

We will show the details about the cell growth and other parameters we used in model 1 here. One should note that the analyses we did here are for individual cells grown on slide, under

the microscope. we grew cells on solid agar, mixed with M9 media with 0.5% glycerol and 1% CAA, and take pictures every five minute (fluorescent pictures are taken every 15 minute). The growing temperature is kept at 30°C by stage heater. The cell lengths and other informations (like time and cell numbers) are extracted from those pictures.

2.3.1 Cell length increases exponentially

To be able to implement cell growth in the simulations we need to figure out if *E.coli* cells increase their mass (and thus it length) exponentially or linearly with time (or in a more complicated way [104]). To do so we took pictures of the cells every 5 minutes and measured the cell lengths. We analyzed the data in two different ways to determine the increment in cell length per time.

1. Rescaled cell length

If cell length L increases exponentially with time t , then

$$L(t) = L_0 \exp\left[\frac{\ln 2}{T}(t - t_0)\right], \quad (2.2)$$

Where L_0 is the newborn cell length, that is different for individual cells. T is the doubling time, and the t_0 is the time, when the cell was born. This can be written as

$$\ln \frac{L}{L_0} = \frac{\ln 2}{T}(t - t_0), \quad (2.3)$$

where on the right hand side $\ln 2/T$ is constant for the cells growing under the same condition. In particular, one obtains for the division length L_d

$$\ln \frac{L_d}{L_0} = \frac{\ln 2}{T}(t_d - t_0). \quad (2.4)$$

By combining Eq.2.3 and Eq.2.4 we can eliminate the difficulties caused by the differences in newborn cell length, i.e.

2. RESULTS

$$\frac{\ln L - \ln L_0}{\ln L_d - \ln L_0} = \frac{t - t_0}{t_d - t_0}, \quad (2.5)$$

Upon introducing the rescaled length increment

$$l_{resc} = \frac{\ln L - \ln L_0}{\ln L_d - \ln L_0}. \quad (2.6)$$

and the rescaled time

$$t_{resc} = \frac{t - t_0}{t_d - t_0}. \quad (2.7)$$

Eq.2.5 then implies $l_{resc} = t_{resc}$, i.e. a linear correlation between cell length increment and time. Thus, for an exponential increase in cell mass all experimental data points should lie on a straight line from (0,0) to (1,1), see Fig.2.7.

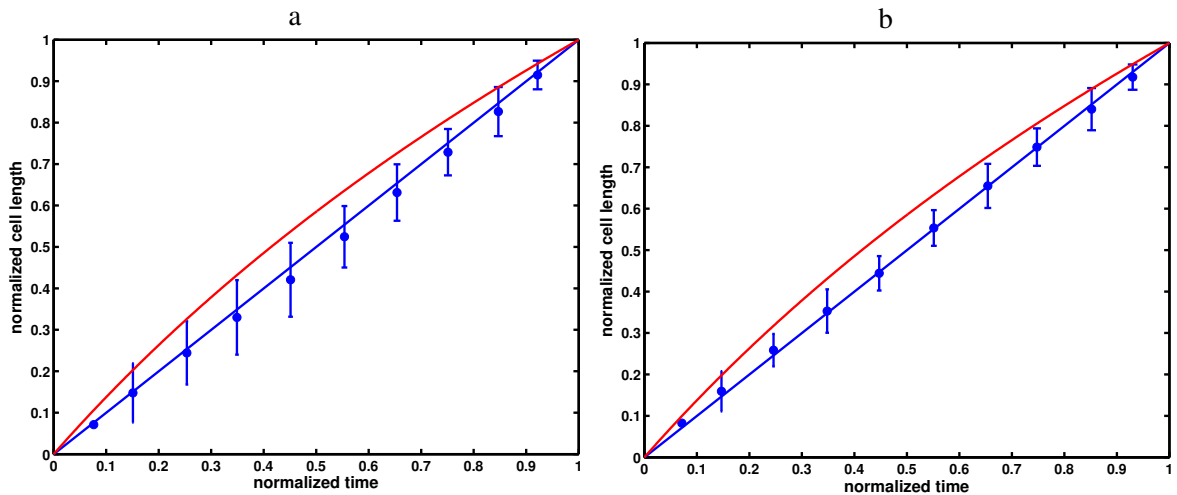


Figure 2.7 – Rescaled cell length increment as function of rescaled time. The blue dots and error bars are experimental data. If cell mass increases exponentially of with time the data points should lie on a straight line from (0,0) to (1,1). (a) shows the result of wildtype strain and (b) represents $minB^-$ data. As a control, the rescaled curves for a linear cell length increment are shown in both figures as red lines.

As can be seen, the rescaled experimental data (represented by blue dots) clearly lie on the straight line from (0,0) to (1,1). The red line shows how the curve would look like if

the cells were increasing the cell length linearly in time. In this way the differences between the two growth modes becomes apparent, indicating that the cells indeed increase their mass exponentially.

2. Cell length increment rate

Another way to distinguish exponential from linear mass increase is to calculate the cell length increment rate. For an exponential time dependence, Eq.2.2 implies

$$\frac{dL}{dt} = \frac{\ln 2}{T}L, \quad (2.8)$$

while for a linear increase one has

$$L = L_0 + \frac{L_d - L_0}{T}t, \quad (2.9)$$

and thus

$$\frac{dL}{dt} = \frac{L_d - L_0}{T}. \quad (2.10)$$

Eq.2.8 shows that for an exponential mass increase the length increment rate is proportional to its length, while for a linear time dependence the length increment rate is constant.

In Fig.2.8 we can see that for both strains the length increment rate is indeed proportional to the cell length, and the ratio is about the same for both strains, this is also consistent with our conclusion that these two strains have similar growth rate.

From the combination of these two methods, we conclude that the cells grow exponentially in length. Otherwise, if cells would grow linearly or bi-linearly, then in Fig.2.8a, we would see all the data points stay in one or two horizontal lines, which means that the length increment rate does not change along with the cell length.

2. RESULTS

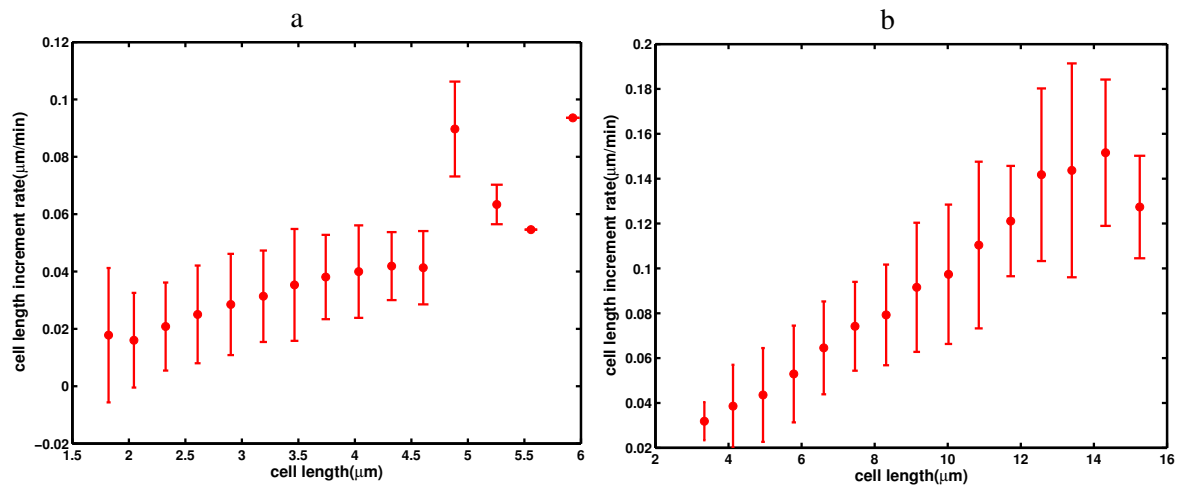


Figure 2.8 – The dependence of length increment rate on cell length. (a) shows result of wild type strain and (b) represents data of *minB*⁻ cells.

For the *minB*⁻ cells, it is more complicated. A filamentous cell which contains several compartments will also increase its length faster when it is longer. If the compartments' length is increased bi-linearly and they are in different growth phases, then we would still get a similar curve as shown in Fig.2.8b by averaging over all cells.

We also checked the cell growth of *M. Xanthus* in flow chamber and found they also grow exponentially.

2.3.2 The doubling time and division waiting time of wild type strain

We use doubling time to represent the growth rate of cells. As we proved above with OD plots, the Min system does not affect cell growth, so we can use the distribution of doubling times from wild type cells (Fig.2.9) and implement it into the simulation for *minB*⁻ cells. Different to the OD plot shown in Fig.2.1, we are tracking here the increment of individual cell lengths in microscope photos. By fitting the individual length increment curves of different cells with straight lines in log scale plot, we get the doubling times, which also represent the growth rates of the cells, shown in Fig.2.9.

Most cells have doubling times in the range of 57 to 91 minutes, some cells grow very slowly. We are not sure what makes cell growth rates vary so much. The individual cells themselves are quite different and have very doubling times. The inhomogeneity of the agar plate

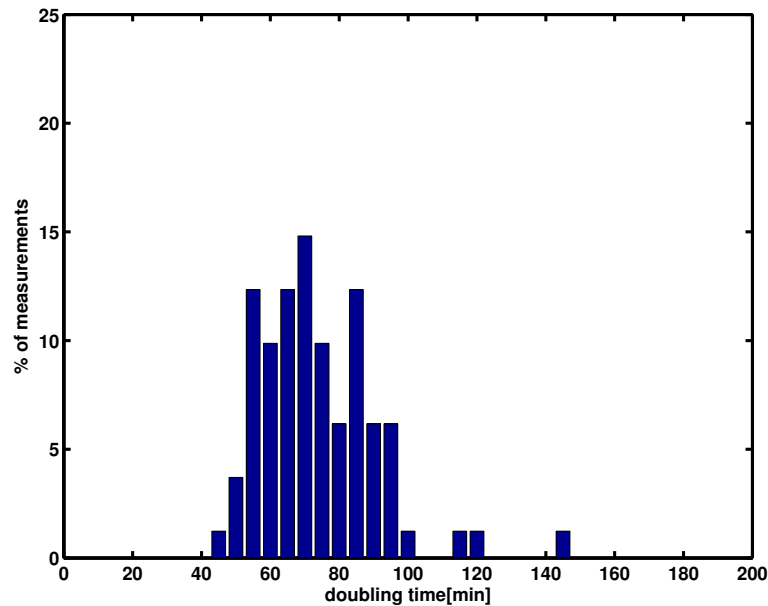


Figure 2.9 – The distribution of doubling time of wild type strain. 81 wild type cells were measured. The doubling time is $74\text{min} \pm 17\text{min}$.

might be another reason, although we tried to mix the agar solution very well, the fluctuation maybe still be big enough to cause the differences in growth rates among cells.

The doubling time also shows the duplication rate of cells and chromosomes, besides representing cell's growth rate. So by counting cell numbers, we should be able to obtain a "cell duplication" curves. And based on this, we can estimate the doubling time as well. Furthermore, because the duplication of chromosome is synchronous with cell grow, we should get similar curve by counting chromosome numbers. As Fig.2.10 shows, in a log-linear scale, the points of cell number and chromosome number are on two parallel lines. The horizontal distance between them results from the phase separation of the cycles of duplication of cell and chromosome. Because the cell division always happens after the chromosome segregation in WT cells, the chromosome number is always larger than the cell number. And this distance actually shows how much earlier the chromosome segregation ends than cell division, which is the division waiting time. The division waiting time obtained from Fig.2.10 is 17.7 minutes.

The distribution of division waiting times of WT cells in Fig.2.5a is measured from individual cells. As the definition of division waiting time, we start measuring the time right after we see a gap appear between two chromosome clusters, and measure until the cell divides.

2. RESULTS

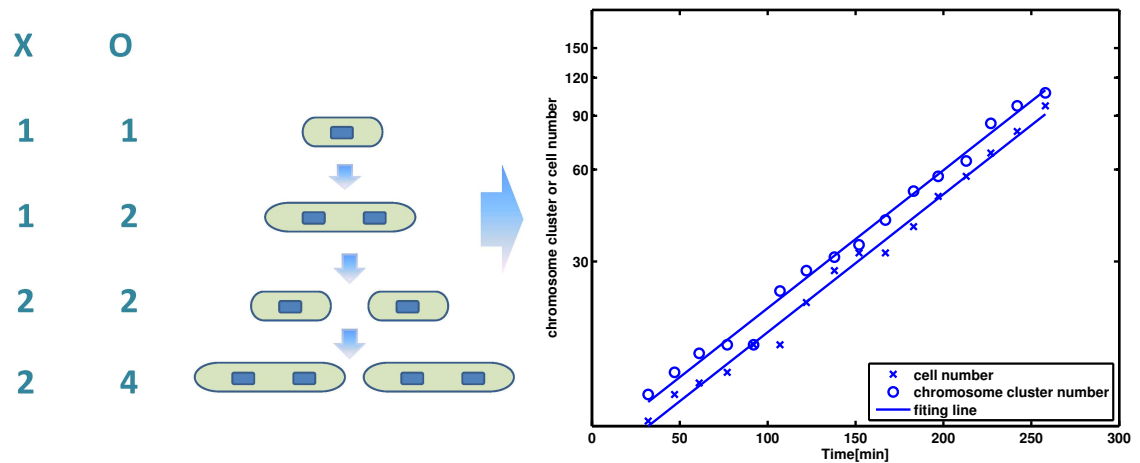


Figure 2.10 – The cell number and chromosome cluster number curves in log scale plot. The points of cell number and chromosome number are on two parallel lines. The horizontal distance between them represents the division waiting time.

A problem we had with this technique is the bleaching of the fluorescent proteins because of the relatively high frequency of taking pictures. In order to avoid the proteins bleaching too fast, we took fluorescent pictures every 15 minutes. So in this case, the chromosomes might already be segregated for some time when we can see the gap. Considering that we take the phase photos every five minutes, the division waiting time might be underestimated by 10 minutes at maximum.

In this respect, it is better to use the division waiting time from Fig.2.10 to calculate other parameters of cell growth, like the starting length of a new compartment of a cell. But from Fig.2.10, we cannot calculate the standard deviation of the distribution of division waiting times. We estimated it to be 12 minutes based on the distribution shown in Fig.2.5a and considering the possible shift of the distribution caused by the underestimation I mentioned above.

The division waiting time of *minB*⁻ cells can only be obtained from the distribution shown in Fig.2.5b. The distributions are different for non-polar (47 ± 35.7 min) and polar (76 ± 34 min) sites. Because mini cells do not contain chromosomes, by counting the cell number and chromosome number, we will get two non-parallel curves in semilogarithmic plot, as shown in Fig.2.11. We are not able to extract a division waiting time from this, plus from Fig.2.5b we knew that the distributions of division waiting time at polar and non-polar sites in *minB*⁻ cells are different. So we will use the data got from Fig.2.5b.

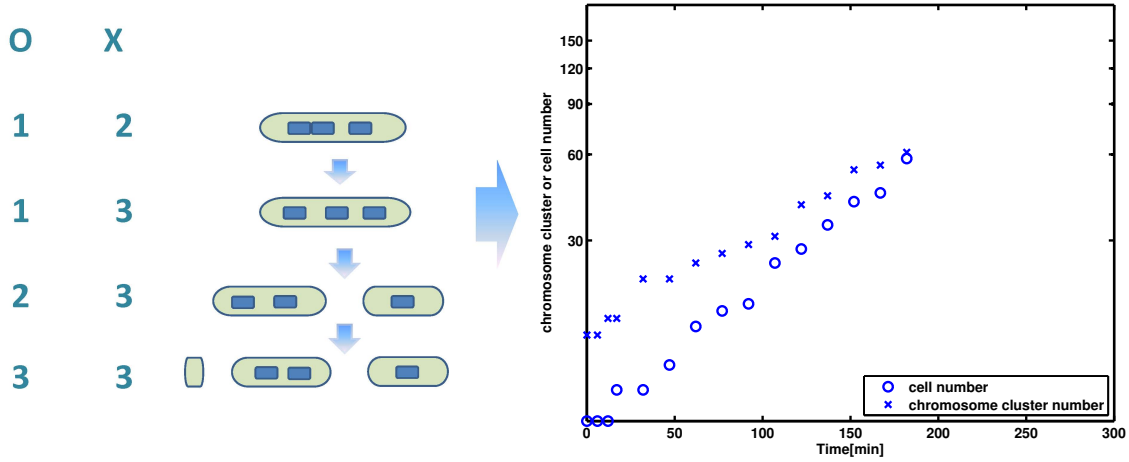


Figure 2.11 – The cell number and chromosome cluster number curves in log scale plot. The division waiting time of $minB^-$ cells cannot be obtained in this way.

2.3.3 The cell length

As we mentioned above, in the simulation we distribute starting length and ending length to each new compartment. The ending length is twice as long as the starting length, but neither of them can be measured directly from the experimental data. What we can measure is the new born cell length of WT cells (Fig.2.12). And then we can calculate the starting length by:

$$L_s = \frac{1}{2}L_0 \exp\left[\frac{\ln 2}{T}(T - T_w)\right], \quad (2.11)$$

Where L_s is the starting length, L_0 is the average new born cell length of WT cells in Fig.2.12, T is the average doubling time in Fig.2.9, T_w is the waiting time in Fig.2.10. This function calculates the cell length when the chromosomes just segregated and form two compartments in one WT cell. The average starting length is half of it.

In the simulation a starting length is drawn from a normal distribution with average L_s and standard deviation $0.1L_s$. This is set according to the distribution of new born cell lengths (Fig.2.12). Again, we used the length distribution of WT cells as a parameter for the $minB^-$ strain in the simulations.

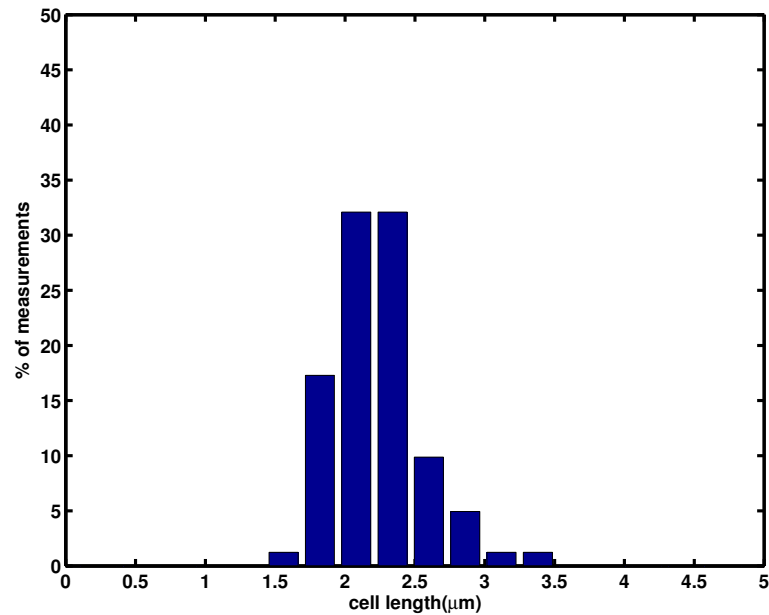


Figure 2.12 – The distribution of cell length of wild type newborn cells. 81 cells were measured. The new born length is $2.2\mu m \pm 0.31\mu m$.

2.4 Results of model 1

In model 1, we took the parameters of individual cell growth and division as input for the simulation and tried to capture the properties of the whole cell culture. There are several things we can look into. First, will the culture enter a steady state and how will it do that? Second, how does the culture look like then? Third, how do the dynamic processes look like? These questions also tell us how to compare the simulation with experimental data.

To see if our model is able to capture the growth dynamics of the *minB*⁻ cells, we performed a series of experiments where we measured the time-dependent fraction of cells in a growing population having zero to four chromosome clusters (the fraction of cells which contain more chromosome clusters is too small for reliable statistics).

In the experiments we can follow the growth dynamics only for about 200 minutes since after ~ 3 -4 doubling times the agar plates become too crowded. In the experiment of WT cells, as a consequence the restriction of the movement of the cells, cells become visibly shorter.

These measured data were compared with the simulation of model 1. To have a meaningful comparison with the experimental data we started simulations with a number of cells that is

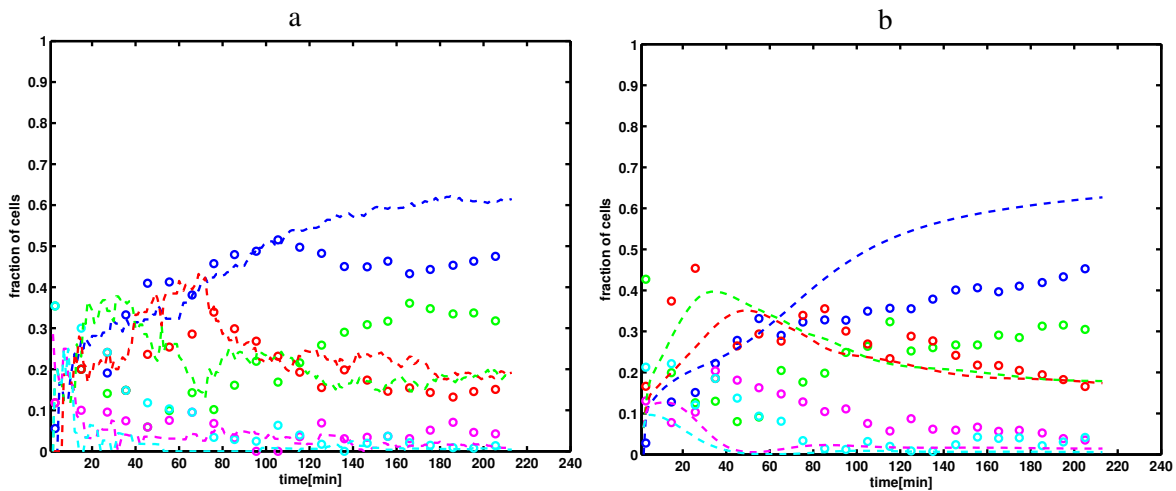


Figure 2.13 – Time dependence of the fraction of cells with zero to four chromosomes. (a). In the experiments (dots) and in the simulations (dashed lines) we start with 7 cells and determine the composition of the growing population. Cells without chromosome (mini cells) are shown in blue, cells with one chromosome in green, with two chromosomes in red, with three chromosomes in magenta and with four chromosomes in cyan. (b) Shows the comparison between the experimental data and calculated data obtained from averaging 50 simulations each one starting with 1000 cells.

comparable with the experimental one (about 7 cells).

To our surprise we were not able to achieve a good agreement between simulations and experiments. The best result we could achieve by adjusting the initial conditions is shown in Fig.2.13a. As one can see there are significant differences between predicted and observed data for all fractions of the populations.

We also tested if the differences could be caused by the fact that the experimental data is obtained by averaging over 2 times experiments. But even in this case the differences are larger than the standard deviations, see Fig.2.14.

A very apparent difference is that the simulation produces too many mini cells compare to the experiment. The differences even remain if we average over many simulations, see Fig.2.13b.

But the results of simulation are not totally wrong, because they still show that the fractions of cells containing more chromosome clusters are smaller, and the whole culture enters steady state after about 200 minutes. So the disagreements between simulation and experiment can be fixed.

To find the origin of these differences, we next tested if our model is able to reproduce the

2. RESULTS

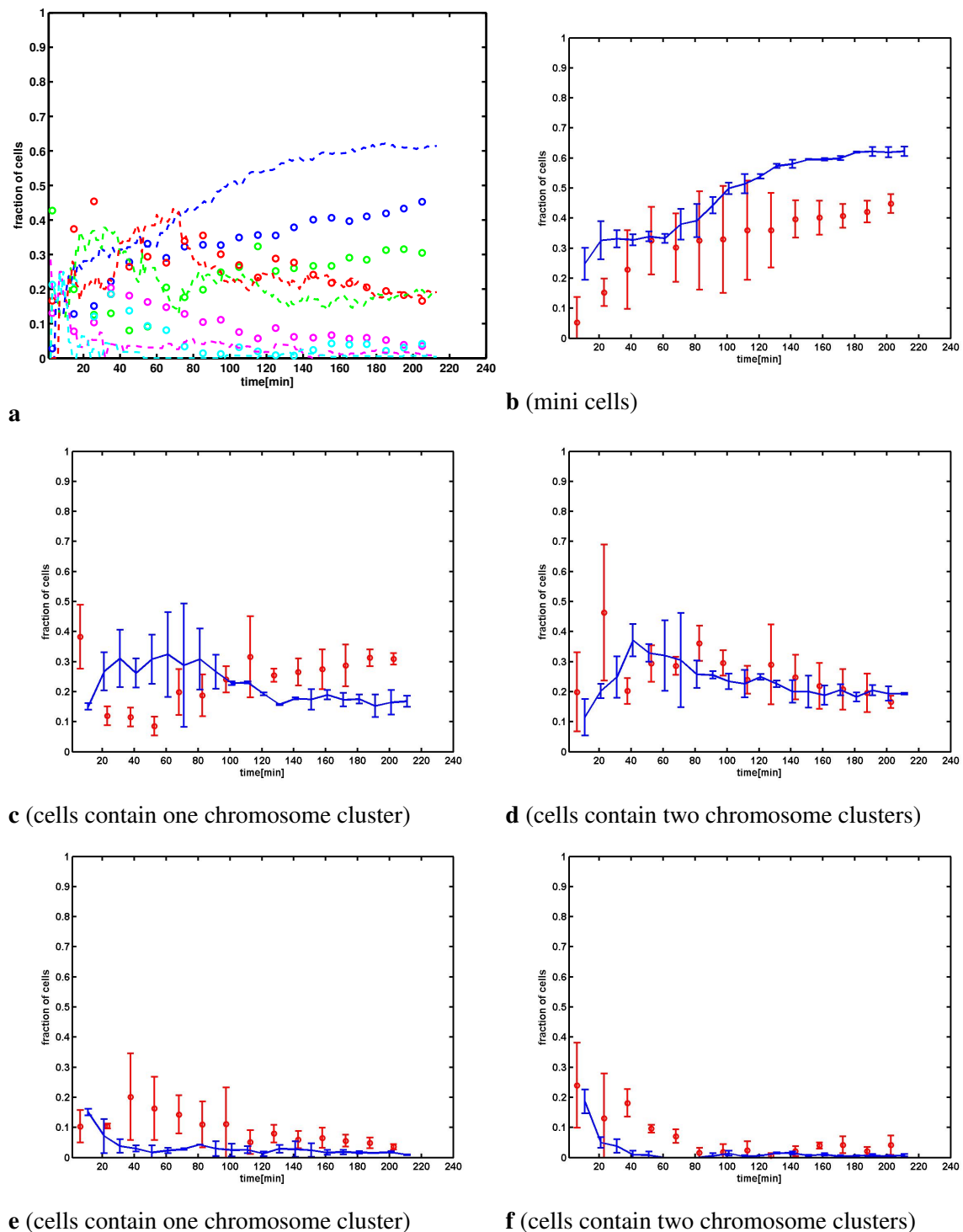


Figure 2.14 – The time dependence of the fraction of cells. (a) is the same as Fig.2.13, but data are obtained by averaging over two simulations respectively two experimental populations. The standard deviations are also shown with error bars. (b) - (f) show the curves separately. In these five figures we show the time dependence of the fraction of different types of cell separately, the simulation (blue) starts with 7 cells and repeat two times, like the experiment (red).

size distribution of cells. In Fig.2.13b, the culture enters steady state in the end. In order to classify cells into different groups, only the number of chromosome clusters has been counted, but the information about the stage of each compartment has not been include in Fig.2.13 and Fig.2.14. By checking the cell length distribution of the culture, we can see the state of the culture more detailed. Of course the length distribution cannot reveal everything, for example, it is possible that a cell containing three new formed compartments is shorter than a cell containing two compartments which are going to divide. But combining the length distribution with the results from Fig.2.13 can give us a complete picture about the state of the culture.

To compare the length distribution in a better way, we measured the distribution of cell lengths of a growing population with 7 initial cells. Fig.2.15a and Fig.2.15b shows the corresponding histogram. Similar results were obtained for the simulations with a different number of initial cells (Fig.2.15a and 2.15b).

As one can see that the calculated distribution (red line) fits the experimental data (blue histogram) only for small cells with lengths below $4\mu m$. The significance of the differences becomes even more apparent by cumulating the distribution of cell lengths (that smoothens out the effects arising from the discrete nature of the data), see Fig.2.15b. This plot also shows that deviations between experiment and simulation occur for cells larger than $4\mu m$.

In Fig.2.15c and Fig.2.15d, we show the average results over 50 simulations and the average results over two experiments for $minB^-$ cultures. The results show even clearer that the simulation results lack filamentous cells. Thus, compared with the experimental system the simulation produces too few filamentous cells. This might indicate that in simulation cells divide too often at non-polar sites.

This would be a significant difference between model and experiment concerning cell division. The over abundance of cell division at non-polar sites could be due to the preference of cell division at non-polar sites, or due to the faster rate of cell division at non-polar site. To analyze if timing or positioning of cell division is the origin of this difference we analyzed the cell division history of individual cells. We measured the spatial positions of two successive division events and the time interval between these two events. To do this in a quantitative way we classified the first division event as being polar or non-polar. The second division event of

2. RESULTS

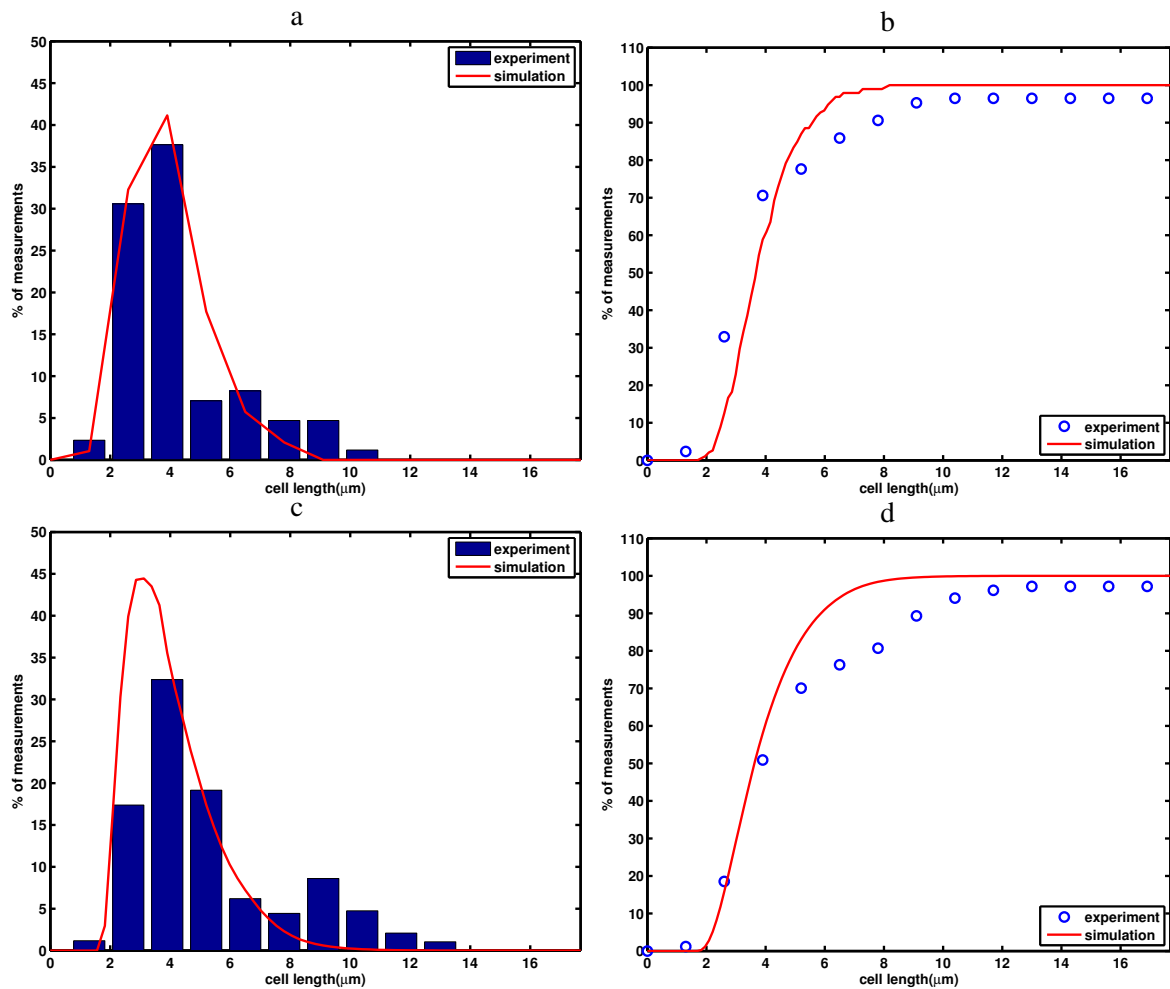


Figure 2.15 – Cell length distribution of a growing population. Cell length distributions (a and c) and cumulative distributions of cell lengths b and d) as obtained experimentally (blue circles) and calculated from the simulations of model 1 (solid red curves). In (a) and (b) the simulations started with 7 cells, in (c) and (d) with 1000 cells. The histogram was obtained at fixed time (213 minutes after start). In the experiment 238 cells were present at that time, out of these 105 mini cells that were not taken into account.

the daughter cells was then classified as being either polar (and division occurs at the old or new pole) or non-polar. Simultaneously we measured the time difference between the two division events. By checking the division history in this way, we can also check if cell divisions at different position in one cell are totally independent as we assumed in model 1.

Table.2.2 summarizes our findings. As one can see the standard deviations of the time between two division events is comparable to the mean, indicating a strong cell to cell variation. This can also be seen from Fig.2.16 where we show the distribution of individual interdivision times for the five different division types.

These results now allow a detailed comparison between experiment and simulations. As can be seen from Table.2.2, in the experiments the chance of the next division occurring at a non-polar site is about 50% no matter if the previous division occurred at a polar or a non-polar site. This is different to the predictions of model 1 where the probability for a non-polar division is very low if the previous division took place at a non-polar site.

This is also in agreement with the above finding that the fraction of mini cells is too high in the simulations, see Fig.2.13. From Table.2.2, we can see that we got more mini cells in the simulation because the fraction of polar divisions in simulation is higher than it is in the experiments. Considering that we set the polar division waiting time according to the experimental data, we thought that the preference of polar division is mainly due to higher ratio of polar sites to all division sites, which means there are too many short cells. This is again in agreement with the above finding that the simulations result in a fraction of filamentous cells which is too small. Furthermore, model 1 predicts a too short interval division time after a non-polar division (Table.2.2).

	%	old pole	non-polar	new pole
Experiment	polar	3(41.2 ± 21.3min)	17(37 ± 21.9min)	13(22.8 ± 19.4min)
Experiment	non-polar	31(31.0 ± 18.4min)	36(39.1 ± 22.3min)	
Simulation	polar	6(35.1 ± 21.2min)	21(29.9 ± 21.8min)	20(24.2 ± 19.4min)
Simulation	non-polar	38(21.9 ± 18.2min)	15(23.3 ± 21.7min)	

Table 2.2 – Cell division history of individual cells as obtained experimentally and from model 1. All cell divisions within ~ 200 minutes are classified into 5 types according to the position of two successive cell divisions. Rows represent the location of the first division event, columns location of the second event. Time in parenthesis represents mean time difference ± standard deviation between the division events.

We ran the simulations under the assumption that cell divisions at different position in one cell are totally independent, but the simulation results for division histories differ quite a bit from the experimental data, which indicates that the polar and non-polar sites are not totally independent.

The shorter interval division time between two non-polar divisions indicates that there might be some timing problem in our model for non-polar divisions. Since the chromosome duplication rate and division waiting time after chromosome segregation are all set by fitting

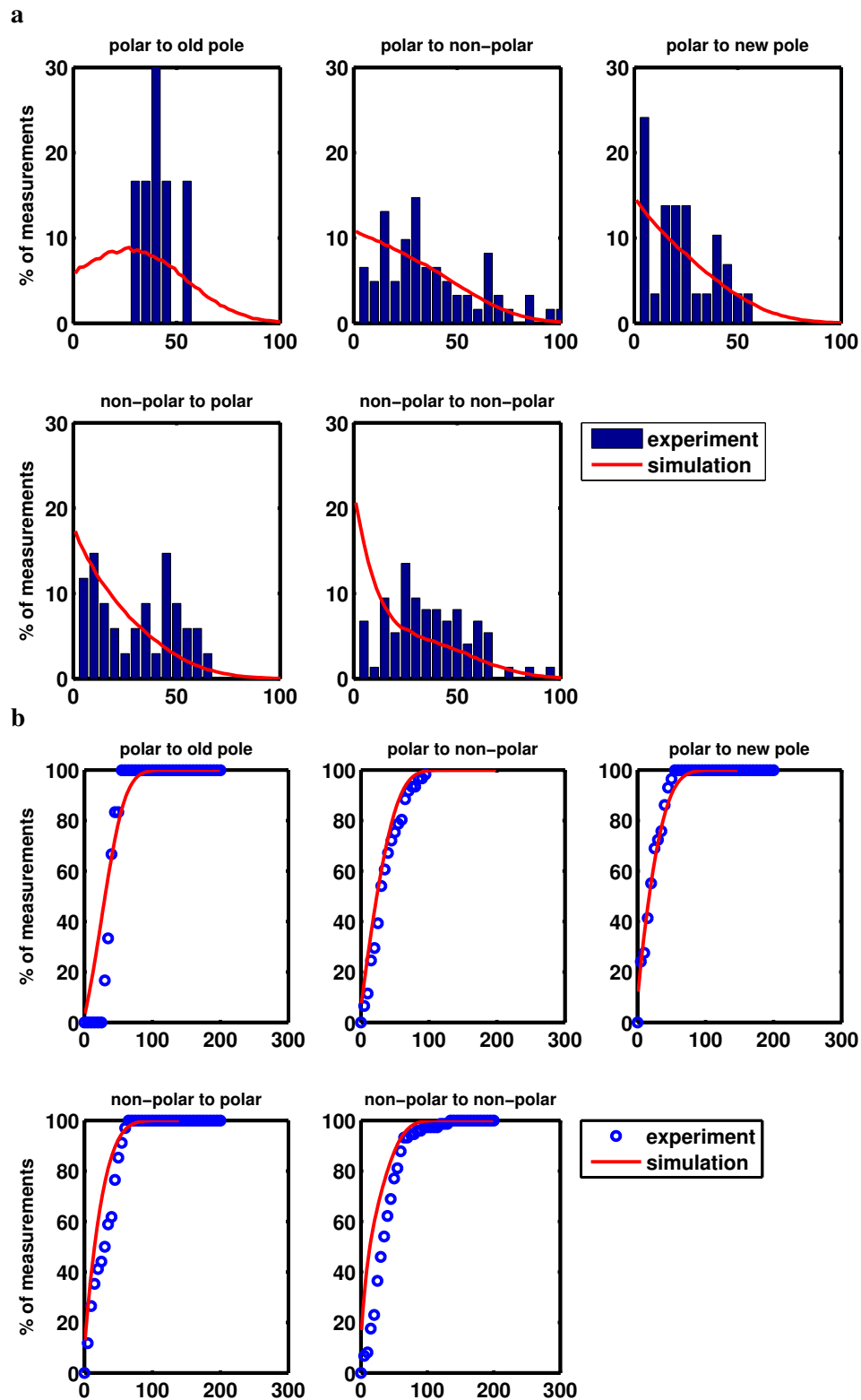


Figure 2.16 – The distribution (a) and cumulative distribution (b) of inter-division time of different types of cell division. The cell divisions are classified into 5 types according to the position of two successive cell divisions. The rows represent the location type of the first cell divisions. The columns represent the location type of the second cell divisions. All the X-axis are time (minute).

experimental data, there must be some systematic process we missed in our model 1.

To conclude, model 1 that is based solely on the experimentally measured waiting time distribution fails to explain the observations in many points. In particular, the simulations yield too few filamentous cells and too many mini cells, indicating that model 1 lacks essential information on where division occurs, information that is not contained in the measured division waiting times that is the basis of model 1. This is also supported by the finding that our model predicts a wrong fraction of two subsequent non-polar divisions. However, these problems could be solved and model 1 is still a good platform for further improvement of our theoretical work.

2.5 Model 1P

In model 1, we tried to establish a platform on which we can continue working to test our hypothesis. As a candidate of a possible platform, a model where cell division events are treated as Poisson distribution events was tested as well.

In this model, the simulation of cell growth and chromosome duplication is the same as in model 1, the only difference is the division waiting time. In model 1, after chromosome duplication, a division waiting time is distributed to the new division site between the two new segregated chromosomes. This gives a trend that older division sites will complete a cell division earlier than newer sites.

In model 1P, the program distributes random numbers to each division site, and the ones getting a number bigger than a certain threshold will divide. This makes an essential difference to model 1, since new and old division sites are not distinguishable. In model 1P, we do not need to take the division waiting distribution as an input, instead, we need to find a good value for the threshold parameter (λ). Since it is not so easy to extract this parameter from the experimental data directly, we used trial and error and ended up using $\lambda = 0.005$. We checked the properties of the simulation culture of model 1P (shown in Fig.2.17 to 2.20, including Table.2.3) as we did for model 1. Because in this model, the distribution of division waiting time was not taken as input, we also checked if we can reproduce these distributions (shown

2. RESULTS

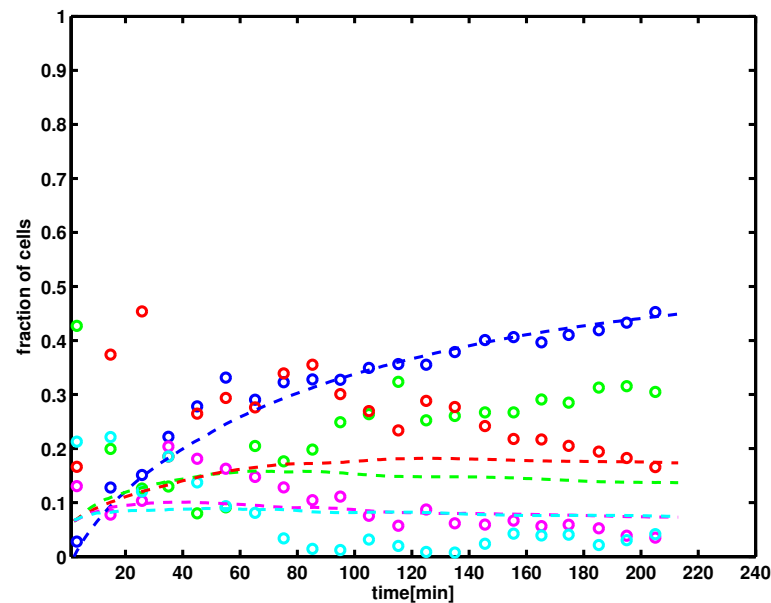


Figure 2.17 – The time dependence of the fraction of cells. In this figure, we averaged the results of 50 simulations, each one starts with 1000 cells. Circles represent experimental data, dashed lines the results of our model. Cells without chromosome (mini cells) are shown in blue, cells with one chromosome in green, with two chromosomes in red, with three chromosomes in magenta and with four chromosomes in cyan.

in Fig.2.19).

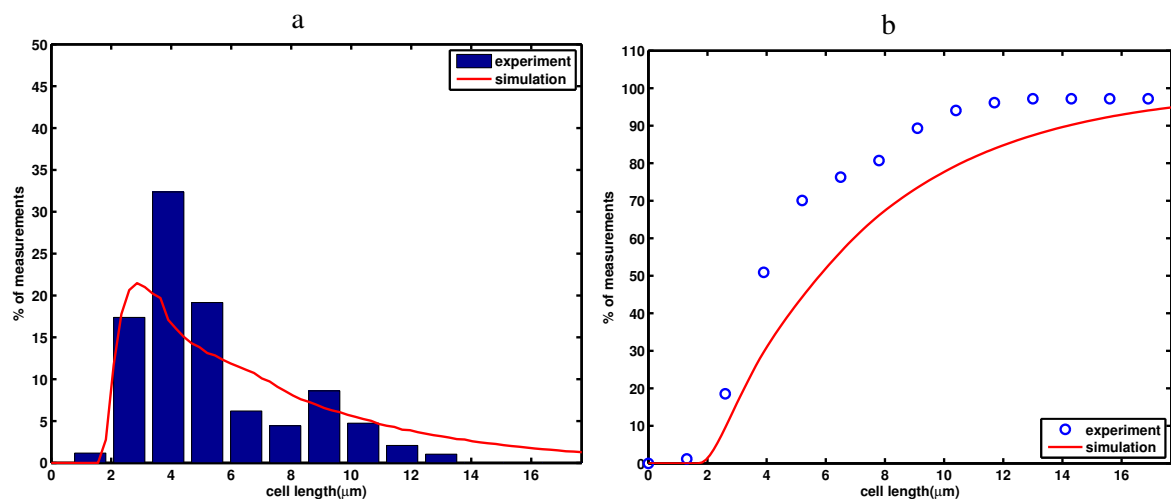


Figure 2.18 – The cell length distribution (the red curves are simulation results, the blue circles or bars are experimental data). (a). The cumulative cell length distribution. It shows the percentage of cells which are shorter than different values. (b). The cell length distribution. It shows the distribution of cells in different length range. 133 cells were measured when the time is 213 minute. Mini cells are not included. 105 mini cells on total were not taken into account.

From Fig.2.17, we can see that the composition of the simulation culture seems to fit a

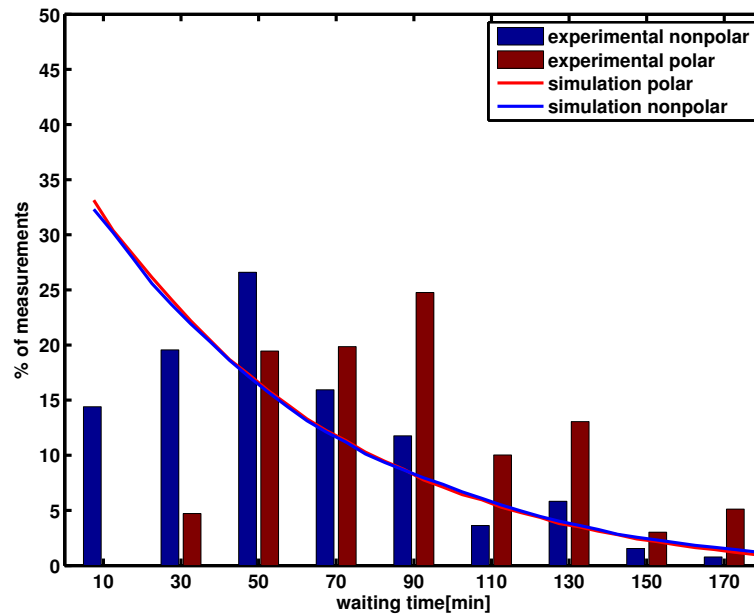


Figure 2.19 – The waiting time distribution of $minB^-$ for polar and non-polar sites. The curves are from simulation and the bars are experimental data (red: polar sites; blue: non-polar sites). The X-axis is the time measured in minutes.

little better than that from model 1. The curve of fraction of mini cells fits the experimental data very well, and the curves for multi-chromosome cluster cells are also improved. But one can see that the simulation cell length distribution gets much worse, especially the cumulative distribution of cell length, as shown in Fig.2.18a.

However, the problem shown in Fig.2.19 is even more serious. There are two problems for the distribution of simulation division waiting time. First, the distributions of division waiting times for polar and non-polar are equal. Second, the simulation curves are decreasing monotonously. There are some ways to solve the first problem (as explained below in detail for model 2), but the monotonic decreasing of the curves cannot be changed because it is an intrinsic property of the poisson process.

The division history shown in Table.2.3 and Fig.2.20 looks good. But if we compare the fraction of polar divisions followed by another polar division, we see an essential difference between model 1P and the experimental data. In the experiment, after one polar division, the probability of the next division happening at the other cell pole is higher than the probability of it happening at the same pole. This shows that the cell division is a history-dependent event. But the simulation results are different. There is no difference in division probability between

the older and the newer cell pole. This means, that in model 1P the old division sites and new appeared division sites are treated equally, and their formation histories do not matter at all. This divergence between model and experiment cannot be solved either.

These essential problems of model 1P show that it is not a good candidate for further research. The Poisson process cannot describe cell division very realistically, and the problems cannot be solved by improving this model or using different parameters while keeping the basic principle. So we will further improve model 1 and use it as a base for further study.

	%	old pole	non-polar	new pole
Experiment	polar	3($41.2 \pm 21.3min$)	17($37 \pm 21.9min$)	13($22.8 \pm 19.4min$)
Experiment	non-polar	31($31.0 \pm 18.4min$)	36($39.1 \pm 22.3min$)	
Simulation	polar	6($26.8 \pm 24.1min$)	16($29.3 \pm 26.6min$)	6($26.1 \pm 23.9min$)
Simulation	non-polar	33($27.9 \pm 25.5min$)	38($30.7 \pm 28.4min$)	

Table 2.3 – Cell division history of individual cells as obtained experimentally and from model 1P. All cell divisions within about 200 minutes are classified into 5 types according to the position of two successive cell divisions. Rows represent the location of the first division event, columns location of the second event. Time in parenthesis represents mean time difference \pm standard deviation between the division events.

2.6 Model 2 and model 3

As we talked above, there are some major details missing in model 1, and this lack results in the production of too many shorter and mini cells. We checked the original microscopy phase and fluorescent images for *minB*⁻ cells, and found some chromosome clusters being larger than others, as shown in Fig.2.21. After a while, these longer chromosome cluster go through a symmetrical or an asymmetrical segregation.

We interpret this situation as the disturbance of chromosome segregation [52, 107, 108]. To get an overview of the disturbance of chromosome segregation, we established a visualization, which we called division map, as shown in Fig.2.22 visualizing cell divisions and chromosome segregations. In those figures, we can follow the cell division and chromosome segregation history, and see how the cells get longer or shorter.

To make sure that missing this phenomenon is really serious in model 1, we analyzed the

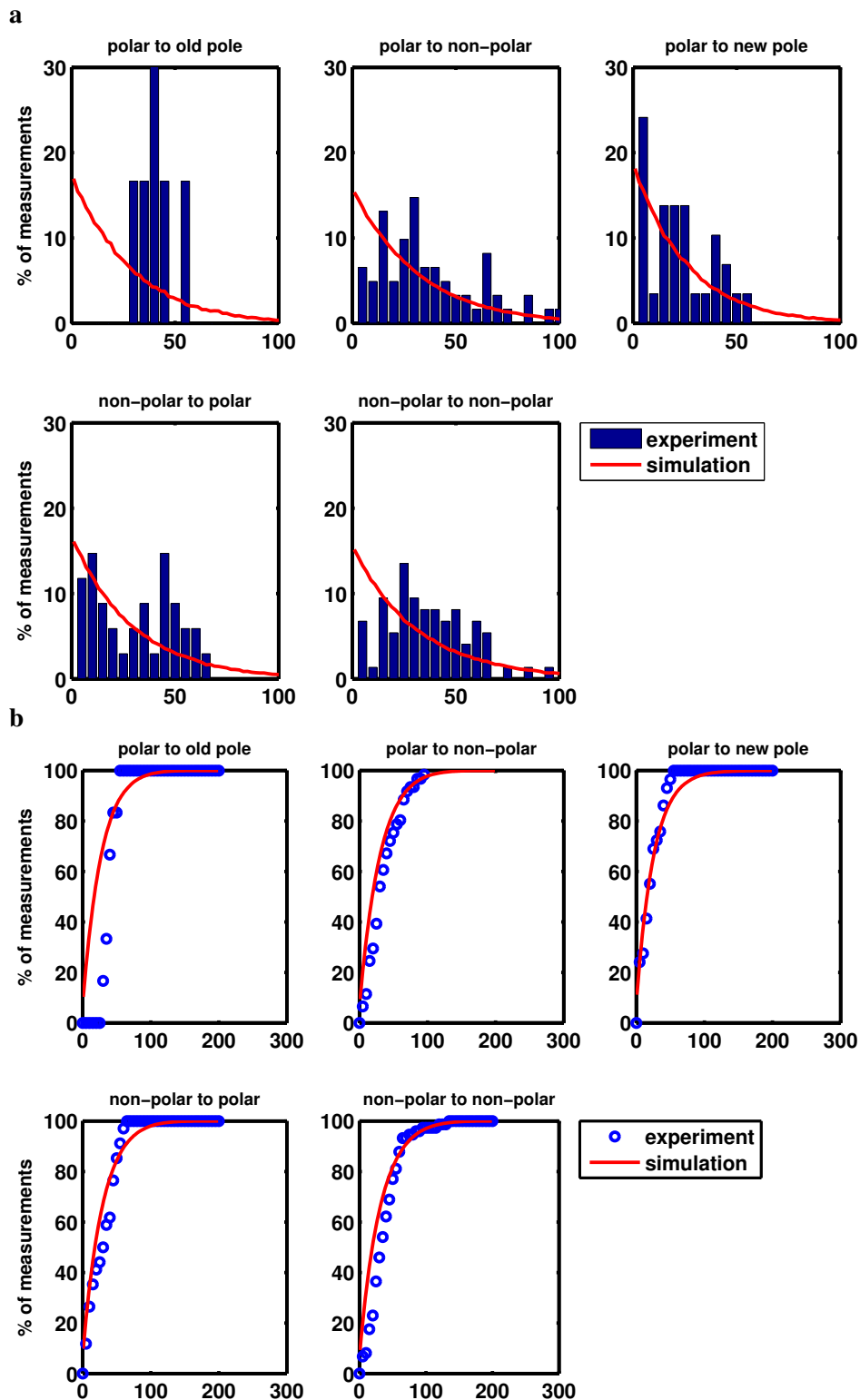
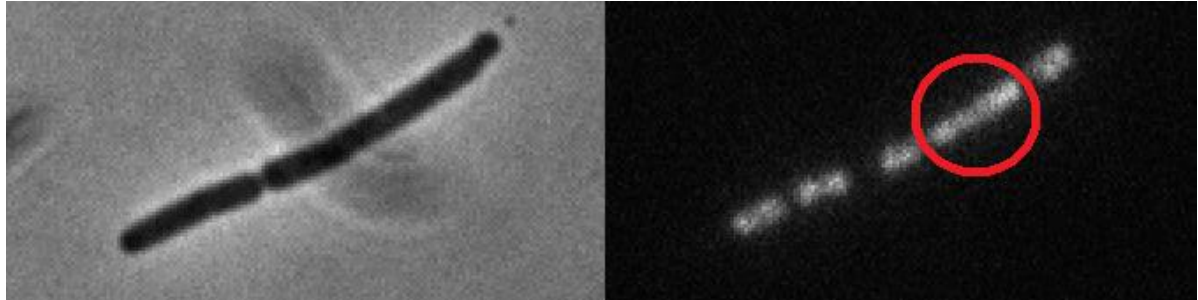


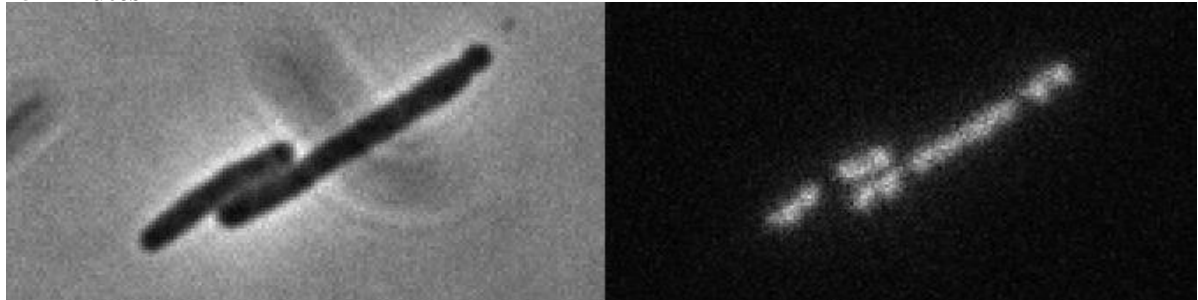
Figure 2.20 – The distribution (a) and cumulative distribution (b) of inter-division time of different types of cell division. The cell divisions are classified into 5 types according to the position of two successive cell divisions. The rows represent the location type of the first cell divisions. The columns represent the location type of the second cell divisions. All the X-axis are time (minute).

2. RESULTS

0 minute



15 minutes



30 minutes

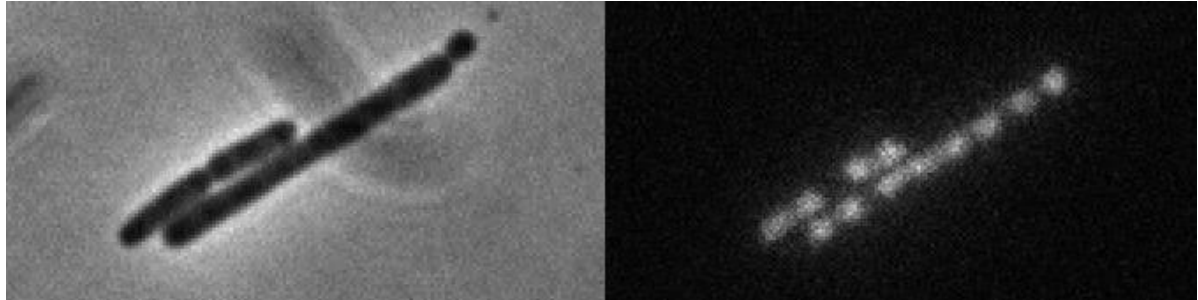


Figure 2.21 – The disturbance of chromosome segregation. The left column: The phase image shows one filamentous cell just divided into two cells; the right column: the fluorescent image shows that in the shorter daughter cell, there are two chromosome clusters, the gap between them is very clear, and from the photo we can see that the two chromosomes are also going to segregate. There are three clusters in the longer daughter cell at $t=0$ min, and the middle one (in the red circle) is apparently longer than the other two, it is even much longer than the two clusters in the shorter daughter cell, which are going to segregate. And after about half an hour, it segregate at the quarter position. This indicates the disturbance of chromosome segregation.

number of division sites per cell length in the growing population. Fig.2.23 shows the time-dependence of this quantity as experimentally observed and as calculated from the simulations of model 1. As one can see there is significant difference between the two curves, showing that in the experiments a smaller number of division sites are available. Thus in the experiments it takes longer until a potential division site becomes available, indicating that in the $minB^-$ cell chromosome segregation is less efficient.

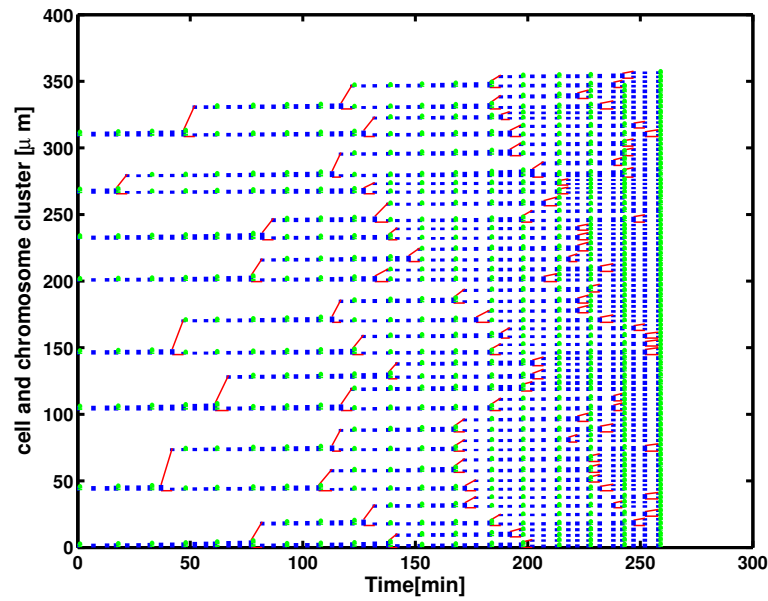


Figure 2.22 – The division map for experiment culture. the blue bars are cells, green bars are chromosome clusters, the length of the bars represents the sizes of the cells or chromosome clusters. The red lines show the division history.

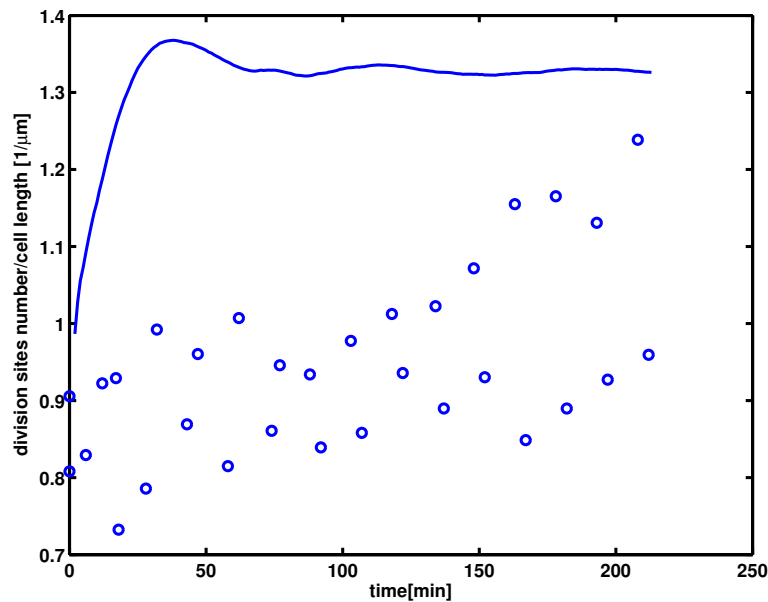


Figure 2.23 – Time dependence of the number of division sites per cell length. Dots represent experimental data obtained by averaging over all cells in the culture at that moment. The solid curve is the prediction of model 1.

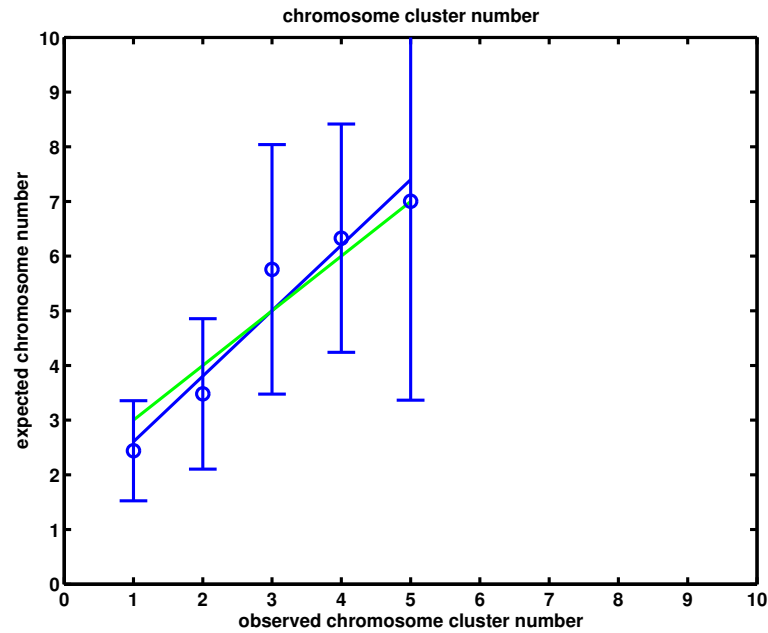


Figure 2.24 – The expected and observed number of chromosome cluster. The y-axis is the expected number of chromosome clusters n_{exp} for a cell of Length L (with $n_{exp} = L/L_C$, where $L_C = 1812nm$ is the length of a single chromosome). The x-axis is the experimentally observed chromosome cluster number. Experimental data were obtained by averaging 133 cells for 212 min. The green line represents the line we are using in the simulation for estimating the blocking sites number. Its slope is one, and it results in $r = 2$.

To quantify this effect, we calculated the number n_{exp} of chromosome clusters that we expect for a cell of Length L (with $n_{exp} = L/L_C$, where $L_C = 1812 nm$ is the length of a single chromosome) and compared this with the experimentally observed chromosome cluster number, see Fig.2.24. As one can see, this figure clearly shows that the $minB^-$ cells have a chromosome segregation problem that is missing in model 1. We fit a straight line to the data points in Fig.2.24, and get a slope of about one. This means that the disturbance of chromosome segregation does not strongly depend on cell length or chromosome number.

To take this effect into account we developed a novel model (model 2). Model 2 extends model 1 by including the chromosome segregation problem of the $minB^-$ strain. Thus, model 2 also includes the experimentally observed waiting time for polar and non-polar sites.

To implement the segregation problem we blocked (on average in each cell) r randomly picked potential division sites (Fig.2.24 suggests $r = 2$) and in the following we show the data for this case. During the simulation, random numbers are distributed to potential division sites and those ones with numbers smaller than a certain threshold are transformed into blocked

sites. The site which is blocked is also the place where the chromosome does not segregate successfully, as shown in Fig.2.25a.

All the sites are treated equally, including the polar sites. But there is not chromosome segregation at cell poles, so we interpreted the block of a polar site as shown in Fig.2.25b. For some reason, cell do not start building septums at all poles immediately after they appeared, and those poles without septum being built are those which are blocked.

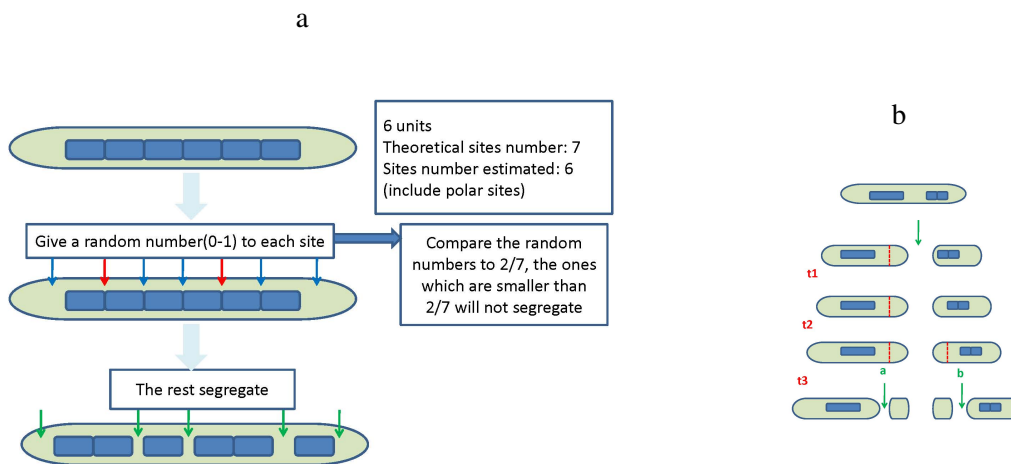


Figure 2.25 – The blocking potential division sites. (a) shows how the program selects the blocking sites. (b) shows the interpretation for the blocked polar site. The red dash line represents the on building division septum. Although cell pole a and b appeared at the same time and have the same division waiting time, they did not start septum building at the same time, so the polar site b was blocked in the beginning.

The results of model 2 are shown in the similar way as for model 1 and model 1P. From Fig.2.26 to Fig.2.29, including Table.2.4, the simulation results for *minB*⁻ culture are compared to the experimental data. As one can see, model 2 is in good agreement with some of the experimental data, it only fails to reproduce the division waiting time distribution of the polar sites (or agrees less with the waiting distribution of the non-polar sites, as shown in Fig.2.28). This is quite surprising given the fact that model 2 is based on this distribution. Evidently the eventual blockage of the polar division site (because of the segregation problem) leads to too long waiting times of the polar division sites. This observation lead us to speculate that the different waiting time distributions of the polar division sites are not an a priori property of the polar sites but rather an emerging property. To test this idea, we developed model 3 that is

identical to model 2 except that the division waiting time of the polar sites is now drawn from the experimentally observed division waiting time distribution of the non-polar division sites.

One should note that, according to our definition of the division waiting time for polar sites, we still start counting the division waiting time when the cell pole is formed, in both simulation and experiment.

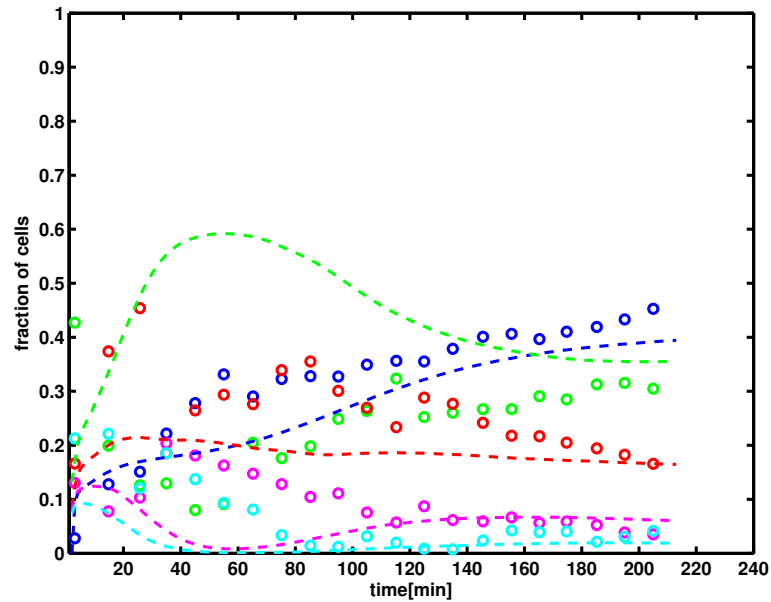


Figure 2.26 – The time dependence of the fraction of cells. In this figure, we averaged the results of 50 simulations, each one starts with 1000 cells. Circles represent experimental data, dashed lines the results of our model. Cells without chromosome (mini cells) are shown in blue, cells with one chromosome in green, with two chromosomes in red, with three chromosomes in magenta and with four chromosomes in cyan.

	%	old pole	non-polar	new pole
Experiment	polar	3(41.2 ± 21.3min)	17(37 ± 21.9min)	13(22.8 ± 19.4min)
Experiment	non-polar	31(31.0 ± 18.4min)	36(39.1 ± 22.3min)	
Simulation	polar	2(55.2 ± 32.3min)	19(48.1 ± 38.3min)	6(30.4 ± 31.2min)
Simulation	non-polar	33(39.8 ± 28.5min)	40(36.2 ± 39.3min)	

Table 2.4 – Cell division history of individual cells as obtained experimentally and from model 2. All cell divisions within ~ 200 minutes are classified into 5 types according to the position of two successive cell divisions. Rows represent the location of the first division event, columns location of the second event. Time in parenthesis represents mean time difference ± standard deviation between the division events.

The results of model 3 are shown from Fig.2.30 to Fig.2.33, including Table.2.5. As one

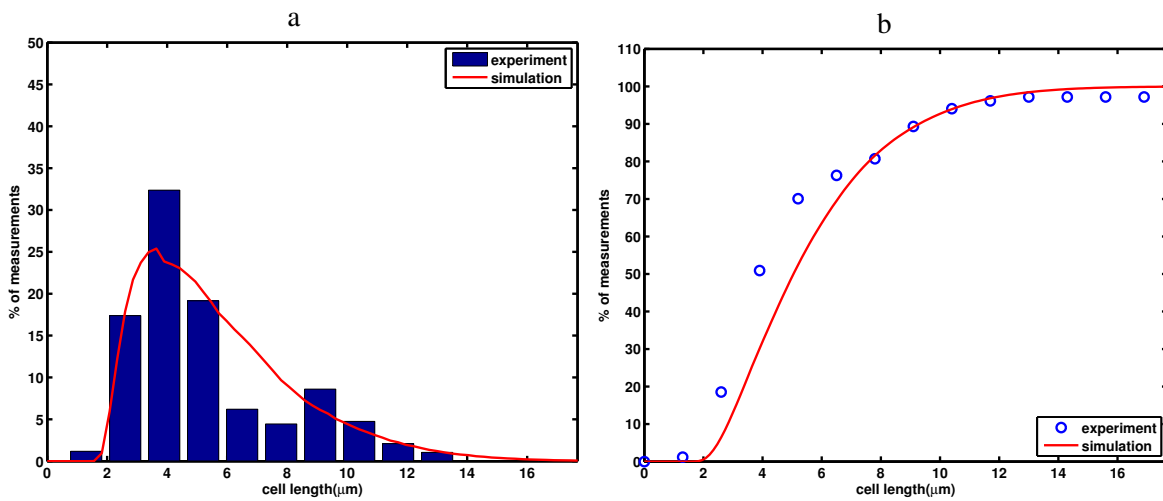


Figure 2.27 – The cell length distribution (the red curves are simulation results, the blue circles or bars are experimental data). (a). The cumulative cell length distribution. It shows the percentage of cells which are shorter than different values. (b). The cell length distribution. It shows the distribution of cells in different length range. 133 cells were measured when the time is 213 minute. Mini cells are not included. 105 mini cells on total were not taken into account.

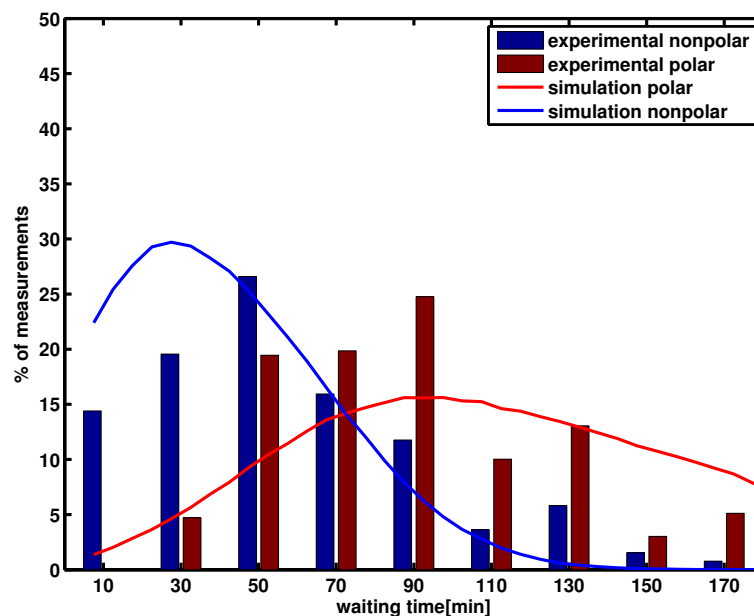


Figure 2.28 – The waiting time distribution of $minB^-$ for polar and non-polar sites. The curves are from simulation and the bars are experimental data (red: polar sites; blue: non-polar sites). The X-axis is the time measured in minutes.

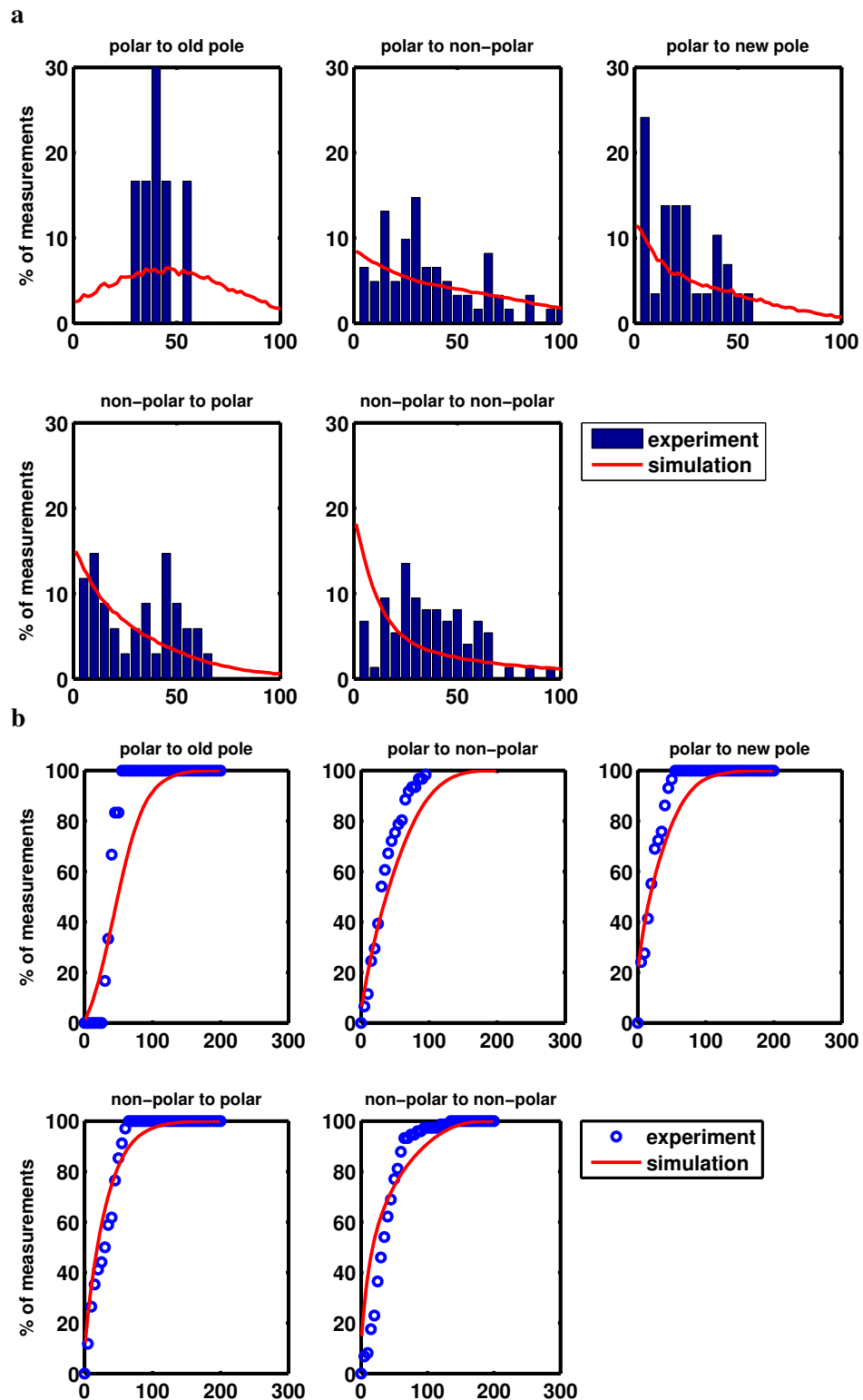


Figure 2.29 – The distribution (a) and cumulative distribution (b) of inter-division time of different types of cell division. The cell divisions are classified into 5 types according to the position of two successive cell divisions. The rows represent the location type of the first cell divisions. The columns represent the location type of the second cell divisions. All the X-axis are time (minute).

can see model 3 is as good as model 2 in reproducing the experimental data but additionally yields the correct waiting time distribution of the polar sites. In Fig.2.30, we can see that the curves of different cells in the simulation culture are in much better agreement to the experimental data than model 1 was.

The simulation does not over produce mini cells now. In Fig.2.30, the blue curve fits the experimental data very well. And although the raising parts of curves for cells with different number of chromosome clusters are still not so good, they saturate at the same values as their corresponding experimental curves after the system entered its steady state. We tried several times with different initial conditions for the simulation, and found the system always converges to the same steady state. This means the steady state of the system does not depend on the history of its development, but is a basic property of the strain in specific growth conditions.

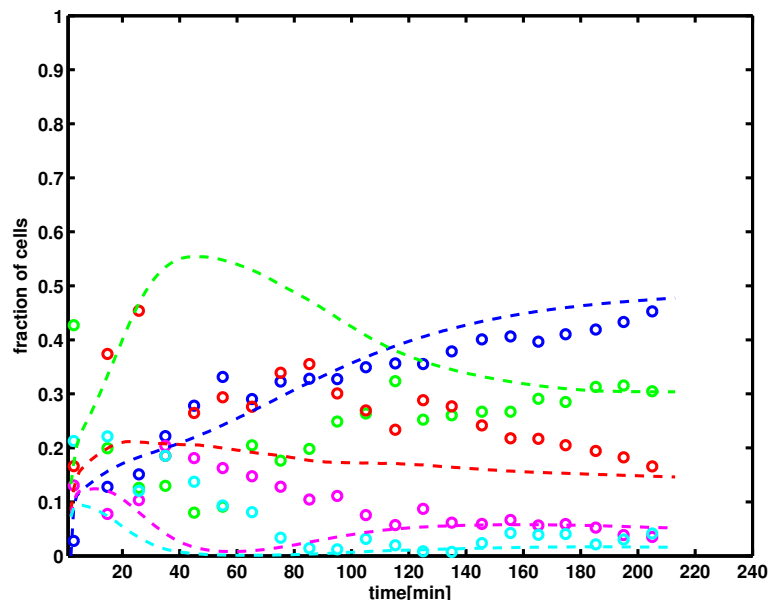


Figure 2.30 – The time dependence of the fraction of cells. In this figure, we averaged the results of 50 simulations, each one starts with 1000 cells. Circles represent experimental data, dashed lines the results of our model. Cells without chromosome (mini cells) are shown in blue, cells with one chromosome in green, with two chromosomes in red, with three chromosomes in magenta and with four chromosomes in cyan.

Fig.2.31 shows that the distribution of the simulated cell lengths has also been changed

2. RESULTS

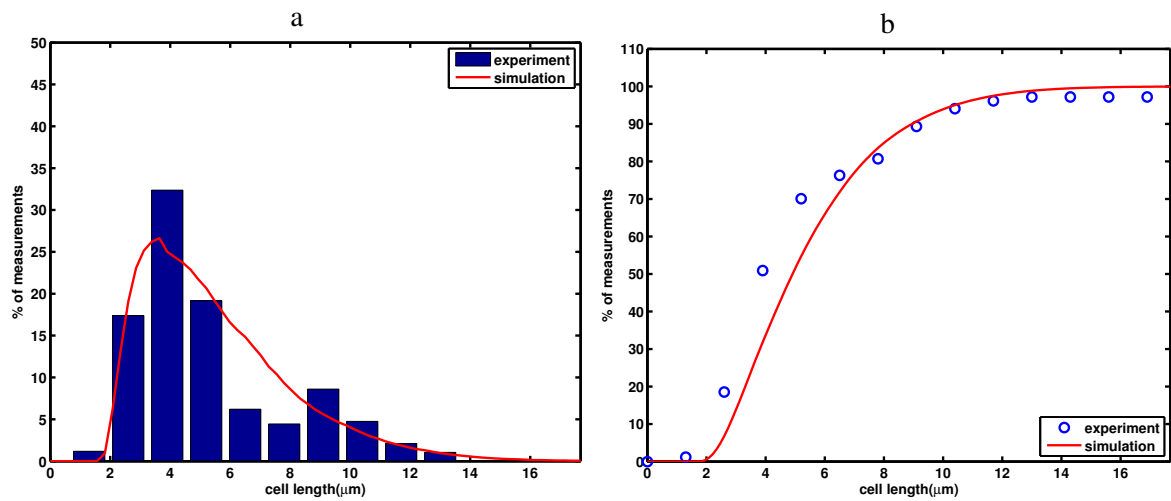


Figure 2.31 – The cell length distribution (the red curves are simulation results, the blue circles or bars are experimental data). (a). The cumulative cell length distribution. It shows the percentage of cells which are shorter than different values. (b). The cell length distribution. It shows the distribution of cells in different length range. 133 cells were measured when the time is 213 minute. Mini cells are not included. 105 mini cells on total were not taken into account.

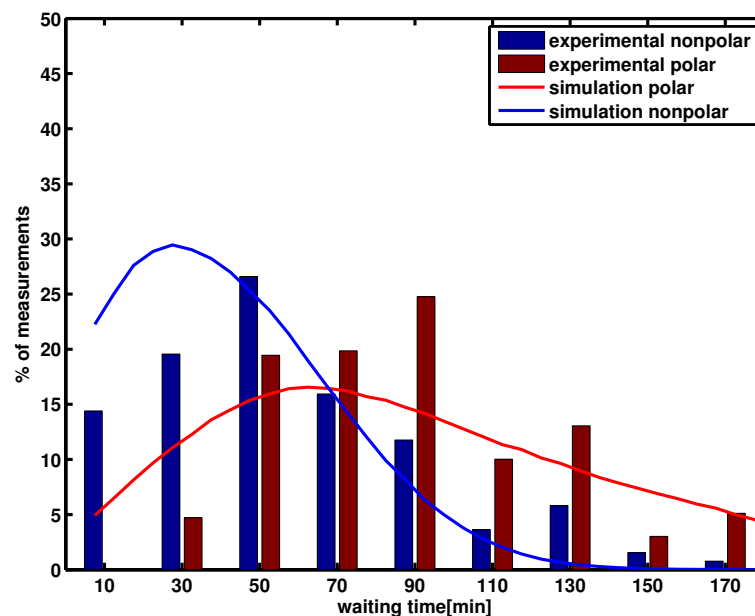


Figure 2.32 – The waiting time distribution of $minB^-$ for polar and non-polar sites. The curves are from simulation and the bars are experimental data (red: polar sites; blue: non-polar sites). The X-axis is the time measured in minutes.

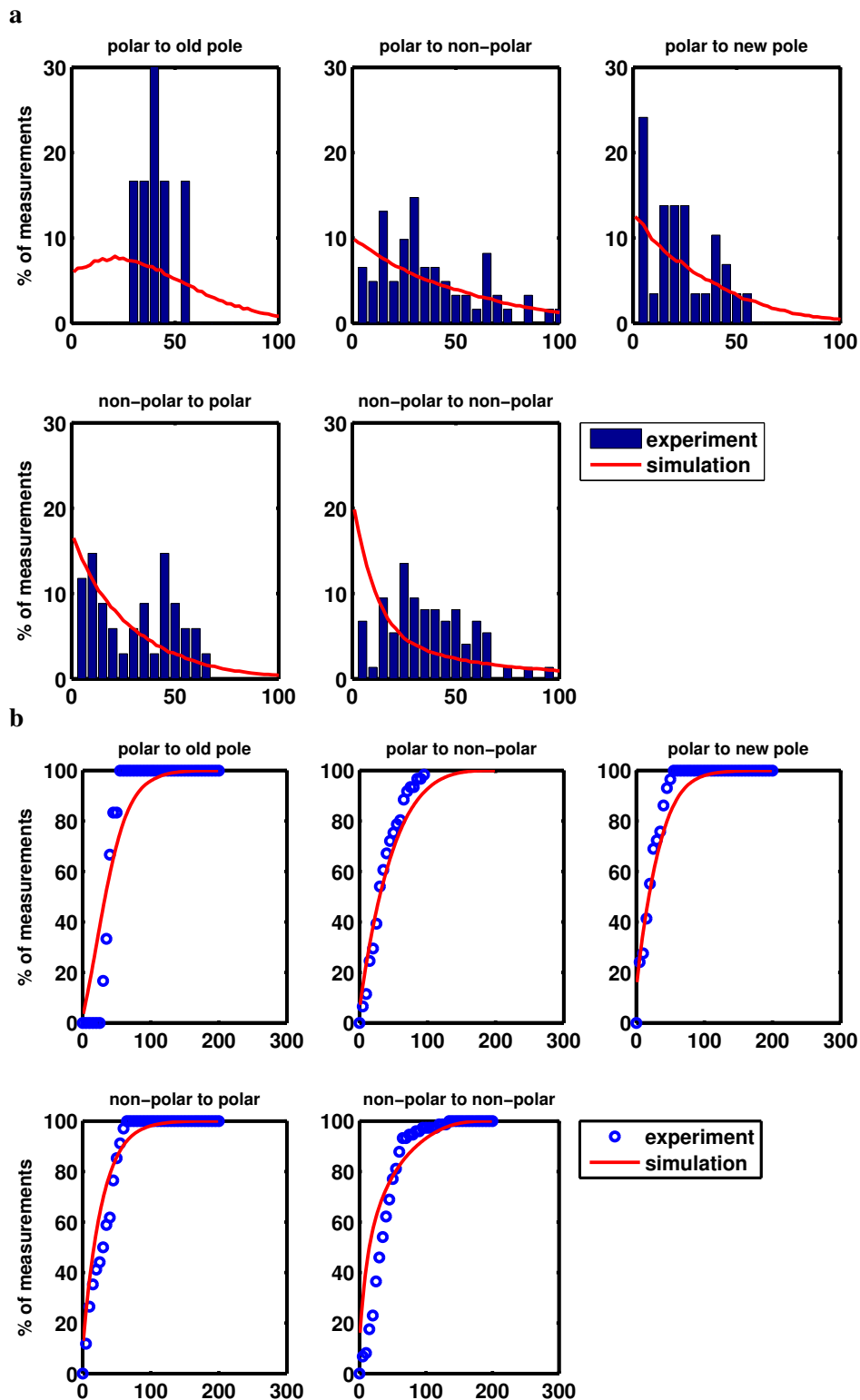


Figure 2.33 – The distribution (a) and cumulative distribution (b) of inter-division time of different types of cell division. The cell divisions are classified into 5 types according to the position of two successive cell divisions. The rows represent the location type of the first cell divisions. The columns represent the location type of the second cell divisions. All the X-axis are time (minute).

2. RESULTS

	%	old pole	non-polar	new pole
Experiment	polar	3(41.2 ± 21.3min)	17(37 ± 21.9min)	13(22.8 ± 19.4min)
Experiment	non-polar	31(31.0 ± 18.4min)	36(39.1 ± 22.3min)	
Simulation	polar	5(41.2 ± 29.3min)	20(41.5 ± 35.1min)	10(28.3 ± 26.8min)
Simulation	non-polar	35(26.8 ± 25.8min)	40(32.3 ± 36.2min)	

Table 2.5 – Cell division history of individual cells as obtained experimentally and from model 3. All cell divisions within about 200 minutes are classified into 5 types according to the position of two successive cell divisions. Rows represent the location of the first division event, columns location of the second event. Time in parenthesis represents mean time difference ± standard deviation between the division events.

compared to the results of model 1. It is consistent with the result of cell fractions shown in Fig.2.30. As we intended to, the problem caused by over abundance of cell division is solved by introducing the blocking number which represents the disturbance of chromosome segregation. At the same time, individual cell division histories obtained from model 3 are also improved. As we mentioned about model 1, corresponding to the lack of filamentous cells and overproduction of mini cells, the probability of polar division after a non-polar division is higher and the time interval between two non-polar divisions is shorter in simulation. Both of these problems are improved a lot, as shown in Table.2.5.

The distributions of simulated division waiting times also look good as shown in Fig.2.32, even when we implemented the same distribution for both polar and non-polar sites.

As we expected, model 3 solved the problem of too long polar division waiting times, which appeared in model 2. This indicates that polar and non-polar division sites are a priori equivalent for cell division. However, the polar division waiting times appear longer. To make sure that the increase in waiting time of the polar sites is not the consequence of the fact that only specific division sites are observed, we also measured the waiting time distribution of division sites close to mid cell in the simulations of model 3.

The waiting time of this site is nearly identical to that of the other non-polar sites (Fig.2.34) indicating that there is indeed something special about the polar sites. As we discussed above, this shows that the cell poles are not always able to act as division sites. For some reason, cell poles could be blocked.

Compared to model 2, which also induced blocking number to solve the problem of over abundance of cell division, the most important finding of model 3 is that there is no difference

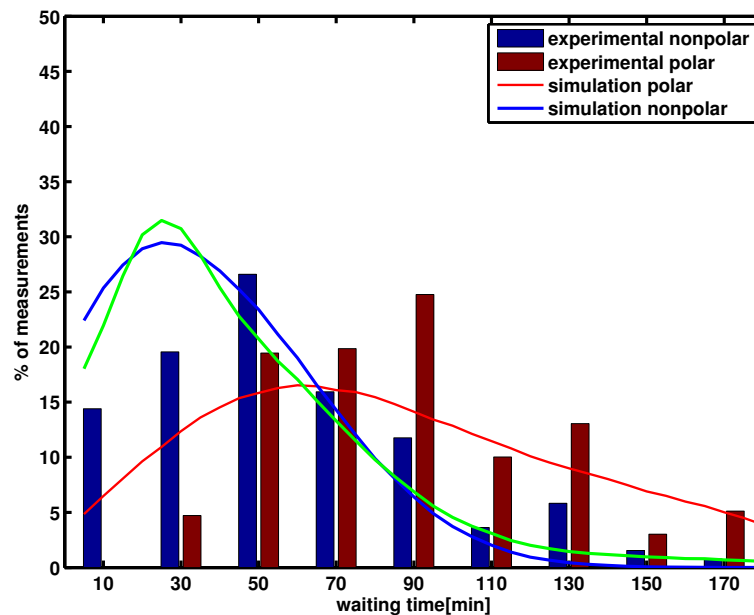


Figure 2.34 – The waiting time distribution of $minB^-$ for polar and non-polar sites. The curves are from simulation and the bars are experimental data (red: polar sites; blue: non-polar sites). The X-axis is the time measured in minutes. Here the distribution of division waiting time at the middle (or the closest to mid-cell) of cells is shown with green curve.

in division waiting times between polar and non-polar sites.

As we just speculated, this indicates that it takes the same time for polar and non-polar sites to form the division septum. Considering the importance of FtsZ for septum formation, to test this experimentally we assumed that the existence time of Z-rings at a division site is a measure for the division waiting time of the division site.

We expressed fluorescent labeled FtsZ by introducing a plasmid (originally from Beckwith's group [109]) and determined the time interval between the first appearance of the Z-ring (at a division site) and cell division at polar and non-polar sites.

Labeling FtsZ with fluorescent protein is a general method for seeing Z-ring structures in vivo [80, 110]. But because FtsZ is so important to cell division, this only works when less than half of the total amount of FtsZ in cell is labeled [80, 110]. We transformed the plasmid with FtsZ-YFP regulated by Plac into wild type and $minB^-$ strain. In order to check if the Z-ring formation is related to division waiting time, we labeled Hu with mCherry instead of GFP (see AppendixA.3). In Fig.2.35, we showed the cells, chromosome clusters and Z-ring structure under microscope with different filters. A division map with all these information is

2. RESULTS

shown in Fig.2.35 as well.

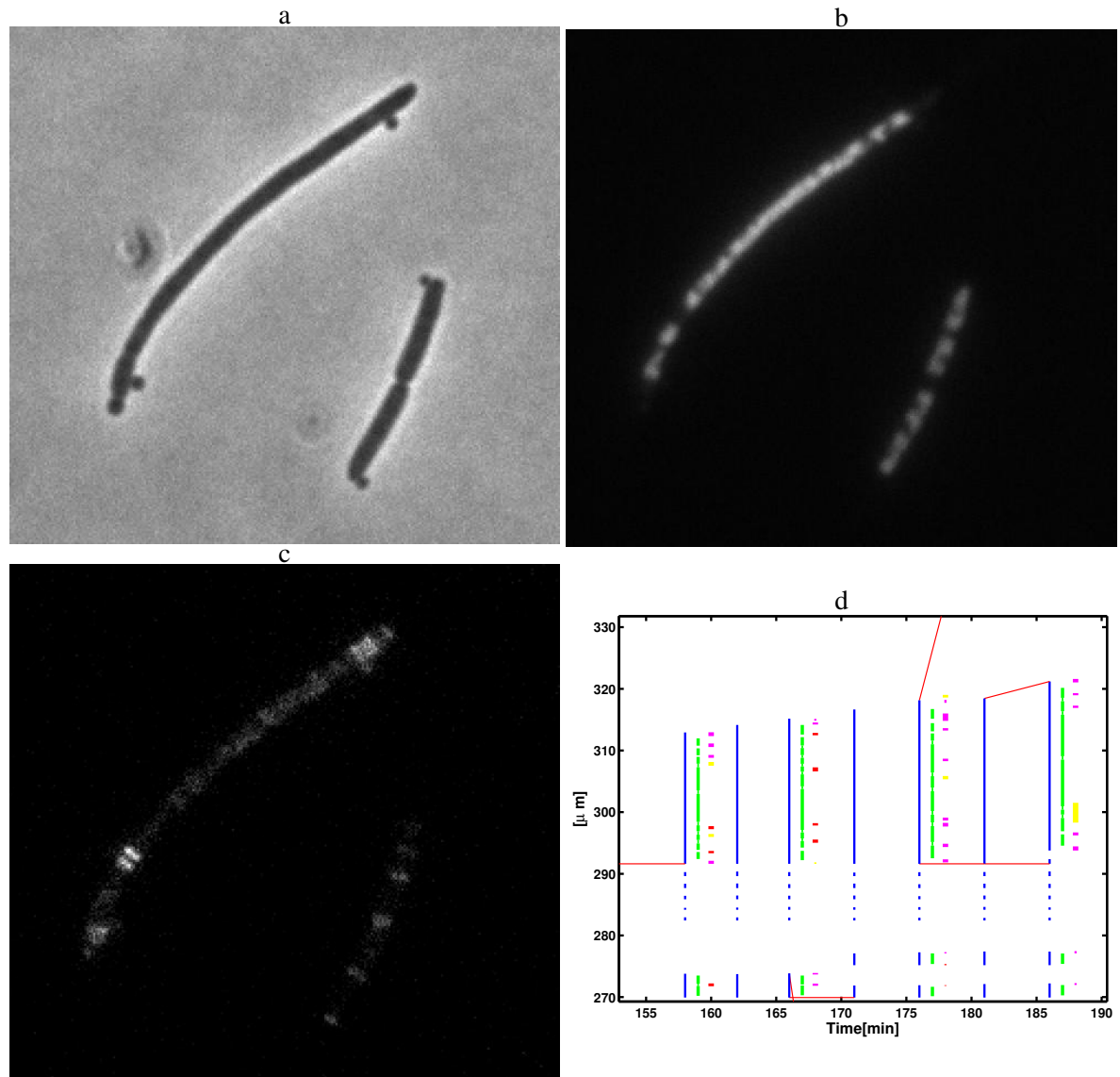


Figure 2.35 – The cell photos and the division map. Fig.2.35(a-c) show the photo of cell, chromosome clusters and Z-ring structures. Fig.2.35(d) shows part of the history about the cell division, the red short bars represent the Z-ring structures we observed in photos.

Fig.2.36a shows this time interval as a function of division waiting time of the division site. One can see that the data points for WT cells and non-polar sites of $minB^-$ cells are almost symmetrically distributed around a straight line with slope one, which means for non-polar sites, division waiting time and Z-ring existence time are comparable. But for polar sites, we can see that most data points are below that straight line, which means the Z-ring existence

time is shorter.

In order to analyze the data quantitatively, we show the cumulative distributions of division waiting times and Z-ring existence times of different strains and division sites in Fig.2.36b. We can see that for WT, those distributions of division waiting times and Z-ring existence times are close to each other and steeper than other distribution curves. The curve of polar division waiting time raises the slowest. Other distributions are in between and close to each other. This means there is a clear difference between the WT and the *minB*⁻ cells but no significant difference between polar and non-polar sites supporting the results and interpretations of model 3.

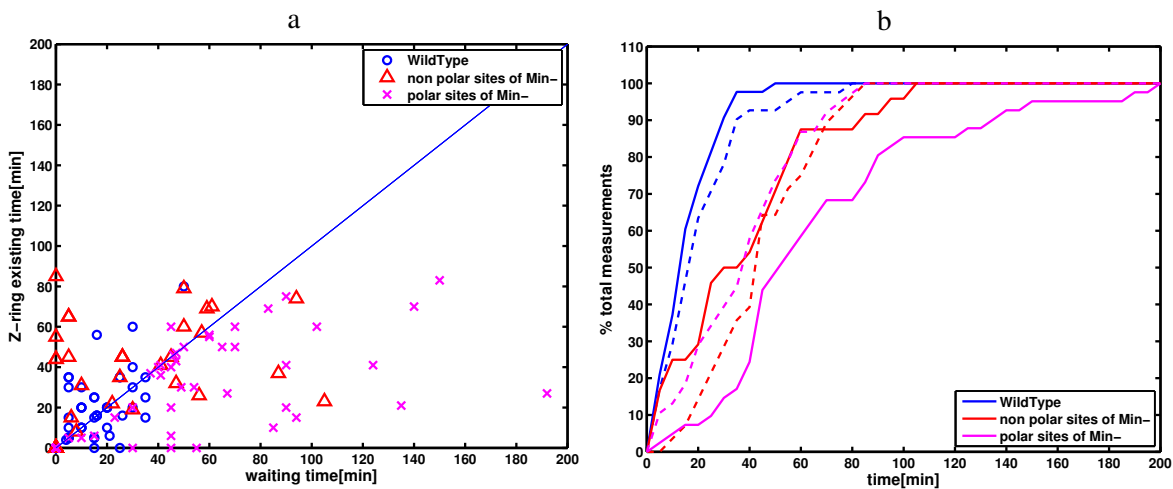


Figure 2.36 – The FtsZ ring measurement. (a) the relation between the waiting time and Z-ring existing time. The circles are for TB43(magenta cross are polar sites, red triangles are non-polar sites), the blue circles represent TB28. (b) The cumulative distribution of the waiting time or Z-ring existing time. The solid curves are division waiting time, and the dashed curves are the Z-ring existence time.

We also calculated the average value for each distribution, as shown in Table.2.6. The results also support our interpretations.

2. RESULTS

	Average division waiting time [min]	Average Z-ring existence time [min]
WT	17.3	22.2
Polar sites in <i>minB</i> ⁻	69.0	39.1
Non-polar sites in <i>minB</i> ⁻	39.4	45.8

Table 2.6 – The average of different time distributions. The average values for division waiting time and Z-ring existence time of different types of division sites shown in Fig.2.36 are calculated. The second column is corresponding the solid lines in Fig.2.36b, and the third one is corresponding to the dash lines.

However, the average Z-ring existence time of WT cells is longer than the division waiting time, and the situation is the same for non-polar sites of *minB*⁻ cells. We cannot rule out the possibility that this is because of the imprecision of the measurement, but it could also indicate that cells start building a septum prior to the chromosome segregation at the same place. This is also consistent with earlier work. It might mean that the Z-ring structure helps the chromosome segregation or cell keeps attempting to build a Z-ring at all potential division sites until it succeeds.

In order to compare our results to earlier work, in Fig.2.37, we estimated the fraction of FtsZ on Z-ring structure by the fluorescent intensity. Limited by the quality of our pictures, we were not able to distinguish the Z-ring structure and FtsZ Helical structure, and we could not see the oscillation of FtsZ helical structures either. But Fig.2.37 shows that in the WT around 30% of FtsZ is bound in a Z-ring. This finding on WT cells is in good agreement with other experimental studies [50, 77]. Interestingly, we found that the fraction in *minB*⁻ cells is about 15%, which is half of that in WT cells.

It has been shown that increasing the amount of FtsZ in *minB*⁻ cells twofold gives rise to a cell size distribution of *minB*⁻ cells that is very similar to that of WT *E.coli* [92]. Fig.2.37 suggests that this effect could be explained by the fact that upon increasing the FtsZ amount twofold the amount of FtsZ bound in Z-rings in *minB*⁻ cells becomes comparable to the amount of bound FtsZ in Z-rings in WT cells.

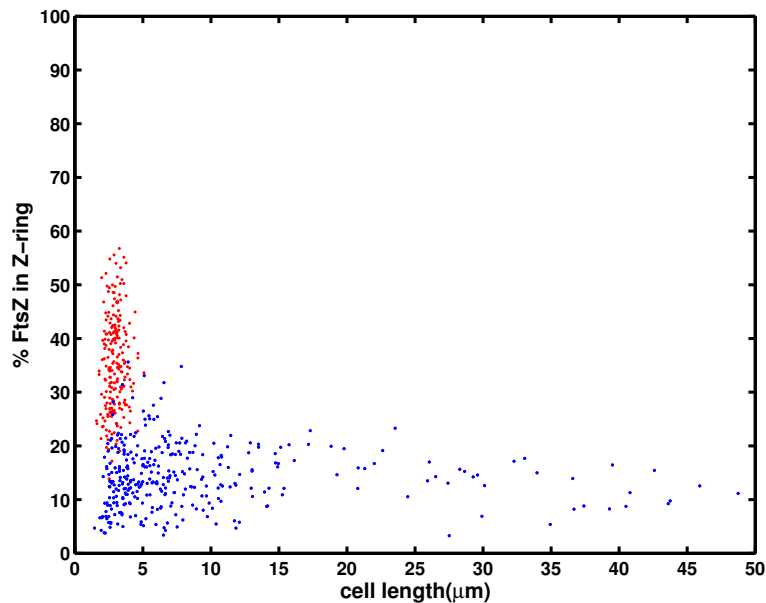


Figure 2.37 – fraction of Z protein on Z-ring in both strains. The red dots are TB28, blue dots are for TB43. Each circle here represent the situation of one cell in one fluorescent photo.

2.7 Model 4

So far, model 3 is able to capture the main experimental observations. But nevertheless, the question remains why the $minB^-$ cells have longer division waiting times than WT cells. We speculated that this could be caused by the fact that $minB^-$ cells are longer and thus have more possible division sites. Thus, a priori a division site in $minB^-$ cells has the same waiting time as a division site in WT cells. However, as we showed above, cells might attempt to build a septum at all potential division sites, and $minB^-$ cells have more of those sites than WT cells. It should, for a given amount of cell division machinery, take longer to finish division at these sites.

To implement this into the model, we assigned a quantity x to every division site that measures how much the division process has proceeded. Upon appearance of the division site we set $x = 0$, division is completed for $x = T_w$, where T_w is the waiting time assigned to the division site drawn from the experimentally distribution of WT ($17.7 \pm 12min$). Between time t_1 and t_2 we increase x by

$$x(t_2) - x(t_1) = \int_{t_1}^{t_2} dt \frac{dx}{dt}. \quad (2.12)$$

In the previous models we simply had $\frac{dx}{dt} = \frac{1}{T_w}$ but now we want to take into account that several division sites compete for the division machinery and that larger cells have a larger amount of division machinery. We therefore set

$$\frac{dx}{dt} = \frac{L/(N-1) - L_c}{C}. \quad (2.13)$$

Here, L is cell length, N is the number of division sites and $L_c = 0.98\mu m$ is the size of a chromosome.

Thus, the waiting time of a site decreases the more the larger the average compartment size $L/(N-1)$ is. The constant C is chosen such that for WT, $\frac{dx}{dt} = 1$, implying $C \simeq 4.3\mu m/1 - L_c = 3.3\mu m$. One should note that as the cell grows or as additional potential division sites appear $\frac{dx}{dt}$ changes. Beside this novel feature model 4 is identical to model 3.

The results of model 4 are shown from Fig.2.38 to Fig.2.41, including Table.2.7. As one can see, model 4 is as good as model 3 in reproducing the experimental data. Of course, the main advantage of this model is that it is independent of the experimentally measured division waiting time distributions.

	%	old pole	non-polar	new pole
Experiment	polar	3(41.2 ± 21.3min)	17(37 ± 21.9min)	13(22.8 ± 19.4min)
Experiment	non-polar	31(31.0 ± 18.4min)	36(39.1 ± 22.3min)	
Simulation	polar	5(37.6 ± 26.9min)	20(37.8 ± 31.7min)	9(26.2 ± 24.7min)
Simulation	non-polar	34(24.1 ± 23.2min)	32(30.7 ± 32.0min)	

Table 2.7 – Cell division history of individual cells as obtained experimentally and from model 4. All cell divisions within ~ 200 minutes are classified into 5 types according to the position of two successive cell divisions. Rows represent the location of the first division event, columns location of the second event. Time in parenthesis represents mean time difference \pm standard deviation between the division events.

Furthermore, we can also use model 4 to simulate WT cells. The essential difference of WT cells to $minB^-$ cells is that in WT cells, the Z-ring formation at polar sites and nearby

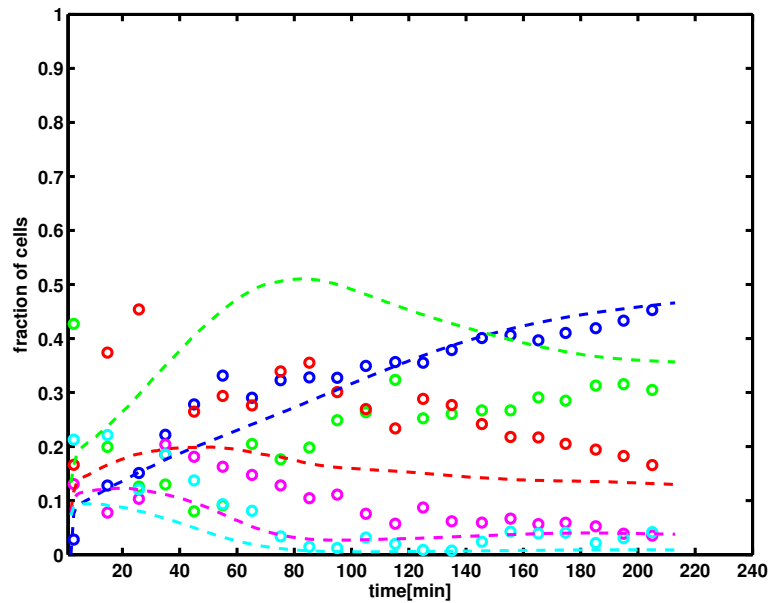


Figure 2.38 – The time dependence of the fraction of cells. In this figure, we averaged the results of 50 simulations, each one starts with 1000 cells. Circles represent experimental data, dashed lines the results of our model. Cells without chromosome (mini cells) are shown in blue, cells with one chromosome in green, with two chromosomes in red, with three chromosomes in magenta and with four chromosomes in cyan.

area is blocked by MinC. So we need to recalculate the number of compartments for WT cells. For this we have to take into account that the Min proteins confine the operation space of the division machinery. To do so, we replace Eq.2.13 by

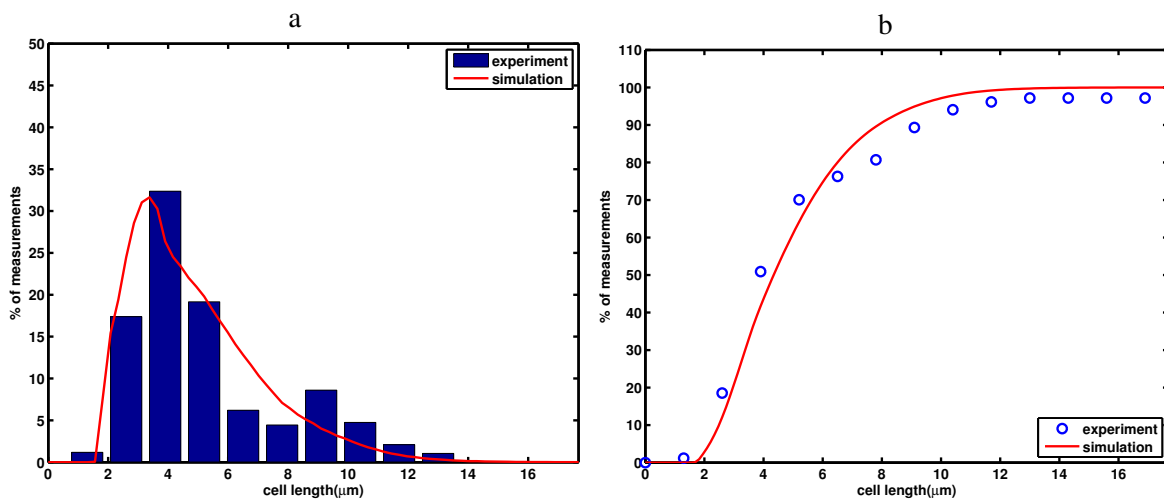


Figure 2.39 – The cell length distribution (the red curves are simulation results, the blue circles or bars are experimental data). (a). The cumulative cell length distribution. It shows the percentage of cells which are shorter than different values. (b). The cell length distribution. It shows the distribution of cells in different length range. 133 cells were measured when the time is 213 minute. Mini cells are not included. 105 mini cells on total were not taken into account.

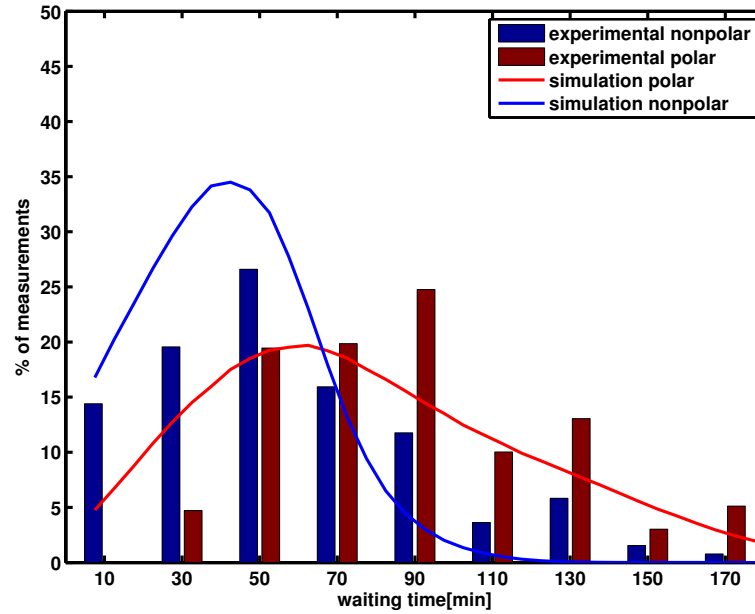


Figure 2.40 – The waiting time distribution of $minB^-$ for polar and non-polar sites. The curves are from simulation and the bars are experimental data (red: polar sites; blue: non-polar sites) . The X-axis is the time measured in minutes.

$$\frac{dx}{dt} = \frac{L - L_c}{C}. \quad (2.14)$$

In this way the Min proteins that oscillate from pole to pole effectively confine the division machinery to a region (around the division site in mid-cell) of roughly half the cell length. This actually means there is a difference of a factor two for the septum formation rate of WT cells compared to that of $minB^-$ cells. We also need to keep the polar sites blocked all the time in the simulation for WT cells. But beside these changes, the simulation is identical to that for $minB^-$ cells.

The predictions of model 4 for WT cells are shown from Fig.2.42 to Fig.2.44. As one can see model 4 is also able to reproduce the experimental data for WT cells.

Like for $minB^-$ culture, we show the time-dependence of the fraction of cells in Fig.2.42. In Fig.2.42a, we averaged the results of 50 simulation runs, and found the curves do not fluctuate as much as the experimental data. In order to make the results more comparable, we reran the simulation with similar initial conditions as the experiment, and only checked

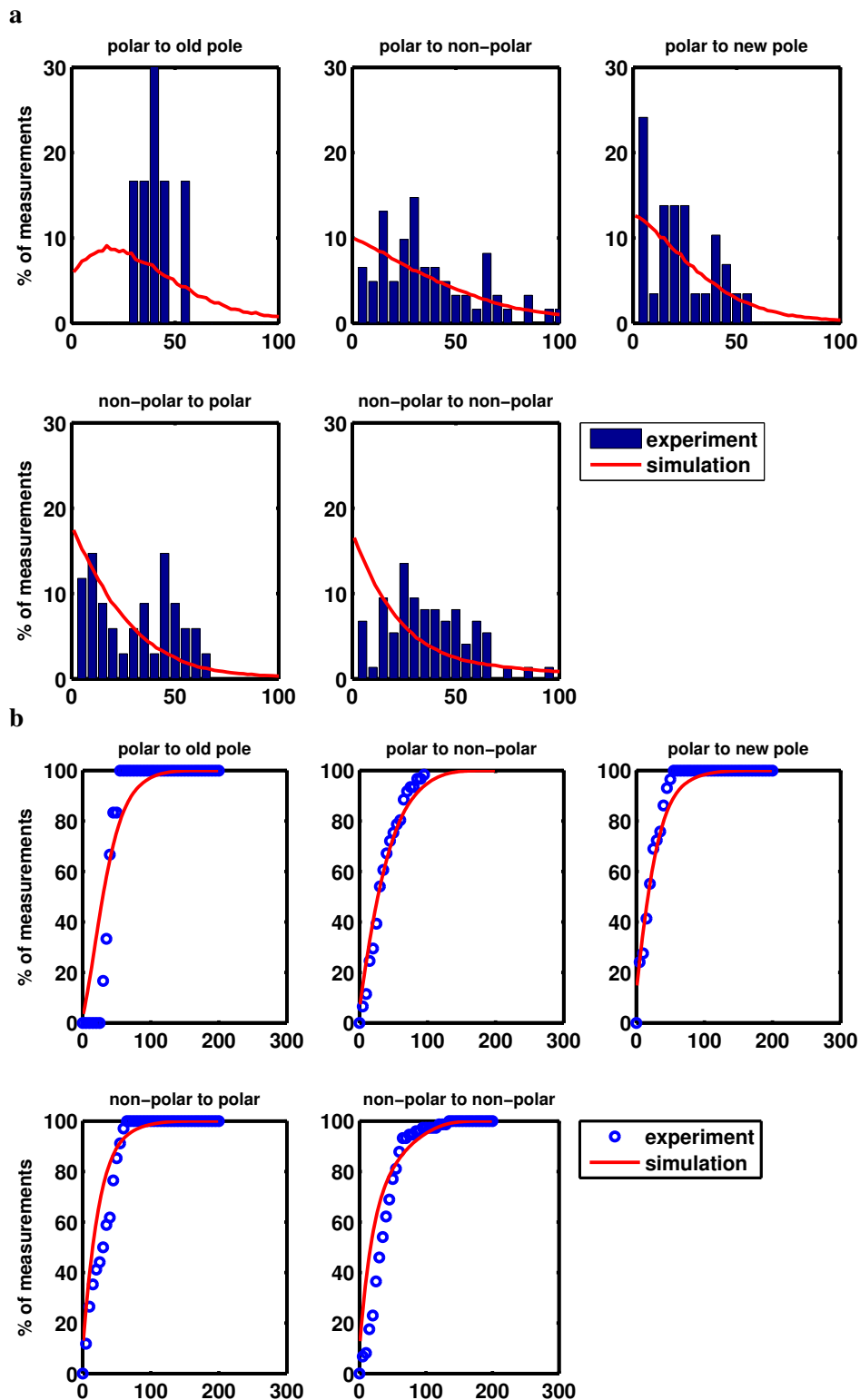


Figure 2.41 – The distribution (a) and cumulative distribution (b) of inter-division time of different types of cell division. The cell divisions are classified into 5 types according to the position of two successive cell divisions. The rows represent the location type of the first cell divisions. The columns represent the location type of the second cell divisions. All the X-axis are time (minute).

2. RESULTS

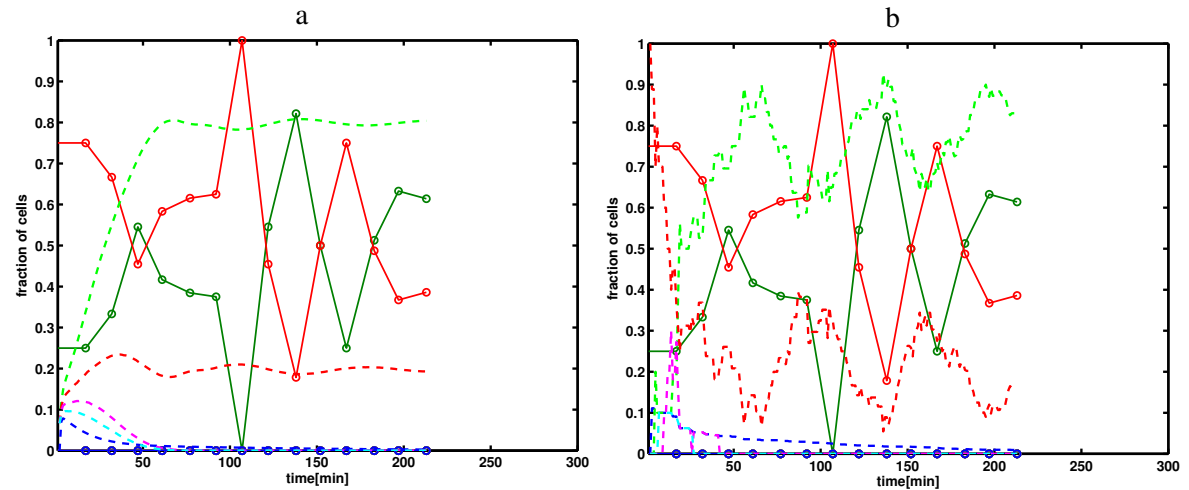


Figure 2.42 – The time dependence of the fraction of cells. The dash lines are simulation results and the solid lines with the circles are the experimental data. The X-axis is calculated by minute. The cells are classified by their chromosome number and represented by different colors (blue: mini cell; green: one chromosome; red: two chromosomes). (a) shows the average simulation results of 50 runs. (b) shows the results of the simulation initialized with similar condition (one runs, starts with five cells). The simulation system is initialized like a *minB*⁻ culture, but very soon the longer cells disappeared .

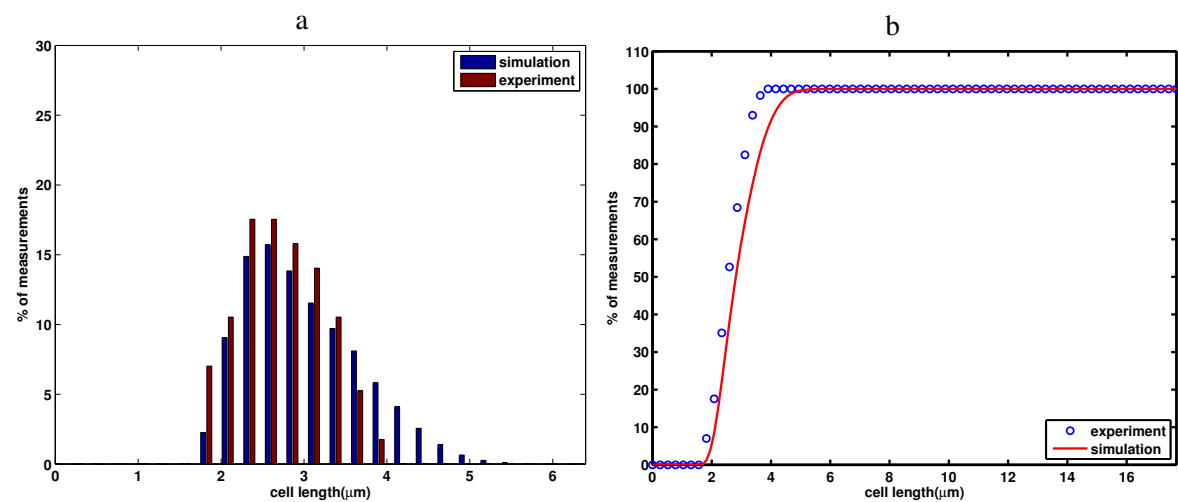


Figure 2.43 – The cell length distribution of WT cells (a, red histogram are experimental data, blue one are simulation). The cumulative cell length distribution of WT cells (b, blue circles are experimental data, red curve is for simulation). 57 cells are measured at about 220 minutes.

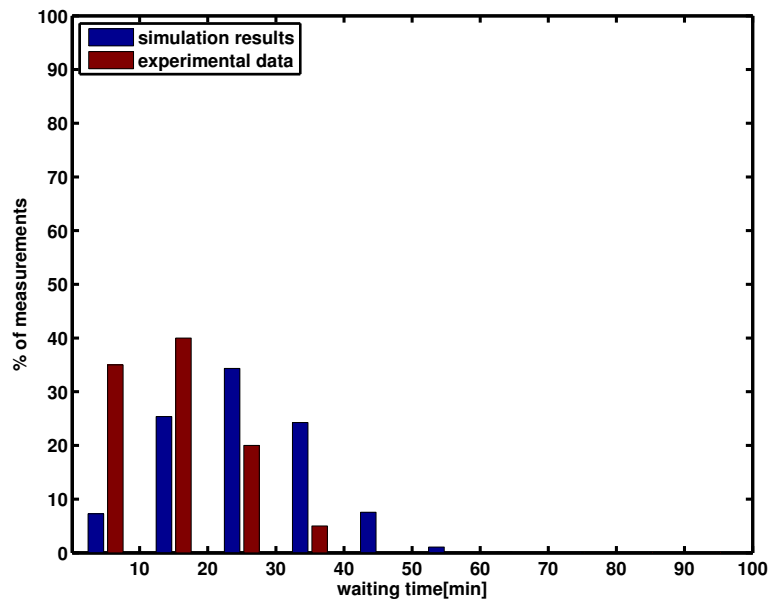


Figure 2.44 – The waiting time distribution of WT cells. The red histogram represents experimental data and the blue one are simulation results.

the result of one simulation run. As Fig.2.42b shows, the simulation curves also fluctuate a lot, although still not as much as the experimental ones, they show more similarities than Fig.2.42a. The culture of *minB*⁻ cells can reach steady state within 200 minutes, but Fig.2.42 shows that the culture of WT cells will need longer time to completely reach it.

The cell length distributions are compared in Fig.2.43. As we can see, the simulation results are very close to experimental ones, except that the simulations produce somewhat longer cells which are about twice as long as a new born cell. This could be caused by the small size of the experimental data set, which is still not big enough compares to the simulations whose results are averaged over 50 runs and which start with 1000 cells each run, or caused by the fact that the experimental system might also have not reached the steady state.

The distribution of simulation division waiting times is compared to experimental data in Fig.2.44. It looks like the simulated division waiting times are a bit longer, but considering the underestimation of the division waiting time of WT cells as we mentioned in the section 2.3.2, the simulation result is actually consistent with experimental data.

We also try to get the distribution of cells according to their “time until division” (Tud) as was done earlier [114] . As Fig.2.45 shows, we can also get similar result, although because of

the different parameters of cell growth, our result is not completely the same to the one shown in the paper.

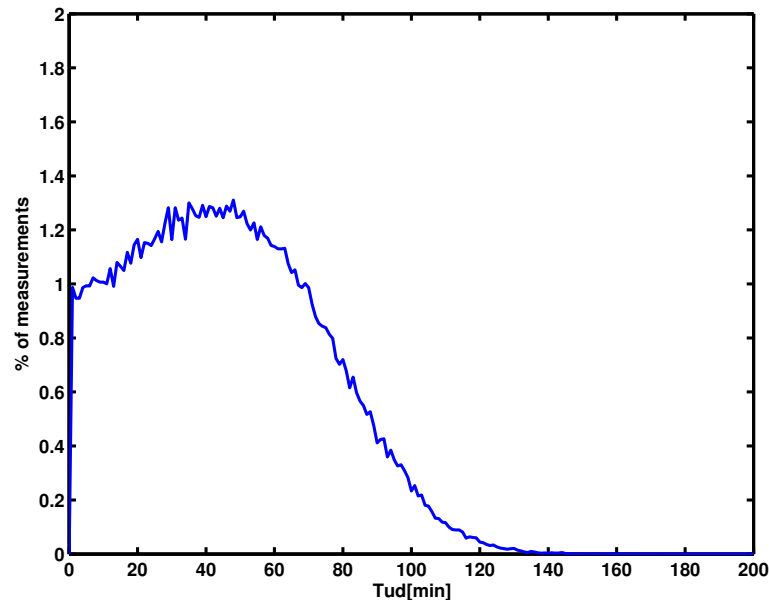


Figure 2.45 – The distribution of cells according to time left to divide. In order to make it comparable to earlier work, the distribution was obtained after 800 minutes in the simulation, which means the culture reached the steady state already. The result is obtained by averaging results of 50 runs of simulations.

2.8 The inter-division time and the ratio of MinD to MinE

The results obtained so far indicated that the Min systems influences timing of cell division. We were therefore wondering if the oscillation frequency of the Min system directly correlates with the interdivision times.

In order to understand the mechanism of the oscillation of Min system, a lot of modeling work has been done [34–36, 38–42]. An interesting finding from simulation and experimental work is that the oscillation frequency is related to the ratio of intracellular concentrations of MinD to MinE [37]. Combined with our hypothesis that the oscillation of Min system affects the formation rate of cell division septum, this gave us the idea of checking if the ratio of MinD to MinE is related to the cell division timing.

To analyze this we fluorescently labeled minD and minE and measured their intensities in WT background that we take as measure for intracellular concentration (for details see

AppendixA.3). We labeled MinD and MinE as others did, but in their original frame and got two strains (as shown in Fig.2.46), and then combine them into one strain. As a control, we first checked if the amount of MinD or MinE affects the cell inter division time and we found no clear correlation between interdivision time and intensities of MinD or of MinE (see Fig.2.47a and Fig.2.47b). However, there is a correlation between inter division times and the ratio of MinD to MinE (see Fig.2.47c). One should keep in mind that the numbers on the x-axis represent the intensity of the fluorescent proteins, we just used it to estimated the amount the MinD or MinE.

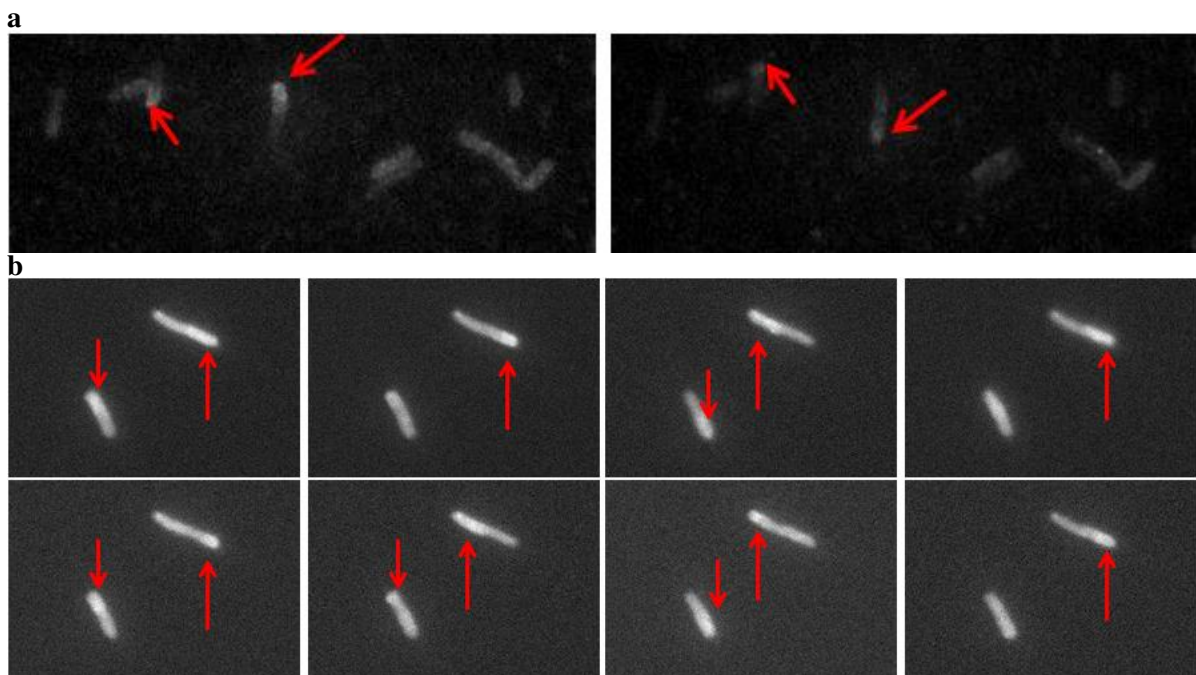


Figure 2.46 – The oscillation of labeled MinD and MinE. (a) shows the oscillation of MinD. (b) shows the oscillation of MinE. The time interval between every two photos is about 30 seconds.

In Fig.2.47c, we measured the correlation between the inter division time and the ratio of MinD to MinE by calculating Pearson product-moment correlation coefficient, which is -0.3662 here. We speculated that the correlation is not so strong because the individual inter division time is affected by many things. For example, the individual doubling time of different cells are different, the born length might be also different for different cells and there are some other fluctuations.

2. RESULTS

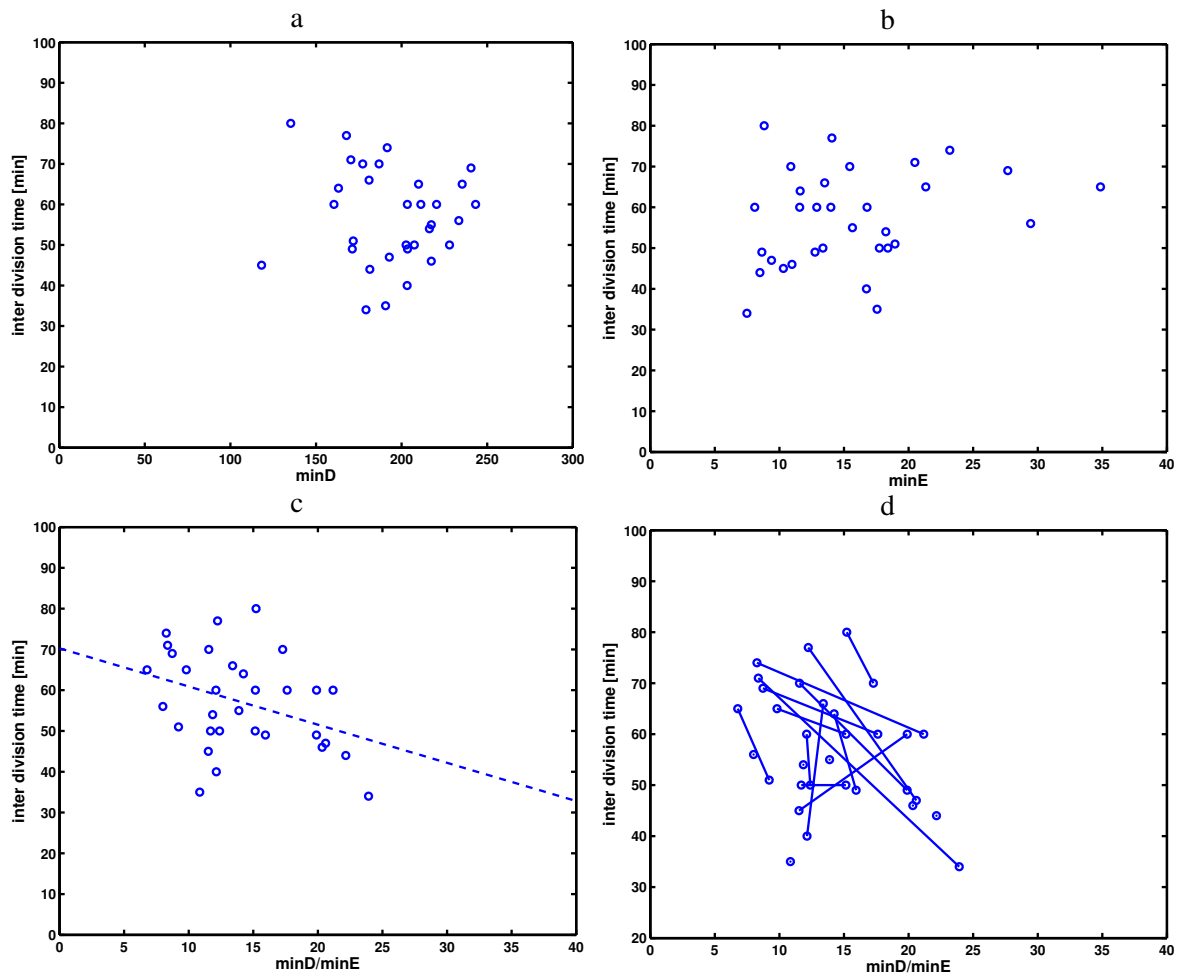


Figure 2.47 – The correlation between the inter-division time and the level of MinD to MinE. (a) and (b) shows the correlation between inter division time and the level of MinD or MinE. (c) shows the correlation between inter division time and the ratio of MinD and MinE, the dash line is got by fitting the data points and shows their trend. In order to see the correlation more clear, the sister cells are connected by lines in (d).

But the variation should be smaller between sister cells which are from the same mother cell than that the variation among totally uncorrelated cells. As Fig.2.47d shows, we marked the sister cells via straight lines, and ten pairs of cells show the correlation very clearly, only two of the 13 pairs we measured showed apparently a different trend.

As we mentioned above, the division waiting time is related to the rate of septum formation in cells. This should be affected by the distribution of the average concentrations of MinC, which is related to the level of MinD and MinE. It might be not only simply correlated to the oscillation period of Min system, but to know more details about this, we need more experimental data.

An interesting thing here is that the ratio in Fig.2.47b varies from about 7 to 25, which is an almost 4 fold increase. This is consistent to the earlier work [37] and probably shows the limit of the wild type cells to tolerate the fluctuation of the oscillation period.

The situation of TB43 is equal to the situation that the concentration of MinE much bigger than MinD so that the oscillation period is infinite.

2.9 The increased FtsZ level in model 4

In model 3, we mentioned the effect of the FtsZ level on cell division of *minB*⁻ cells. As we always speculated in model 4, the prolongation of division waiting time is due to the slow-down of the formation of the septum, and combined with the earlier experimental results, it seems this effect is mainly related to FtsZ.

We used the cell length to represent the division machinery in model 4, and we want to know if we can mimic the experimental finding about the effect of the FtsZ level. To test this, we performed a new round of simulations of model 4 where we now effectively increase the amount of FtsZ by replacing Eq.2.13 by

$$\frac{dx}{dt} = \frac{2L/(N-1) - L_c}{C}. \quad (2.15)$$

As we mentioned above, we add a factor two to the cell length L here to represent the level of FtsZ is doubled.

And as it is claimed in that paper [92], that the distance between two septa is also similar to that distance in WT cells, we took it as an indication that the blocking number goes to zero. This is also consistent with our interpretation of the change in the rate of septum formation. If there are enough FtsZ proteins, then all the potential division sites will be taken as available sites.

In Fig.2.48a and b, we compared the cell length distribution from the new simulation to the distribution of experimental WT cell lengths. In order to see the effect of a change in the FtsZ level more clearly, we also showed the simulation result for *minB*⁻ cells with a normal FtsZ level in Fig.2.48a and b. In Fig.2.48a and b, the distribution from the new simulation

(red curve) is very similar to that of WT cells, and very different to the simulation result for *minB*⁻ cells with normal FtsZ levels (green curve).

We changed the septum formation rate and the blocking number in the simulation. In order to see which one is more important to get the new distribution, we also did simulations with only one of them changed. As the magenta curves show in Fig.2.48c and d, being the results of an increment of FtsZ level, both of the changes of formation rate and blocking number are equally important.

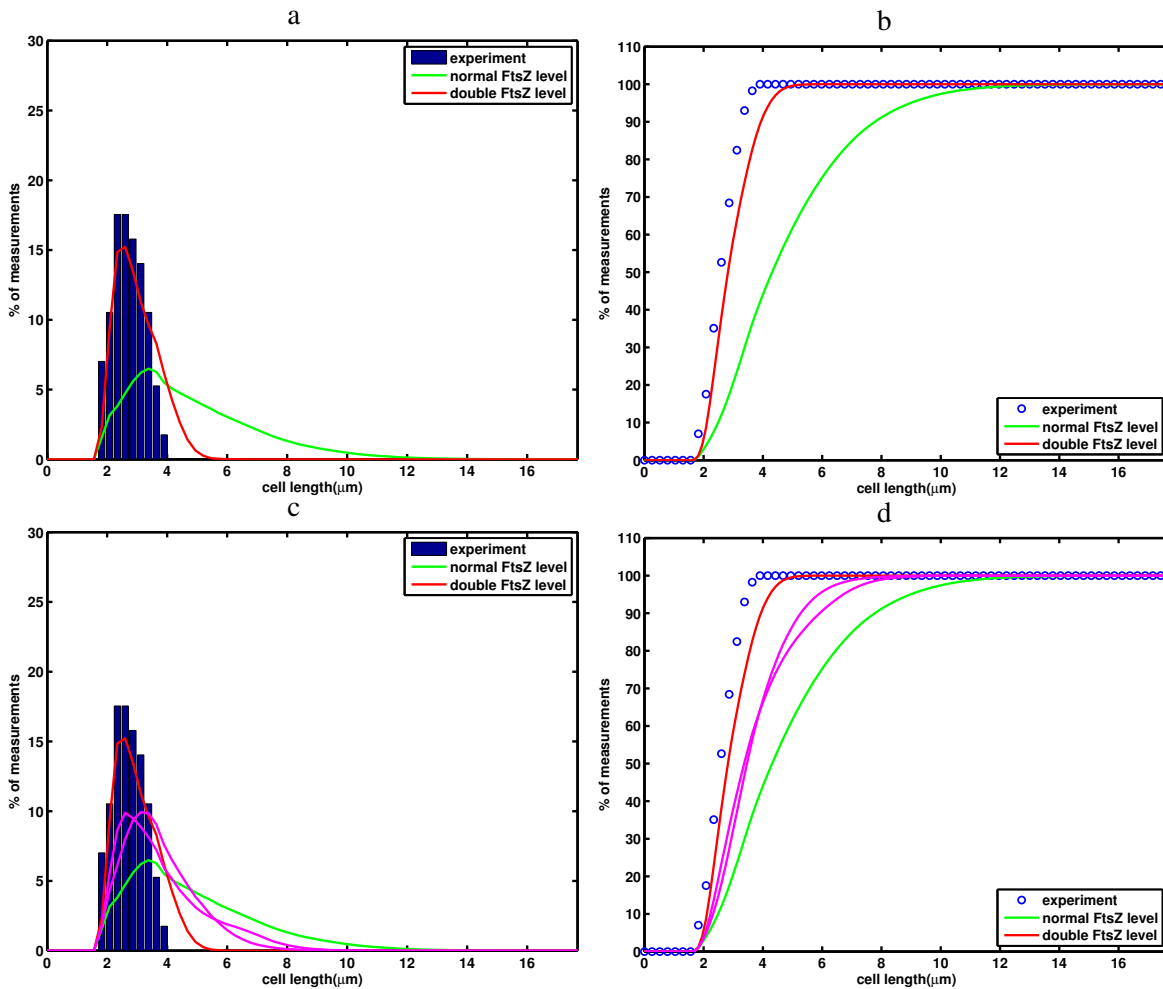


Figure 2.48 – The cell length distribution of $minB^-$ with the FtsZ concentration doubled in the simulation and the cell length distribution of WT from experimental data (blue bars and circles). (a) is the cumulative cell length distribution (blue circles are experimental data, red curve is for simulation of higher FtsZ level $minB^-$ cells). (b) is the cell length distribution (blue bars are experimental data, red ones are simulation). The simulation result for $minB^-$ cells with normal level of FtsZ is also shown in both figures (green curves). Like mentioned in the literature, the cell length distribution of TB43 after raising FtsZ concentration is comparable with WT cells. The simulation shows the cell length distribution at about 710 minutes. In (c) and (d), simulation results with only formation rate or blocking number changed are additionally shown with magenta curves.

Chapter 3

Discussion

In this work, we mainly focused on the effect of the Min system of *E.coli* on cell division timing. While the mechanism and role of the spatial oscillations of this system have been well studied [5, 17, 64, 111] these timing effects have not been addressed before [36]. Our interest in this aspect was triggered by the observation that cell inter-division time varies a lot without Min system. However, a problem is to quantify the irregularity of cell division timing in *minB*⁻ cells in a meaningful way. Inter-division time itself is not a very good quantity because it is closely connected with the cell size that is irregular because of the lack of Min oscillations. A longer cell, that has several available division sites has, of course, a higher probability to divide earlier. In order to avoid this difficulty, we studied the timing of cell division by comparing division sites rather than comparing cells. There are mainly two major processes in cell growth that affect the timing of cell division: duplication of the chromosome and septum formation between two chromosome clusters. The growth curves of WT and *minB*⁻ strain in different liquid media at 37°C show that the Min system does not change the growth rate of the cell. This indicates that the chromosome duplication rate should be the same in *minB*⁻ strain and in wild type strain. So to compare the timing at each division site, we only need to measure how long cells take to divide at each site after the chromosomes segregate. We refer to this quantity as division waiting time. For the cell poles the division waiting time is the time difference between appearance of the pole and the polar division event. To be able to track the segregation of the chromosomes, we labeled the Hu protein with a fluorescent protein.

Our results show that there is a significant difference in the timing of cell division between WT and *minB*⁻ strain. The average division waiting time of the *minB*⁻ cells is longer than that of the wild type cells. Given that the only genotype difference between these two strains is the lack of Min this indicates, that Min has an effect on the timing of cell division. Furthermore, we found that the waiting time at cell poles is longer than that at other division sites (the non-polar sites). In order to understand these findings in a quantitative way, we developed several models to explain and reproduce the experimental observations.

We first developed model 1 that is completely based on experimental observations. As described in section 2.2, in model 1 each cell consists of one or several compartments that each contains one chromosome. Each compartment has a starting, an ending length and growth rate all drawn from a normal distribution (as suggested by the experimental data). When the compartment reaches its ending length, its chromosome segregates into two and it also splits into two compartments. The gap between two chromosome clusters is taken as a division site.

Furthermore, the division waiting time assigned to the polar and non-polar sites are drawn from the experimental distributions (see Fig. 2.5). When it reaches zero the cell divides. In model 1 all parameters are set to the values obtained from the experimental data without further assumptions. This guarantees that the disagreement between the simulation and experiment is not related to any arbitrary assumptions, but directly to the model itself.

We compared the results of the simulations of model 1 with the experimental data, and found that the model is able to reproduce some of the main observations of the Min mutant culture. For example, the simulation results showed, the fraction of mini cells is the highest and most of the cell lengths are between 2 and 5 μm in the end (see Fig.2.13 and Fig.2.15). So starting from the level of individual cells, we can calculate some of the properties of the culture indicating that model 1 is a good basis for further investigations.

However, model 1 fails in explaining some properties. Major deficiency is that the simulations produce more mini cells and shorter cells, but less filamentous cells than the experiments. This indicates that the simulated cells divide too frequently. Furthermore, shorter cells have less non-polar division sites leading to an increase of the ratio of polar sites to all division sites. This leads to a too low fraction of two subsequent non-polar divisions events, see Table.2.2.

These deviations are caused by the fact that model 1 does not take into account the chromosome segregation defect that the *minB*⁻ cells exhibit leading to a too high relative number of division sites per cell length. The chromosome segregation defect has also been observed in [52, 107, 108]. The mechanism of this effect is not totally clear yet, but evidently Min seems to play an important role in chromosome segregation [101, 102].

In the improved models we take this effect into account. To mimic it we keep (on average) two potential division sites blocked. When we suppose that the polar sites can be also blocked as the non-polar sites and distributed division waiting time to polar sites according to the experimental data (Fig.2.5b), we found the simulated division waiting time is amazingly longer than the experimental results (Fig.2.28). Apparently, blocking polar sites also prolongs the polar division waiting time. This reminds us that the longer observed polar division waiting time is probably due to the random blockage of polar sites and there might be no essential difference between polar and non-polar sites. In model 3 we therefore assigned the same waiting time distribution to the polar and non-polar division sites. With this modification we were able to significantly better results on cell sizes, division timing and division history. This justifies our assumption, that the disturbance of chromosome segregation is random and all the division sites are essentially equal. While blockage of non-polar sites mimics the chromosome segregation defect, the interpretation of the blockage of polar sites is less evident. Our interpretation is that the polar sites are blocked if, for example, the chromosome is too close to the pole to allow septum assembly. Of course further questions could be about how thick the septum is and how much spaces it needs. The discovery of the equality of division waiting times at polar and non-polar sites achieved with model 3 indicates that the time needed to finish the septum and cell division is the same for all potential division sites. Furthermore, the fact that the assumption that polar and non-polar sites have the same blockage probability indicates that the same mechanism might be at work at both kinds of sites.

In this study we have set the blocking number (i.e. the number of blocked division sites) to two, since we found that the real chromosome cluster number is about two less than the expected cluster number (see Fig.2.24). In WT cells, the two cell poles are always blocked, although results from different mechanism. This leads us to think that there are always two

potential division sites are blocked in *minB*⁻ cells maybe because the two polar division sites sometimes are not blocked anymore. Understanding the disturbance of chromosome segregation better will help us to understand the blockage of potential division sites. But to achieve a deeper understanding about the disturbance of chromosome segregation, we obviously need more information about the mechanism of chromosome segregation. Random movement of chromosome clusters apparently plays an important role in this process. And fixed blocking number also builds a weak connection between different potential division sites, which makes them not totally independent. But anyhow, our simple setting about the blocking number in the simulation works so far and we are more interested in the timing of cell division, so we just kept this part as it is, and tried to improve the distribution of the waiting time.

The equivalency of the timing of polar and non-polar division is further tested by experimentally measuring the life time of the Z-ring. As we saw the life time distribution of a Z-ring is identical at polar and non-polar sites in *minB*⁻. As for the waiting time the life time of a Z-ring is longer in *minB*⁻ than in WT for all division sites. In the experiments, we sometimes found that there are two or even more Z-ring structures at the same cell poles. In other cases the Z-ring structures were quite extended possibly consisting of several ring structures. Inclusion of such effects will make the model more complicated. So far we have included them as the good agreement between experiment and simulation does not make this necessary. Nevertheless, because FtsZ is one of the first proteins working on building division septum, this experiment has two important implications: First, concerning timing of appearance of FtsZ there is no fundamental difference between polar and non-polar sites division sites. Second, compared with WT, the time interval between initiation of Z-ring formation and cell division is larger for *minB*⁻ cells

This second finding shows again that the lack of Min has an effect on the timing of cell division. There are at least two hypothetical explanations for this effect. The longer division waiting time of Min mutant cells could be caused (i) by a delay in a checkpoint or (ii) by the change of the formation rate of the septum. For the first mechanism, however, it is hard to explain how to make one division site pass the checkpoint by some signals while keeping the others not pass in the same cell. For that reason we find the second scenario more likely

because it can keep the division sites which are available earlier divide earlier. In the absence of Min there are more available positions for FtsZ to assemble a Z-ring structure. At the same time the total amount of division machinery does not change, so the formation rate of a septum is affected. To quantify this effect we introduced an effective model where the division waiting time depending is set by a combination of cell length and compartment number of the cells. Here the cell length represents the amount of division machineries in each cell, while the compartment number relates to the possible spaces for Z-ring assembly. This number is actually halved in wild type strain because the area nearby cell poles is unreachable for the division machinery including FtsZ. And it also shows how strong the effect of Min system on septum formation in WT cells is. In WT cells, this could be different in different cases, for example, different oscillation frequencies or concentration of MinC will lead different septum formation rates.

In this study we cannot analyze the mechanism that leads to a lower rate of septum formation. Being one of the essential proteins for septum formation, the assembly of FtsZ on the cell membrane is affected by the Min system in a complex manner. The stiffness of FtsZ structure is affected by MinC, and so is the function of the Z-ring as a scaffold [30]. Furthermore, both experimental and theoretical approaches have shown that FtsZ can form helical structures [51, 94]. These structures are then pushed by Min to oscillate in the cell as well [51]. But without Min system, the assembly of FtsZ is different. In the absence Min the recovery time of the Z-ring after photo-bleaching is twice as long as in WT indicating that the Z-ring is more dynamical in wild type cells [50]. Actually, this effect might give rise to the factor of two mentioned above, where we calculated the compartment number in WT cells. We tried to include all these effects into model 4. The results show that it can capture almost every experimental observation, for both strain cultures.

This means our assumption and estimation of the septum formation rates are reasonable. And before going further based on this, we tried to find more supportive evidence. One of the deductions of this assumption is that with different oscillation frequencies, which are the result of different ratios of MinD to MinE [37], the rate of septum formation will be changed, too. As we analyzed above, lack of a Min system makes different septum formation rates (as shown

with Eq.2.13 and Eq.2.14), and of course, with different oscillating frequency, this rate could be different as well, resulting in different inter-division times. In our experiments we found supporting evidence for this. As shown, we found a correlation between the inter-division time and the ratio of the concentrations of MinD and MinE in individual cells.

Furthermore, we artificially doubled the cell length when we implement Eq.2.15 into the simulations and found that the distribution of the cell lengths of the Min mutant strain is similar to that of the wild type strain. This is consistent with the findings where the cell length distribution of the *minB*⁻ cells becomes similar to that of wild type cells if the level of FtsZ is doubled or higher [92]. We also found that, as shown in Fig.2.37, the fraction of FtsZ in the Z-ring in *minB*⁻ cells is half of that fraction in wild type cells. This could be a reason why the level of FtsZ needs to be increased at least two fold to get a similar cell length distribution as for wild type strains. All this hints that the change of the rate of septum formation probably mainly relates to the assembly of a Z-ring, although it is normally believed that the time scale of Z-ring formation is very short.

Chapter 4

Summary and outlook

4.1 Summary

E. coli cells divide precisely in mid-cell position with the help of two protein systems, the “NO” system [43–45] and the Min system [5, 17, 64, 111]. They collaboratively regulate the spatial positioning of the Z-ring, a protein structure that marks the position of cell division and whose formation is initiated by assembly of a FtsZ ring. The NO prevents Z-ring formation over the chromosome while the Min system exhibits spatial oscillations and in this way inhibits Z-ring formation at the cell poles. While these self-organized spatial oscillations have been studied in great detail the influence of the Min system on the timing of cell division has so far not been analyzed. In this study, we analyze this aspect by comparing the behavior of WT and *minB*⁻ strain. In order to do this in a quantitative way, we experimentally measure the division waiting time (defined as the time interval between chromosome segregation and cell division, see Chapter 2). We find that the *minB*⁻ strain has a longer division waiting time than WT and that for *minB*⁻ cells, polar sites have longer division waiting time than non-polar sites.

To theoretically explain these findings we introduce a series of models whose numerically obtained predictions are compared with the experimental data. In this way we demonstrate that the minimal model that accounts for all observations needs to include the experimentally observed disturbance of chromosome segregation in *minB*⁻. The theoretical analysis also shows that all available division sites are equivalence despite an apparently longer division waiting of the polar sites. We show that this effect arises because the polar sites can be blocked

as well as non-polar sites. We also show that the increase in division waiting time could be the result of a decreased rate of septum formation associated with the lack of the *minB*⁻ system. This is supported by our experimentally obtained correlation between the inter-division time and the ratio of MinD and MinE. The theoretical and experimental results on the FtsZ levels in *minB*⁻ cells suggest that the change in the septum formation rate is mainly related to the assembly of the Z-ring. Combining all these results, we conclude that the Min system also has an important effect on cell division timing, by changing the rate of septum formation through manipulating the assembly of FtsZ.

4.2 Outlook

The development of model 1 to model 4 demonstrates the interplay between theoretical analysis and quantitative experimentation to improve the understanding of biological systems. We first collected all relevant parameter values for the basic model and compared the theoretical predictions with the experimental data. The disagreement between model and data then lead us to take into account the defect of chromosome segregation and the differences between polar and non-polar sites.

Recently, it was shown that the Min system also affects chromosome segregation [101, 102]. Evidently, there are also other processes affecting this process and the *minB*⁻ strain can give us some clues about these possible processes. Our theoretical models might provide means to do so. The theoretical analysis already lead to the suggestion to regulate the level of FtsZ, and check if this is related to the blocking number that we are using in our simulations. We predicted theoretically that the probability to be blocked should be the same for polar and non-polar sites, and according to Model 4, higher levels of FtsZ will make the division waiting time shorter leading to a smaller blocking number. On the other hand, the division waiting time of polar sites is also affected by the blocking number. So the change of the waiting time of polar and non-polar sites caused by the change in FtsZ level should be different. Therefore, in further experiments, we need to check if the division waiting time of these two types of division sites changes differently or not. In the experiments where we introduced expression of labeled FtsZ via plasmid, the total level of FtsZ is changed, we found that on average the division waiting times of polar and non-polar sites are about six to seven minutes shorter than in the original *minB*⁻ strain (in Fig.2.36). This seems to indicate that the blocking number stays constant. But the increment and activity of labeled FtsZ is very small, so the difference might be very weak, and the data set is not big enough to get strong conclusion from this small difference.

In the earlier experiment, where the level of FtsZ is increased twofold or even higher, the distance between two septums is similar to wild type cells, which indicates that the blocking number is close to zero [92]. This supports our speculation. To analyze this further we suggest to experimentally introducing expression of wild type FtsZ from a plasmid to get a higher

concentration and to check then how the distribution of division waiting time changes.

If the blocking number is related to the FtsZ level, chromosome segregation is also related to FtsZ, and getting more details in this direction will help us to calculate the blocking number analytically or in a numerical simulation.

From Model 4 we also obtain a possible way to calculate the rate of septum formation, Eq.2.13. In that model, we tried to include information about the amount of cell division machinery, the number of complete chromosomes, and the effect of the Min system on the septum formation rate. The simulation results are as good as in Model 3, but based on Eq.2.13, we can get the distribution of division waiting times for the *minB*⁻ strain from the simulation. This shows a possible direction for the next step: If we change the level of FtsZ, we would expect the division waiting time of all division sites to change as explained above. Furthermore, we can check if our simulation can predict the experimental changes.

On the other hand, we also suggest regulating the level of wild type MinD or MinE expressed on plasmids to get different oscillation periods and to check if the ratio of MinD to MinE correlates to division waiting time. Our experiments with labeled MinD and MinE expressed at the original location on the chromosome showed that, on the individual cell level, the ratio of MinD to MinE is related to the inter division time. In a next series of experiments the expression of MinD or MinE could be regulated without tagging them fluorescently. This would allow us to track the chromosome segregation by fluorescent protein and check the division waiting time without risking a large overlap of the fluorescent spectra. One experiment also showed the change of the N-terminal of MinE will also change the oscillation frequency [27]. So another option could be getting different oscillation frequency by changing the sequence of MinE. From the information obtained in this way combined with a theoretical simulation of the oscillation of the Min proteins, the rate of septum formation could be estimated from the distribution of the average concentration of MinCDE and the oscillation frequency. These can replace the septum formation rate function we are using now in Model 4.

To test the model in a better way, we need larger data set from experiment. To do this in a more automated way it would be necessary to develop a numerical method to find and contour

cells in the microscope phase-contrast photos. However, this is a quite challenging task. If two cells are too close, they look like fused to each other. Trying to get the contour according to the gray value of pixels will not work in such a scenario. Using gradients of the gray value might improve the results a bit, but probably won't be sufficient. This situation gets even worse after several generations, because one cell will form a colony of four or eight cells in close proximity. A long filamentous cell has a similar problem: because the gray value changes a lot over the length the program might treat the long filamentous cell as several short cells. Another problem is tracking cell divisions. Although the cells on the slide are not motile, they also change their position when being pushed by another cell's growth. So the program has to include tracking of the cell motion.

A possible solution to the first problem is to take the shape of the cell into account. The situation of wild type is easier because all cells have a similar length and all look rod shaped. However, the filament cells of *minB*⁻ strains sometimes are bent several times. Trying to capture the cap shape of the cell poles might be a good first attempt. Although there is some software that can solve part of our problem here, a cell recognition program perfectly suitable for this is still very challenging but would be very useful.

To sum up, based on this work, we can get deeper understanding on the timing of cell division and the chromosome segregation. The complete and detailed understanding of the Min system in *E.coli* will be very helpful to understand division timing in all kinds of microorganisms.

Appendix A

Materials and Methods

A.1 Materials

Reagents, antibiotics, enzymes and kits which were used in this study are listed in Table.A.1, including the respective supplier. Technical equipment and software to analyse the data is listed in Table.A.2.

Table A.1 – Chemicals and kits

Reagents	Supplier
Pure chemicals	Roth (Karlsruhe), Merck (Darmstadt), Sigma-Aldrich (Taufkirchen)
Media components, agar	Roth (Karlsruhe), Merck (Darmstadt), Difco (Heidelberg), Invitrogen (Darmstadt)
Antibiotics	
Kanamycin sulfate	Roth (Karlsruhe)
Chloramphenicol	Roth (Karlsruhe)
Ampicillin sodiumsulfate	Roth (Karlsruhe)
Enzymes	
<i>PfuUltratmIIDNA – Polymerase</i>	Stratagene (Amsterdam)
T4-DNA-Ligase	MBI Fermentas (St. Leon-Rot)
Kits	
DNA purification (Plasmid DNA), PCR purification, Gel purification	Zymo Research (Freiburg), Qiagen (Hilden)

E.coli cells were cultivated in LB/M9 Media and on LB plate, M9 is mainly used for the Microscope experiment, in this study, glucose in M9 is replaced by glycerol and Casamino

Table A.2 – Equipment and software

Application	Device	Manufacturer
Cell disruption	Branson sonifier	Heinemann (Schwaebisch Gmuend)
Centrifugation	RC 5B plus, Ultra Pro 80, Multifuge 1 S-R, Biofuge frasco, Biofuge pico	Sorvall/Thermo Scientific (Dreieich) Heraeus/Thermo Scientific (Dreieich)
PCR	MasteCycler personal MasteCycler epgradient	Eppendorf (Hamburg)
Electroporation	GenePulser Xcell	Bio-Rad (Munche)
Imaging	Leica DM6000B and DM	Leica Microsystems (Wetzlar)
Determination of optical densities	Ultrospec 2100 pro spectrophotometer	Amersham Biosciences (Muenchen)
Determination of nucleic acids absorption	Nanodrop ND-1000 UV-Vis spectrophotometer	Nanodrop (Wilmington)
DNA illumination and documentation	UVT 20 LE UV table	Herolac (Wiesloch)
Fluorescence microscopy data analysis	Metamorph®v 7.5 Image-Pro®6.2 ImageJ	Molecular Devices (Union city, CA) MediaCybernetics (Bethesda, MD) National Institutes of Health (US)
Checking sequences, sequence alignments	Vector NTI advance software, suite 11	Invitrogen (Darmstadt)

acid is added. Composition of media is described in Table.A.3.

Table A.3 – Media

Medium	Composition
<i>E.coli</i>	
Luria-Bertani (LB)	1% (w/v) tryptone, 0.5% (w/v) yeast extract, 1% (w/v) NaCl
LB agar plates	LB medium, 1% (w/v) agar
M9(Recipes for 1 Liter)	Mix 8.501g $\text{Na}_2\text{HPO}_4 - 2\text{H}_2\text{O}$, 3g KH_2PO_4 , 0.5g NaCl and 1g NH_4Cl in 750 ml H_2O Adjust the pH to 7.4 with 10 M NaOH . Adjust the volume to 1 liter with H_2O . Sterilize by autoclaving and cool to room temperature. Add 2ml 1M $\text{MgSO}_4 - 7\text{H}_2\text{O}$, 0.1ml 1M CaCl_2 . Sterilize by filtration and store at room temperature. Add 25ml 20% glycerol and 50ml 20% Casamino Acid which are sterilized by filtration.
LB for looping out the plasmid from chromosome	1% (w/v) tryptone, 0.5% (w/v) yeast extract, 10% Sucrose
LB plate for looping out the plasmid from chromosome	1% (w/v) tryptone, 0.5% (w/v) yeast extract, 10% Sucrose, 1% (w/v) agar
<i>M.xanthus</i>	
1% CTT	1% (w/v) Bacto™ casitone, 10 mM $\text{Tris} - \text{HCl}$ pH 8.0, 1 mM potassium phosphate buffer pH 7.6, 8 mM MgSO_4
1% CTT agar plates	1% CTT medium, 1.5% agar
Microscopy	
M9 microscopy agar	M9 medium, 1% agar

For selection antibiotics have been added if needed (Table.A.4). To induce the proteins Isopropyl β -D-1-thiogalactopyranoside (IPTG) was added.

Table A.4 – Additives

Additive	Stock solution (dissolved in)	Final concentration
<i>E.coli</i>		
Ampicillin sodium sulfate	100mg/ml in H ₂ O	100µg/ml
Kanamycin sulfate	50mg/ml in H ₂ O	50µg/ml
IPTG	1M in H ₂ O	5µM

A.2 Methods

A.2.1 Cultivation of *E.coli*

E.coli cells were grown in LB liquid suspension or on plates containing LB supplemented with 1.5% agar at 37 °C . When appropriate, antibiotics were added at the concentrations showed in A.4. Liquid cultures were incubated shaking with 220 rpm at 37 °C . The cultures prepared for microscope experiment were grown in M9 [116], incubated shaking with 170 rpm at 30°C . The solid media included 1% agar. In order to induce FtsZ-YFP in pJC68, 5µM is added to the liquid or solid media, and 50 µg/ml ampicillin is also used. Other media we used is Luria Broth (LB) Media supplemented with 0.2% glucose, M9 Media, M9 Media with 0.5% glycerol instead of glucose.

A.2.2 Storage of *E.coli*

E.coli strains were kept on plates for short time storage at 4°C . For long time storage strains were grown to an OD600 > 1, and after adding 50% Glycerol (200µl Glycerol + 200µl culture) the cells were quickly frozen in liquid nitrogen and then stored at -80°C .

A.2.3 Polymerase chain reaction (PCR)

Amplification of specific DNA fragments was performed in 50 µl reaction volume using *Pfu-UltraII*-polymerase (Stratagene, Amsterdam) with either the provided buffer or Buffer J (Epicentre). The PCR reaction mix was prepared as shown in Table.A.5

Table A.5 – PCR reaction mix

Genomic DNA or Plasmid DNA	1 μ l
10 μ M Primer (each)	1 μ l
10mM dNTPs (each)	1 μ l
10 \times <i>PfuII</i> Ultra buffer	5 μ l
DMSO	5 μ l
<i>PfuUltraII</i> Polymerase	0.5 μ l
H ₂ O (HPLC)	36.5 μ l

Alternatively, 2 \times Buffer J (Epicentre) was used instead of 10 \times *PfuII* Ultra buffer, already containing 10 mM dNTPs (each).

For Check PCR to test plasmid integration or in-frame deletions, colony PCR were conducted in 20 μ l reaction volume using Eppendorf®MasterMix (Eppendorf), containing *Taq* polymerase. The PCR reaction mix was prepared as shown in Table.A.6.

Table A.6 – PCR reaction mix

Crude Genomic DNA	3 μ l
10 μ M Primer (each)	1 μ l
2.5 \times Master Mix	8 μ l
DMSO	2 μ l
H ₂ O (HPLC)	6 μ l

The PCR programs used in this study are represented in Table.A.7. PCR conditions were modified based on the predicted primer annealing temperature (T_m) and expected product sizes. Depends on the sequence of primers, the primer annealing temperature is modified. Depends on the gene length, the elongation time is also modified.

PCR product size was verified by agarose gel electrophoresis. Correct PCR products were either directly purified using DNA Clean & Concentrator-5 kit or extracted from the agarose gel and purified with Gel Recovery Kit (ZymoResearch Hiss Diagnostics).

Table A.7 – PCR programme (Standard/Check PCR)

Step	Temperature	Time	
Initial denaturation	94°C	5 min	
Denaturation	94°C	1 min	30 cycles
Primer annealing	~57°C	45 sec	
Elongation	72°C	~ 2min	
Final elongation	72°C	3min	
Hold	4°C		

A.2.4 Agarose gel electrophoresis

Nucleic acid fragments were separated by size using agarose gel electrophoresis at 120 V in TAE buffer (Invitrogen). Ethidium bromide was added to agarose in the final concentration of 0.01% (v/v). DNA samples were mixed with 5× sample loading buffer (Bioline). Agarose gels were imaged using 2UV transilluminator (UVP-Bio-Doc-It-System, UniEquip) at 365 nm.

A.2.5 Restriction and ligation of DNA fragments

For restriction, Plasmid DNA or PCR products were incubated with restriction endonucleases for 1 hour up to 3 hours at 37°C (for some special enzymes, the temperature are also different), according to the specific requirements for the enzyme used, and the correct buffer can be find from the respective company's database on internet. Restricted DNA was purified with DNA Clean&Concentrator kit or Gelpurification kit according to the instructions (ZymoResearch Hiss Diagnostics). Ligation reactions were performed with T4 DNA ligase. DNA fragments were ligated into vectors applying 3 to 5 folds molar excess of insert DNA. The ligation reaction was ligated for 2 hours at room temperature or at 18°C over night, followed by the inactivation of the enzyme at 65°C for 10 min.

A.2.6 DNA sequencing

For sequencing purified plasmids or PCR products were sent to Eurofins MWG Operon as recommended by the company; Sequencing Primer were either sent additionally or provided by

Eurofins MWG Operon. Received DNA sequences were analyzed using Vector NTI Advance suite 11 (Invitrogen).

A.2.7 Preparation of chemical- and electrocompetent *E. coli* cells

To prepare electrocompetent *E. coli* cells, overnight cultures were diluted 1:200 to inoculate 1 liter of LB medium. Cells were grown at 37°C on horizontal shakers at 230 rpm. At OD₆₀₀ from about 0.3 to 0.5 cells were harvested by centrifugation at 4700 rpm for 20 min at 4°C. The cell pellet was resuspended in 500 ml ice-cold sterile 10% glycerol and centrifuged again. The washing steps were carried out with 10% glycerol and repeated with 100 ml, 50 ml and 10 ml volumes. Final cell pellet was resuspended in 2 ml sterile 10% glycerol, 50 µl aliquots were fast frozen in liquid nitrogen and stored at -80°C for later use.

A.2.8 Transformation of *E. coli* cells

For electroporation, 10 µl to 15 µl of heat-inactivated ligation reaction plasmid DNA were first dialysed against sterile water (VSWP membrane from Millipore) for 30 min and then added to 50 µl electrocompetent *E. coli* cells on ice. The mixture was transferred into an electroporation cuvette (Bio-Rad, Munchen) and pulsed with 1.8 kV, 25 µF and 200 Ω. Then 1 ml LB medium was added; the suspension was transferred into a sterile plastic tube and incubated for 1 hour at 37°C shaking at 220 rpm. After 1 hour incubation cells were harvested by centrifugation at 4000 rpm for 3 min to 5 min, resuspended in 50 µl to 100 µl of LB medium and plated on LB agar plates containing appropriate antibiotics. The plates were incubated at 37°C overnight; grown colonies were transferred onto fresh agar plates and screened for the presence of the plasmid containing the insert by restriction digestion with subsequent agarose gel electrophoresis. For sequencing obtained constructs were sent to Microfins MWG Operon; received DNA sequences were analyzed using Vector NTI Advance suite 11 (Invitrogen).

A.2.9 The construction of the plasmid for homologous recombination

Depending on the way we labeled the protein, a 300bp to 500 bp sequence from the upstream or downstream of the gene of interest is amplified by primers A and B, including the linker.

Part or the whole sequence of the gene interested is amplified by primers C and D, and the sequence of fluorescent protein is amplified by primers E and F. In the end, these three fragments (AB,CD and EF) will be ligated on vector pNPTS138-R6KT, so that the appropriate restriction enzymes cutting sites sequence and the start/stop codon are included in the primers. After every ligation reaction, the plasmid is checked by PCR and the sizes of the products are compared by agarose gel electrophoresis. The plasmids are checked by sequencing in the end before transformation. (Here is a general procedure and therefor the primers are named with letters A to D as place holders. It is the same in below.)

A.2.10 Homologue recombination and looping out the plasmid from the chromosome

The vector contains fragments AB,EF,CD together are transformed into cells and then plated on LB plate with Kanamycin. In the second day, only the cells with the plasmid on the chromosome can form colonies. Several colonies are picked up, and grown in LB medium without NaCl at 30°C shaking with 220 rpm for 1 hour . Then different dilution products were plated on LB plates (without NaCl and with 10% Sucrose). Only the cells where the plasmid is looped out successfully can survive and form colonies on this LB plate (without NaCl and with 10% Sucrose) after overnight. In the third day, around 30 to 50 colonies were picked up and cultivated overnight on two types of LB plates, one is without NaCl but with 10% Sucrose, the other one is without NaCl but with Kanamycin. In the fourth day, the cells which form colonies on the sucrose plate but can not form colonies on Kanamycin plate were picked up and checked by PCR and sequencing to make sure that the correct part of the plasmid is looped out.

A.2.11 The microscopy and measurement

The microscope we used is Leica DM6000B, and we facilitated a stage heater to keep the temperature of the slide constant. The temperature of the stage heater itself is regulated by a water bath (ministat CC3) and a feedback system. The slide is made of aluminum and with a hole in the middle. The solid media will be put in the hole and covered by cover slips on both sides. This design and material of the slide can help the stage heater control the temperature of

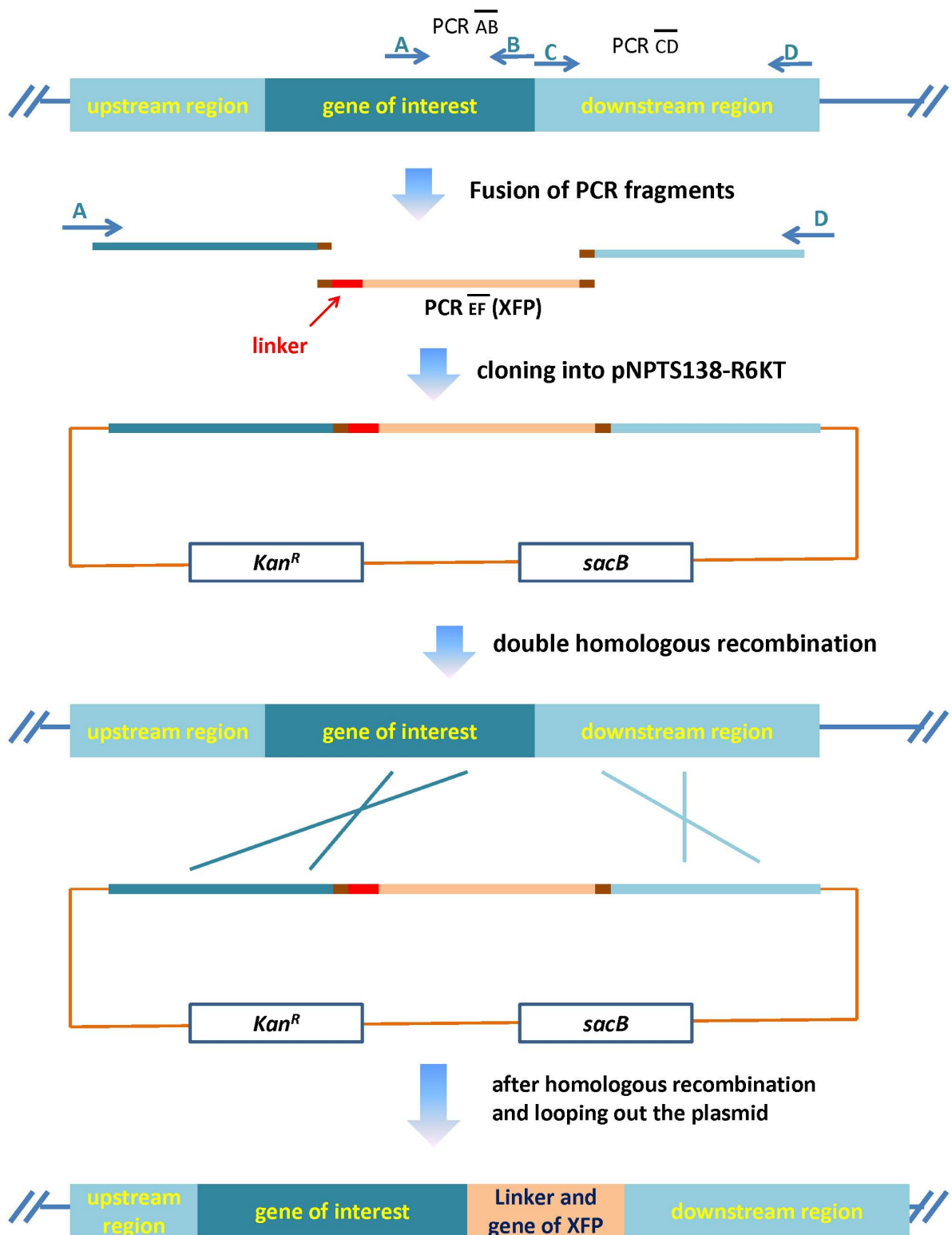


Figure A.1 – Strategy to generate in frame fusion in *E. coli*. Details in the text.

the solid media. We learned the design of slide from personal communication with Barbara Di Ventura. And the stage heater was designed and made by Mr.Reinhard Boecher and Mr.Horst Hensenling.

The cells in the photos were measured with ImageJ software. The cell lengths and the chromosome cluster lengths are measured by the straight/segment line selections tool and the cell outlines were manually marked with the freehand selections tool, so that the relative density of the fluorescence mCherry and Venus in cells can be estimated according to the intensity in within this area and we use them to estimate the relative density of MinD and MinE. To estimate the relative density of FtsZ in the cell, we just measured the intensity on the cell length with the straight/segment line selections tool of ImageJ, and the same to the place where the Z-ring formed, but for Z-ring, we measure the intensity on the diameter of Z-ring, which is the width direction of the cell.

A.3 strains and plasmids

TB28/TB43 Hu-GFP/mCherry: Strain TB28/TB43 with hupB has been fused with fluorescent protein on the chromosome at the native site. In order to achieve this, three PCR fragments were amplified, the AB fragment, the C-terminal part sequence of hupB is amplified from E.coli chromosome with the primers hupBprimerA and hupBprimerB, the CD fragment, the downstream region of hupB is amplified from E.coli chromosome with the primers hupBprimerC and hupBprimerD, and the egfp/mCherry sequence which is amplified with the primers GFPfw and GFPrv from the plasmids pGFPC-2 or pCHYC-2. These three fragments are ligated with the order from AB fragment to fluorescent protein to CD fragment on plasmid pBlueskript II SK-. A fragment containing those three fragments is generated by digesting the plasmid with BamH I and EcoR I and insertion to the plasmid pNPTS138-R6KT which has also been digested by BamH I and EcoR I. The plasmid is then transformed into TB28/TB43, and the fluorescent protein sequence is finally fused to hupB on the chromosome by homologous recombination.

TB28 mCherry-MinD MinE-venus: This strain produces MinD labeled by mCherry (red

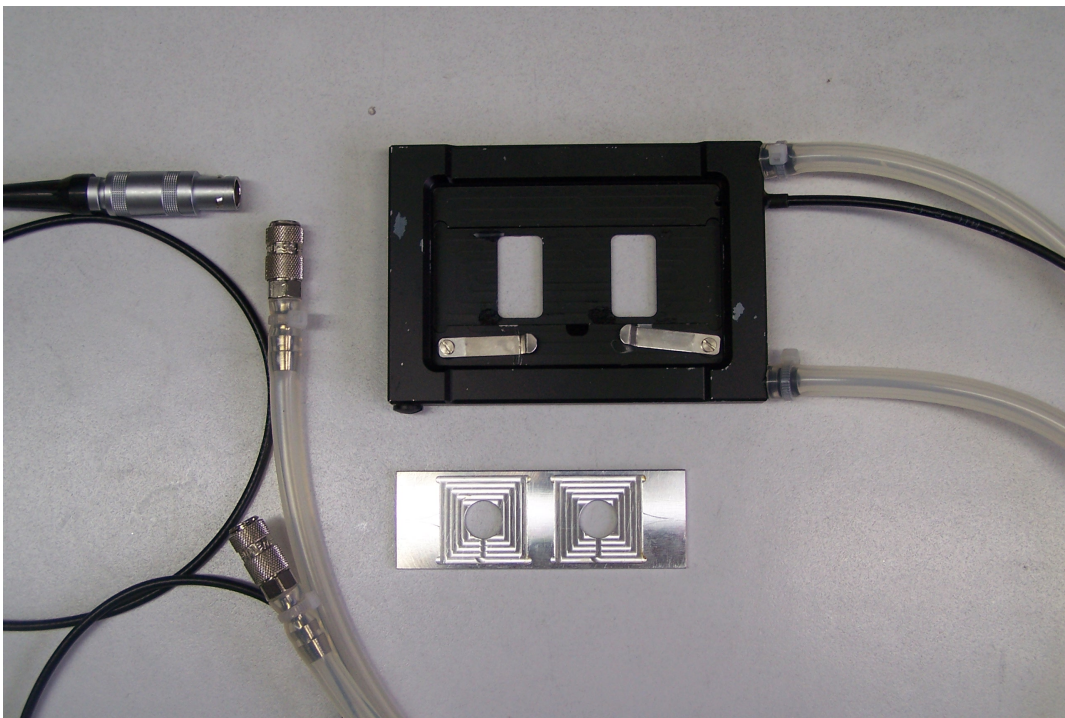
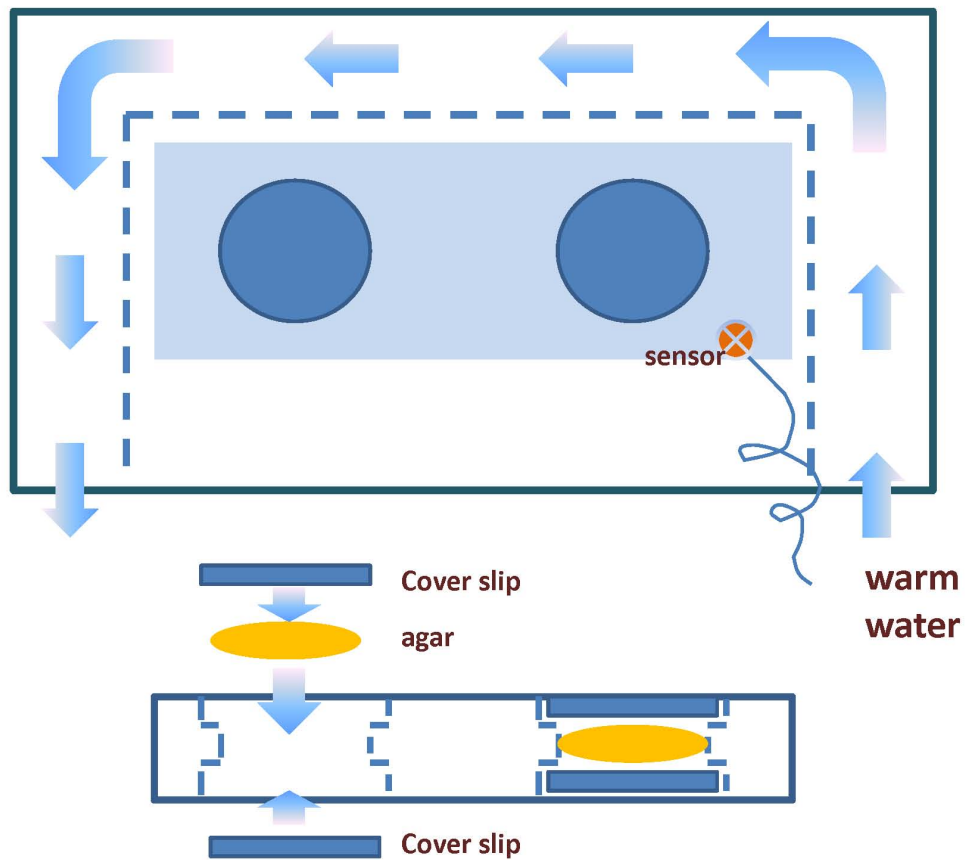


Figure A.2 – The structure of the stageheater and the slide. It is designed and made by Mr.Reinhard Boecherand Mr.Horst Hensenling.

fluorescent protein) and MinE labeled by Venus (yellow fluorescent protein). These two Min proteins were labeled one by one. The upstream region of minD and the 5' end of minD were first amplified from E.coli chromosome with the primers US-minD-up-XhoI, US-minD-down-ClaI, minD-up-EcoRI and minD-down-BamHI. Then the mCherry sequence from the plasmid pCHYC-2 was amplified with the primers XFP-linker-up-ClaI and XFP-linker-down-EcoRI. These three fragments were ligated on the plasmid pBlueskript II SK- as mentioned above. Then a fragment containing those three fragments is generated by digesting the plasmid with Apa I and BamH I and inserted into the plasmid pNPTS138-R6KT which was also digested by the same enzymes. The plasmid is then transformed into TB28, and the fluorescent protein sequence is finally fused to the 5' end of minD sequence on the chromosome by homologous recombination. Then with the primers minE-up-XhoI, minE-down-ClaI, XFP-up, Pvcn-down-EcoRI, DS-minE-up-EcoRI and DS-minE-down-BamHI, the 3' end sequence of minE, the fluorescent protein Venus sequence and the downstream region of minE from E.coli chromosome were amplified and ligated on the plasmid pBlueskript II SK- as a whole fragment. Then with the same way, enzymes and plasmid pNPTS138-R6KT, the Venus sequence was fused to the 3' end of minE on E.coli chromosome.

Then the plasmids are looped out as described in A.2.10. (All the primers used above are shown in Table.A.9 and the strains involed are shown in Table.A.8.)

A.4 Simulation

The simulation of the models started with 1000 randomly initialized cells with different number of chromosomes and cell lengths at time $t = 0$. Each cell contains one or several compartments, according to how many chromosomes it has. To determine when the chromosome is ready to segregate, we keep track of t_c , which is initialized by

$$t_c = T \cdot \frac{\ln L_d - \ln L_s}{\ln 2}. \quad (\text{A.1})$$

L_s, L_d are the starting and ending length of the corresponding compartment, T is the dou-

Table A.8 – Strains and plasmids

Strain	Description	Source
TB28	MG1655 <i>lacZYA<>frt</i>	(Bernhardt and Boer, 2003 [103])
TB43	TB28 <i>minCDE<>frt</i>	(Bernhardt and Boer, 2005 [46])
TB28 Hu-GFP	TB28 <i>hupB<>hupB-egfp</i>	This work
TB43 Hu-GFP	TB43 <i>hupB<>hupB-egfp</i>	This work
TB28 Hu-mCherry	TB28 <i>hupB<>hupB-mCherry</i>	This work
TB43 Hu-mCherry	TB43 <i>hupB<>hupB-mCherry</i>	This work
TB28 mCherry-MinD	TB28 <i>jinD<>mCherry-minD</i>	This work
TB28 MinE-venus	TB28 <i>minE<>minE-venus</i>	This work
TB28 mCherry-MinD &MinE-venus	TB28 <i>minD<>mCherry-minD</i> <i>minE<>minE-venus</i>	This work
DH5 α pir	80 <i>dlacZ</i> M15 (<i>lacZYA-argF</i>)U196 <i>recA1</i> <i>hsdR17 deoR thi-1 supE44 gyrA96 relA1/pir</i>	(Miller and Mekalanos, 1988 [112])
pJC68	P ₂₀₈ - <i>ftsZ-eyfp</i>	(Jon Beckwith, 2001 [109])
pBluescript II SK-	cloning vector	Fermentas
pNPTS138-R6KT	<i>mobRP4⁺ori⁻R6K sacB</i>	(Lassak et al, 2010 [115])
pCHYC-2		(Thanbichler, Iniesta and Shapiro, 2007 [113])
pVENC-2		
pGFPC-2		

Table A.9 – Primers

Name	Sequence(5-3)
hupBprimerA	atcggGGATCCATCTCTAAAGCTGCGGCTGGC
hupBprimerB	atcggCCCGGGGTTTACCGCGTCTTTCAGTGCT
hupBprimerC	atcggCTGCAGgcggtgccccagtgg
hupBprimerD	atcggGAATTCCGGCGTAGTTATTGCCTCCG
GFPfw	atcggCCCGGGgccggcgggagccggccgatccATGGTGAGCAAGGGCGAGGA
GFPrv	atcggCTGCAGTTACTTGTACAGCTCGTCCATGCC
US-minD -up-XhoI	ATACTCGAGCGGTTTGCGGGTTATTG
US-minD -down-ClaI	CTAATCGATAGAAATTCCTTGTTAAAAAGGGA
XFP-linker -up-ClaI	CTAATCGATATGGTGAGCAAGGGCGA
XFP-linker -down-EcoRI	CGTGAATTCggatcgccggctccgcccgccgCCTGTACAGCTCGTCCATGC
minD-up-EcoRI	CGTGAATTCGCACGCATTATTGTTGTTACTT
minD-down -BamHI	ATTGGATCCAGACTTCCGGGTTGGTG
minE-up-XhoI	ATACTCGAGATGGCATTACTCGATTTCTTT
minE-down-ClaI	CTTATCGATTTTCAGCTCTTCTGCTTCC
XFP-up	atcggATCGATgccggcgggagccggccgatccATGGTGAGCAAGGGCGAGGA
Pvenc-down -EcoRI	CGTGAATTCTTACTTGTACAGCTCGTCCA
DS-minE -up-EcoRI	ATAGAATTCGCCCCGCTGTAAAAGCG
DS-minE -down-BamHI	TAAGGATCCCAAAAAAAGCCCGCC

bling time. A simulation step represents one time step and in every time step t_c is reduced by one for all compartments, cell length is increased by ΔL , calculated by Eq.2.1. At a given time all chromosomes with $t_c = 0$ are duplicated completely and ready to segregate. And so a new potential division site formed in each corresponding compartment. In model 1, those chromosomes and corresponding compartments will divide. In model 2-4, random numbers r_x from zero to one are distributed to those potential division sites and compared to thresholds R_t . Those ones with numbers larger than threshold will be blocked and the corresponding chromosome will not segregate. They wait until another potential division site in the same cell is formed. The thresholds are set according to the total number of blocked and new formed potential division sites. For example, for a cell with n_x potential division sites were blocked, when a new one formed,

$$R_t = \frac{n_x + 1 - 2}{n_x + 1} = \frac{n_x - 1}{n_x + 1}. \quad (\text{A.2})$$

This will make sure there are two potential division sites are blocked on average in each cell. The unblocked division sites are available for cell division. In model 4, all the available division sites are initialized with division waiting times T_w drawn from a normal distribution (17.7 ± 12 min). A simulation step represents one time step and in every time step T_w is reduced by dx/dt , which is calculated by Eq.2.13. In other models, T_w is drawn from different distribution (47 ± 35.7 min for non-polar sites and 76 ± 34 min for polar sites) and reduced by one in every time step. At a given time cells with division sites whose $T_w=0$ divide into two daughter cells. After cell divides, new cell poles formed, the program selects again which potential division sites will be blocked according to Eq.A.2.

To mimik the presence of noise in division site placement, L_s is drawn from normal distribution (1812 ± 18 nm), and the difference of L_s of two compartments divided from one mother compartment is smaller than 10% of L_d of their mother compartment. The cell division occurs at the same position where compartments divide, which is determined by L_s . When the cell number of the whole system is larger than 10000, program randomly selects 30% of them to continue the simulation.

For the simulations custom written C-programs were used.

List of Figures

1.1	The comparison of inter-division times.	4
2.1	OD plots.	13
2.2	OD plots.	14
2.3	cell division waiting time	14
2.4	Snapshot of growing population	15
2.5	Division waiting time distribution	16
2.6	OD curve as determined from the simulations.	17
2.7	Rescaled cell length increment as function of rescaled time.	20
2.8	The dependence of length increment rate on cell length.	22
2.9	The distribution of doubling time of wild type strain.	23
2.10	The cell number and chromosome cluster number curves in log scale plot.	24
2.11	The cell number and chromosome cluster number curves in log scale plot.	25
2.12	The distribution of cell length of wild type newborn cells.	26
2.13	Time dependence of the fraction of cells with zero to four chromosomes.	27
2.14	The time dependence of the fraction of cells.	28
2.15	Cell length distribution of a growing population.	30
2.16	The distribution of inter-division time of different types of cell division.	32
2.17	The time dependence of the fraction of cells.	34
2.18	The cell length distribution.	34
2.19	The waiting time distribution of <i>minB</i> ⁻ for polar and non-polar sites.	35
2.20	The distribution of inter-division time of different types of cell division.	37

2.21	The disturbance of chromosome segregation.	38
2.22	The division map for experiment culture.	39
2.23	Time dependence of the number of division sites per cell length.	39
2.24	The expected and observed number of chromosome cluster.	40
2.25	The blocking potential division sites.	41
2.26	The time dependence of the fraction of cells.	42
2.27	The cell length distribution.	43
2.28	The waiting time distribution of <i>minB</i> ⁻ for polar and non-polar sites.	43
2.29	The distribution of inter-division time of different types of cell division.	44
2.30	The time dependence of the fraction of cells.	45
2.31	The cell length distribution.	46
2.32	The waiting time distribution of <i>minB</i> ⁻ for polar and non-polar sites.	46
2.33	The distribution of inter-division time of different types of cell division.	47
2.34	The waiting time distribution of <i>minB</i> ⁻ for polar and non-polar sites.	49
2.35	The cell photos and the division map.	50
2.36	The FtsZ ring measurement.	51
2.37	fraction of Z protein on Z-ring in both strains.	53
2.38	The time dependence of the fraction of cells.	55
2.39	The cell length distribution.	55
2.40	The waiting time distribution of <i>minB</i> ⁻ for polar and non-polar sites.	56
2.41	The distribution of different types of cell division.	57
2.42	The time dependence of the fraction of cells.	58
2.43	The cell length distribution of WT cells.	58
2.44	The waiting time distribution of WT cells.	59
2.45	The distribution of cells according to time left to divide.	60
2.46	The oscillation of labeled MinD and MinE.	61
2.47	The correlation between the inter-division time and the level of MinD to MinE.	62
2.48	The cell length distribution of <i>minB</i> ⁻ with the FtsZ concentration doubled.	65
A.1	Strategy to generate in frame fusion in E.coli.	87

A.2 The structure of the stageheater and the slide. 89

List of Tables

2.1	The average doubling times calculated from the growth curves in Fig.2.1. . . .	12
2.2	Cell division history of individual cells as obtained experimentally and from model 1. All cell divisions within ~ 200 minutes are classified into 5 types according to the position of two successive cell divisions. Rows represent the location of the first division event, columns location of the second event. Time in parenthesis represents mean time difference \pm standard deviation between the division events.	31
2.3	Cell division history of individual cells as obtained experimentally and from model 1P. All cell divisions within about 200 minutes are classified into 5 types according to the position of two successive cell divisions. Rows represent the location of the first division event, columns location of the second event. Time in parenthesis represents mean time difference \pm standard deviation between the division events.	36
2.4	Cell division history of individual cells as obtained experimentally and from model 2. All cell divisions within ~ 200 minutes are classified into 5 types according to the position of two successive cell divisions. Rows represent the location of the first division event, columns location of the second event. Time in parenthesis represents mean time difference \pm standard deviation between the division events.	42

2.5	Cell division history of individual cells as obtained experimentally and from model 3. All cell divisions within about 200 minutes are classified into 5 types according to the position of two successive cell divisions. Rows represent the location of the first division event, columns location of the second event. Time in parenthesis represents mean time difference \pm standard deviation between the division events.	48
2.6	The average of different time distributions. The average values for division waiting time and Z-ring existence time of different types of division sites shown in Fig.2.36 are calculated. The second column is corresponding the solid lines in Fig.2.36b, and the third one is corresponding to the dash lines.	52
2.7	Cell division history of individual cells as obtained experimentally and from model 4. All cell divisions within \sim 200 minutes are classified into 5 types according to the position of two successive cell divisions. Rows represent the location of the first division event, columns location of the second event. Time in parenthesis represents mean time difference \pm standard deviation between the division events.	54
A.1	Chemicals and kits	79
A.2	Equipment and software	80
A.3	Media	81
A.4	Additives	82
A.5	PCR reaction mix	83
A.6	PCR reaction mix	83
A.7	PCR programme (Standard/Check PCR)	84
A.8	Strains and plasmids	91
A.9	Primers	92

Bibliography

- [1] Andrew W. Murray (2004) Recycling the cell cycle: cyclins revisited. *Cell* 116, 221-234. 1
- [2] Michael T. Laub, Harley H. McAdams, Tamara Feldblyum, Claire M. Fraser, Lucy Shapiro (2000) Global analysis of the generic network controlling a bacterial cell cycle. *Science* 290, 2144-2148. 1
- [3] Emanuele G. Biondi, Sarah J. Reisinger, Jeffrey M. Skerker, Muhammad Arif, Barrett S. Perchuk, Kathleen R. Ryan and Michael T. Laub (2006) Regulation of the bacterial cell cycle by an integrated genetic circuit. *Nature* 444, 899-904
- [4] Antonio A. Iniesta, Patrick T. McGrath, Ann Reisenauer, Harley H. McAdams and Lucy Shapiro (2006) A phospho-signaling pathway controls the localization and activity of a protease complex critical for bacterial cell cycle progression. *Proc.Natl Acad.Sci USA*103(29), 10935-10940. 1
- [5] Peter Lenz and Lotte Søgaard-Andersen (2011) Temporal and spatial oscillations in bacteria. *Nature Reviews Microbiology*, 9. 565-577. 1, 67, 73
- [6] Michael T. Laub, Lucy Shapiro and Harley H. McAdams (2007) Systems biology of *Caulobacter*. *Annu. Rev. Genet.* 41, 429-441. 2
- [7] Urs Jenal (2009) The role of proteolysis in the *Caulobacter crescentus* cell cycle and development. *Res. Microbiol.* 160, 687-695.
- [8] Harley H. McAdams, Lucy Shapiro (2009) System-level design of bacterial cell cycle control. *FEBS Lett.* 583, 3984-3991. 2

- [9] Masato Nakajima, Keiko Imai, Hiroshi Ito, Taeko Nishiwaki, Yoriko Murayama, Hideo Iwasaki, Tokitaka Oyama, Takao Kondo (2005) Reconstitution of circadian oscillation of cyanobacterial KaiC phosphorylation in vitro. *Science* 308, 414-415. 2
- [10] Ximing Qin, Mark Byrne, Yao Xu, Tetsuya Mori, Carl Hirschie Johnson (2010) Coupling of a core post-translational pacemaker to a slave transcription/translation feedback loop in a circadian system. *PLoS Biol.* 8, e1000394. 2
- [11] Simone Leonardy, Mandy Miertzschke, Iryna Bulyha, Eva Sperling, Alfred Wittinghofer and Lotte Sogaard-Andersen (2010) Regulation of dynamic polarity switching in bacteria by a Ras-like G-protein and its cognate GAP. *The EMBO Journal* 29, 2276-2289. 2
- [12] Yong Zhang, Michel Franco, Adrien Ducret, Tam Mignot (2010) A bacterial Ras-like small GTP-binding protein and its cognate GAP establish a dynamic spatial polarity axis to control directed motility. *PLoS Biol.* 8(7), e1000430. 2
- [13] Gitte Ebersbach, Simon Ringgaard, Jakob Møller-Jensen, Qing Wang, David J. Sherratt and Kenn Gerdes (2006) Regular cellular distribution of plasmids by oscillating and filament-forming ParA ATPase of plasmid pB171. *Molecular Microbiology* 61(6), 1428-1442. 2
- [14] Simon Ringgaard, Jeroen van Zon, Martin Howard and kenn Gerdes (2009) Movement and equipositioning of plasmids by ParA filament disassembly. *Proc.Natl Acad.Sci USA*106(46), 19369-19374. 2
- [15] Jerod L. Ptacin, Steven F. Lee, Ethan C. Garner, Esteban Toro, Michael Eckart, Luis R. Comolli, W. E. Moerner and Lucy Shapiro (2010) A spindle-like apparatus guides bacterial chromosome segregation. *Nature Cell Biol.* 12, 791-798. 2
- [16] Whitman B Schofield, Hoong Chuin Lim and Christine Jacobs-Wagner (2010) Cell cycle coordination and regulation of bacterial chromosome segregation dynamics by polarly localized proteins. *The EMBO Journal* 29, 3068-3081. 2

-
- [17] Joe Lutkenhaus (2007) Assembly dynamics of the bacterial MinCDE system and spatial regulation of the Z ring. *Annu. Rev. Biochem.* 76, 539-562. 2, 67, 73
- [18] Xiaoli Fu, Yu-Ling Shih, Yan Zhang, and Lawrence I. Rothfield (2001) The MinE ring required for proper placement of the division site is a mobile structure that changes its cellular location during the *Escheria coli* division cycle. *Proc.Natl Acad.Sci USA*98, 980-985. 2, 3, 8
- [19] David M. Raskin and Piet A. J. de Boer (1999) Rapid pole-to-pole oscillation of a protein required for directing division to the middle of *Escheria coli* . *Proc.Natl Acad.Sci USA*96, 4971-4976. 8
- [20] Zonglin Hu and Joe Lutkenhaus (1999) Tpoological regulation of cell division in *Escheria coli* involves rapid pole to pole oscillation of the division inhibitor MinC under the control of MinD and MinE. *Molecular Microbiology* 34(1), 82-90. 8
- [21] David M. Raskin and Piet A. J. de Boer (1999) MinDE-dependent pole-to-pole oscillation of division inhibitor MinC in *Escheria coli* . *Journal of Bacteriology*181(2), 6419-6424.
- [22] Cynthia A. Hale, Hans Meinhardt and Piet A. J. de Boer (2001) Dynamic localization cycle of the cell division regulator MinE in *Escheria coli* . *The EMBO Journal* 20(7), 1563-1572. 2
- [23] Erfei Bi and Joe Lutkenhaus (1991) FtsZ ring structure associated with division in *Escheria coli* . *Nature* 354, 161-164. 2
- [24] Xiaolan Ma, David W. Ehrhardt and William Margolin (1996) Colocalization of cell division proteins FtsZ and FtsA to cytoskeletal structures in living *Escheria coli* cells by using green fluorescent protein. *Proc.Natl Acad.Sci USA*93, 12998-13003.
- [25] Joe Lutkenhaus (2002) Dynamic proteins in bacteria. *Curr Opin Microbiol* 5, 548-552.
- [26] Lawrence Rothfield, Aziz Taghbalout and Yu-Ling Shih (2005) Spatial control of bacterial division-site placement. *Nat Rev Microbiol* 3, 959-968. 2

- [27] Zonglin Hu and Joe Lutkenhaus (2001) Topological regulation of cell division in *E.coli* : Spatiotemporal oscillation of MinD requires stimulation of its ATPase by MinE and Phospholipid. *Molecular Cell* 7, 1337-1343. 3, 7, 8, 76
- [28] Piet A. J. de Boer, Robin E. Crossley and Lawrence I. Rothfield (1992) Roles of MinC and MinD in the site-specific septation block mediated by the MinCDE system of *Escheria coli* . *Journal of Bacteriology*174(1), 63-70. 3, 7
- [29] Zonglin Hu and Joe Lutkenhaus (2000) Analysis of MinC reveals two independent domains involved in interaction with MinD and FtsZ. *Journal of Bacteriology*182(14), 3965-3971. 2, 7
- [30] Alex Dajkovic, Ganhui Lan, Sean X. Sun, Denis Wirtz, and Joe Lutkenhaus (2008) MinC spatially controls bacterial cytokinesis by antagonizing the scaffolding function of FtsZ. *Current Biology* 18, 235-244. 2, 8, 71
- [31] Jay E. Johnson, Laura L. Lackner, and Piet A. J. de Boer (2002) Targeting of ^DMinC/MinD and ^DMinC/DicB complexes to septal rings in *Escheria coli* suggests a multistep mechanism for MinC-Mediated Destruction of Nascent FtsZ rings. *Journal of Bacteriology*184(11), 2951-2962. 3, 8
- [32] Sheryl S. Justice, Jorge Garc a-Lara, Lawrence I. Rothfield (2000) Cell division inhibitors Sula and MinC/MinD block septum formation at different steps in the assembly of the *Escheria coli* division machinery. *Molecular Microbiology* 37(2), 410-423. 2, 8
- [33] Zongling Hu, Edward P. Gogol and Joe Lutkenhaus (2002) Dynamic assembly of MinD on phospholipid vesicles regulated by ATP and MinE. *Proc.Natl Acad.Sci USA*99(10), 6761-6766. 3, 8
- [34] Martin Howard, Andrew D. Rutenberg and Simon de Vet (2001) Dynamic Compartmentalization of Bacteria: accurate division in *E.coli* . *Physical Review Letters* 87(27), 278102 3, 60

-
- [35] Hans Meinhardt and Piet A. J. de Boer (2001) Pattern formation in *Escheria coli* : a model for the pole-to-pole oscillations of Min proteins and the localization of the division site. Proc.Natl Acad.Sci USA98(25), 14202-14207.
- [36] Karsten Kruse (2002) A dynamic model for determining the middle of *Escheria coli* . Biophysical Journal 82, 618-627. 4, 60, 67
- [37] Kerwyn Casey Huang, Yigal Meir, and Ned S. Wingreen (2003) Dynamic structures in *Escheria coli* : Spontaneous formation of MinE rings and MinD polar zones. Proc.Natl Acad.Sci USA100(22), 12724-12728. 60, 63, 71
- [38] Donald A. Drew, Mary J. Osborn and Lawrence I. Rothfield (2005) a polymerization-depolymerization model that accurately generates the self-sustained oscillatory system involved in bacterial division site placement. Proc.Natl Acad.Sci USA102(17), 6114-6118. 60
- [39] G Meacci, J Ries, E Fischer-Friedrich, N Kahya, P Schwille and K Kruse (2006) Mobility of Min-proteins in *Escheria coli* measured by fluorescence correlation spectroscopy. Physical Biology 3, 255-263.
- [40] Rex A. Kerr, Herbert Levene, Terrence J. Sejnowski and Wouter-Jan Rappel (2006) Division accuracy in a stochastic model of Min oscillations in *Escheria coli* . Proc.Natl Acad.Sci USA103(2), 347-352.
- [41] Filipe Tostevin and Martin Howard (2005) A stochastic model of Min oscillations in *Escheria coli* and Min protein segregation during cell division. Physical Biology 3, 1-12
- [42] Barbara Di Ventura and Victor Sourjik (2011) Self-organized partitioning of dynamically localized proteins in bacterial cell division. Molecular Systems Biology 7:457. 3, 60
- [43] C. L. Woldringh, E. Mulder, J. A. C. Valkenburg, F. B. Wlentjes, A. Zurisky and N. Nanning (1990) Role of the nucleoid in the toporegulation of division. Res. Microbiol. 141. 39-49. 3, 6, 73

- [44] Xuan-Chuan Yu and William Margolin (1999) FtsZ ring cluster in *min* and partition mutants: role of both the Min system and the nucleoid in regulating FtsZ ring localization. *Molecular Microbiology* 32(2), 315-326.
- [45] Qin Sun, Xuan-Chuan Yu and William Margolin (1998) Assembly of the FtsZ ring at the central division site in the absence of the chromosome. *Molecular Microbiology* 29(2), 491-503. 6, 73
- [46] Thomas G. Bernhardt and Piet A. J. de Boer (2005) SlmA, a nucleoid-associated, FtsZ binding protein required for blocking septal ring assembly over chromosomes in *E.coli* . *Molecular Cell* 18, 555-564. 6, 11, 91
- [47] Jaan Männik, Fabai Wu, Felix J. H. Hol, Paola Bisicchia, David J. Sherratt, Juan E. Keymer and Cees Dekker (2011) Robustness and accuracy of cell division in *Escheria coli* in diverse cell shapes. *Proc.Natl Acad.Sci USA*109, 6957-6962. 3, 6, 18
- [48] Yu-Ling Shih, Xiaoli Fu, Glenn F.King, Trung Le and Lawrence Rothfield (2002) Division site placement in *E.coli* : mutations that prevent formation of the MinE ring lead to loss of the normal midcell arrest of growth of polar MinD membrane domains. *The EMBo Journal* 21(13), 3347-3357. 3, 8
- [49] Yu-Ling Shih, Trung Le, and Lawrence Rothfield (2003) Division site selection in *Escheria coli* involves dynamic redistribution of Min proteins within coiled structures that extend between the two cell poles. *Proc.Natl Acad.Sci USA*100, 7865-7870. 3, 9
- [50] David E. Anderson, Frederico J. Gueiros-Filho, and Harold P. Erichson (2004) Assembly dynamics of FtsZ ring in *Bacillus subtilis* and *Escheria coli* and effects of FtsZ-regulating proteins. *Journal of Bacteriology* 186, 5775-5781. 3, 52, 71
- [51] Swapna Thanedar and William Margolin (2004) FtsZ exhibits rapid movement and oscillation waves in helix-like patterns in *Escheria coli* . *Current Biology* 14, 1167-1173. 3, 6, 71
- [52] Thomas Akerlund, Rolf Bernander and Kurt Nordstroem (1992) Cell division in *Escheria coli minB* mutants. *Molecular Microbiology* 6(15), 2073-2083. 3, 36, 69

- [53] R.M.Teather, J.F.Collins and W.D.Donachie (1974) Quantal behavior of a diffusible factor which initiates septum formation at potential division sites in *Escheria coli* . Journal of Bacteriology 118.407-413. 3
- [54] Adele L. Marston, Helena B. Thomaidis, David H. Edwards, Michaela E. Sharpe and Jeffery Errington (1998) Polar localization of MinD protein of *Bacillus subtilis* and its role in selection of the mid-cell division site. Genes Dev. 12, 3419-3430. 4
- [55] Margaret D. Migocki, Marcelle K. Freeman, R. Gerry Wake and Elizabeth J. Harry (2002) The Min system is not required for precise placement of the midcell Z ring in *Bacillus subtilis*. EMBO Rep. 3, 1163-1167. 4
- [56] Ana I. Prieto, Christina Kahramanoglou, Ruhi M. Ali, Gillian M. Fraser, Aswin S. N. Seshasayee and Nicholas M. Luscombe (2012) Genomic analysis of DNA binding and gene regulation by homologous nucleoid-associated proteins IHF and HU in *Escheria coli* K12. Nucleic Acids Research 40(8), 3524-3537. 5
- [57] Talukder Ali Azam, Akira Iwata, Akiko Nishimura, Susumu Ueda and Akira Ishihama (1999) Growth Phase-dependent variation in protein composition of the *Escheria coli* nucleoid. Journal of Bacteriology 181(20), 6361-6370. 5
- [58] Aline Jaffé, Daniel Vinella, and Richard D'Ari (1997) The *Escheria coli* Histone-like protein HU affects DNA initiation, Chromosome partitioning via MukB, and cell division via MinCDE. Journal of Bacteriology 179(11), 3494-3499. 5
- [59] Muriel Wery, Conrad L. Woldringh, Josette Rouviere-Yaniv (2001) Hu-GFP and DAPI co-localize on the *Escheria coli* nucleoid. Biochimie 83, 193-200. 5, 12, 13
- [60] Yasunobu Kano, Morimasa Wada and Fumio Imamoto (1988) Genetic characterization of the gene *hupA* encoding the HU-2 protein of *Escheria coli* . Gene 69, 331-335. 5
- [61] Yasunobu Kano, Katsuaki Osato, Morimasa Wada, and Fumio Imamoto (1987) Cloning and sequencing of the HU-2 gene of *Escheria coli* . Mol Gen Genet 209,408-410.

- [62] Bernard Laine, Daniel Kmiecik, Pierre Sautiere, Gérard Biserte, and Michel Cohen-Solal (1980) Complete Amino-Acid sequences of DNA-binding proteins HU-1 and HU-2 from *Escheria coli* . Eur. J. Biochem. 103, 447-461. 5
- [63] Laurent Claret and Josette Rouviere-Yaniv (1997) Variation in HU composition during growth of *Escheria coli* : the heterodimer is required for long term survival. J. Mol. Biol. 273, 93-104. 5
- [64] William Margolin (2005) FtsZ and the division of prokaryotic cells and organelles. Nature Reviews Molecular Cell Biology 6, 862-871. 5, 6, 67, 73
- [65] Kevin D. Stokes, Katherine W. Osteryoung (2003) Early divergence of the *FtsZ1* and *FtsZ2* plastid division gene families in photosynthetic eukaryotes. Gene 320, 97-108. 5
- [66] Katherine W. Osteryoung and Jodi Nunnari (2003) The division of endosymbiotic organelles. Science 302, 1698-1704.
- [67] Shin-ya Miyagishima, Hisayoshi Nozaki, Keishin Nishida, Keiji Nishida, Motomichi Matsuzaki, Tsuneyoshi Kuroiwa (2004) Two types of FtsZ proteins in mitochondria and Red-Lineage chloroplasts: The duplication of FtsZ is implicated in endosymbiosis. J Mol Evol 58, 291-303.
- [68] Sue Vaughan, Bill Wickstead, Keith Gull, Stephen G. Addinall (2003) Molecular evolution of FtsZ protein sequences encoded within the genomes of archaea, bacteria, and eukaryota. J Mol Evol 58, 19-39. 5
- [69] Sambra D. Redick, Jesse Stricker, Gina Briscoe, and Harold P. Erickson (2005) Mutants of FtsZ targeting the protofilament interface: effects on cell division and GTPase activity. Journal of Bacteriology 187(8), 2727-2736 5
- [70] Jan Loewe, Linda A. Amos (1998) Crystal structure of the bacterial cell-division protein FtsZ. Nature 391, 203-206. 5

-
- [71] Xiaolan Ma and William Margolin (1999) Genetic and functional analyses of the conserved C-terminal core domain of *Escheria coli* FtsZ. *Journal of Bacteriology* 181(24), 7531-7544. 6
- [72] Xuan-Chuan Yu and William Margolin (1997) Ca²⁺-mediated GTP-dependent dynamic assembly of bacterial cell division protein FtsZ into asters and polymer networks *in vitro*. *The EMBO Journal* 16,5455-5463. 6
- [73] Maria A Oliva, Suzanne C Cordell and Jan Loewe (2004) Structural insights into FtsZ protofilament formation. *Nature Struct. Mol. Biol.* 11, 1243-1250. 6
- [74] Harold P. Erickson, Dianne W. Taylor, Kenneth A. Taylor, and David Bramhill (1996) Bacterial cell division protein FtsZ assembles into protofilament sheets and minirings, structural homologs of tubulin polymers. *Proc.Natl Acad.Sci USA*93, 519-523.
- [75] Jan Loewe and Linda A. Amos (1999) Tubulin-like protofilaments in Ca²⁺ induced FtsZ sheets. *EMBO J.* 18, 2364-2371. 6
- [76] Yaodong Chen, Keith Bjornson, Samba D. Redick, Harold P. Erickson (2005) A rapid Fluorescence assay for FtsZ assembly indicates cooperative assembly with a dimer nucleus. *Biophysical Journal* 88, 505-514. 6
- [77] Jesse Stricker, Paul Maddox, E. D. Salmon, and Harold P. Erickson (2002) Rapid assembly dynamics of the *Escheria coli* FtsZ-ring demonstrated by fluorescence recovery after photobleaching. *Proc.Natl Acad.Sci USA*99(5), 3171-3175. 6, 52
- [78] José Manuel González, Marisela Vélez, Mercedes Jiménez, Carlos Alfonso, Peter Schuck, Jesús Mingorance, Miguel Vicente, Allen P. Minto, and Germán Rivas (2004) Cooperative behavior of *Escheria coli* cell-division protein FtsZ assembly involves the preferential cyclization of long single-stranded fibrils. *Proc.Natl Acad.Sci USA*102, 1895-1900. 6
- [79] Michael R. Caplan and Harold P. Erickson (2003) Apparent cooperative assembly of the bacterial cell-division protein FtsZ demonstrated by isothermal titration calorimetry. *J. Biol. Chem.* 278, 13784-13788. 6

- [80] Guo Fu, Tao Huang, Jackson Buss, Carla Coltharp, Zach Hensel, Jie Xiao (2010) *In Vivo* structure of the *E.coli* FtsZ-ring revealed by photoactivated localization microscopy (PLAM). PLoS ONE 5(9)e12680. 6, 49
- [81] Cynthia A. Hale and Piet A. J. de Boer (1997) Direct binding of FtsZ to ZipA, an essential component of the septal ring structure that mediates cell division in *E.coli* . Cell 88(2), 175-185. 6
- [82] Sebastien Pichoff and Joe Lutkenhaus (2005) Tethering the Z ring to the membrane through a conserved membrane targeting sequence in FtsA. Molecular Microbiology 55(6), 1722-1734. 6
- [83] Sonsoles Rueda, Miguel Vicente, and Jesús Mingorance (2003) Concentration and assembly of the division ring proteins FtsZ, FtsA, and ZipA during the *Escheria coli* cell cycle. Journal of Bacteriology 185(11),3344-3351. 6, 7
- [84] Kang Dai and Joe Lutkenhaus (1992) The proper ratio of FtsZ to FtsA is required for cell division to occur in *Escheria coli* . Journal of Bacteriology 174,6145-6151. 6, 7
- [85] David W. Adams and Jeff Errington (2009) Bacterial cell division: assembly, maintenance and disassembly of the Z ring. Nature Reviews Microbiology 7, 642-653. 6
- [86] Tanneke den Blaauwen, Nienke Buddelmeijer, Mirjam E. G. Aarsman, Cor M. Hameete, and Nanne Nanninga (1999) Timing of FtsZ Assembly in *Escheria coli* . Journal of Bacteriology 181, 5167-5175. 7
- [87] Daisuke Shiomi and William Margolin (2007) A sweet sensor for size-conscious bacteria. Cell 130, 216-218 7
- [88] Olivier Huisman and Richard D'Ari (1981) an inducible DNA replication-cell division coupling mechanism in *E.coli* . Nature 290, 4490-4494. 7
- [89] Olivier Huisman, Richard D'Ari and Susan Gottesman (1984) Cell division control in *Escheria coli* : Specific induction of the SOS function SfiA protein is sufficient to block septation. Proc.Natl Acad.Sci USA 81, 4490-4494 7

-
- [90] Martí Aldea, Teresa Garrido, Jesús Pla and Miguel Vicente (1990) Division genes in *Escheria coli* are expressed coordinately to cell septum requirements by gearbox promoters. The EMBO Journal 9, 3787-3794. 7
- [91] John E. Ward, Jr., and Joe Lutkenhaus (1985) Overproduction of FtsZ induces minicell formation in *E.coli* . Cell 42, 941-949. 7
- [92] Erfei Bi and Joe Lutkenhaus (1989) FtsZ regulates frequency of cell division in *Escheria coli* . Journal of Bacteriology 172,2765-2768. 7, 52, 63, 72, 75
- [93] R Tsukanov, G Reshes, G Carmon, E Fischer-Friedrich, N S Gov, I Fishov and M Feingold (2011) Timing of Z-ring localization in *Escheria coli* . Phys. Biol 8, 066003(13pp). 7
- [94] Elisabeth Fischer-Friedrich, Benjamin M Friedrich and Nir S Gov (2012) FtsZ rings and helices: physical mechanisms for the dynamic alignment of biopolymers in rod-shaped bacteria. Phys. Biol 9, 016009 (10pp). 6, 71
- [95] Jay E. Johnson, Laura L. Lackner, Cynthia A. Hale and Piet A. J. de Boer (2004) ZipA is required for Targeting of ^DMinC/DicB, but not ^DMinC/MinD, complexes to septal ring assemblies in *Escheria coli* . Journal of Bacteriology 186(8), 2418-2429. 8
- [96] Tim H. Szeto, Susan L. Rowland, Cheryl L. Habrukowick, and Glenn F. King (2003) The MinD membrane targeting sequence is a transplantable lipid-binding helix. J. Biol. Chem. 278, 40050-40056. 8
- [97] Zongling Hu, Cristian Saez and Joe Lutkenhaus (2003) Recruitment of MinC, an inhibitor of Z-ring formation, to the membrane in *Escheria coli* : role of MinD and MinE. Journal of Bacteriology 185(1), 196-203. 8
- [98] Laura L. Lackner, David M. Raskin and Piet A. J. de Boer (2003) ATP-dependent interactions between *Escheria coli* Min proteins and the phospholipid membrane in vitro. Journal of Bacteriology 185(3), 735-749. 8

- [99] Lu-Yan Ma, Glenn King and Lawrence Rothfield (2003) Mapping the MinE site involved in interaction with the MinD division site selection protein of *Escheria coli* . Journal of Bacteriology 185(16), 4948-4955. 8
- [100] S. L. Rowland, X. Fu, M. A. Sayed, Y. Zhang, W. R. Cook and L. I. Rothfield (2000) Membrane redistribution of the *Escheria coli* MinD protein induced by MinE. Journal of Bacteriology 182(3), 613-619. 8
- [101] Thomas ÅKERlund, Björn Gullbrand and Kurt Nordström (2002) Effects of the Min system on nucleoid segregation in *Escheria coli* . Microbiology 148, 3213-3222. 4, 69, 75
- [102] Barbara Di Ventura, Benoît Knecht, Helena Andreas, William J Godinez, Miriam Fritsche, Karl Rohr, Walter Nickel, Dieter W Heermann and Victor Sourjik (2013) Chromosome segregation by the *Escheria coli* Min system. Molecular Systems Biology 9:686. 4, 69, 75
- [103] Thomas G. Bernhardt and Piet A.J. de Boer (2003) The *Escherichia coli* amidase AmiC is a periplasmic septal ring component exported via the twin-arginine transport pathway. Molecular Microbiology 48(5), 1171-1182. 11, 91
- [104] Galina Reshes, Sharon Vanounou, Itzhak Fishov and Mario Feingold (2008) Cell shape dynamics in *Escheria coli* . Biophysical Journal 94, 251-264. 19
- [105] Rex A. Kerr, Herbert Levine, Terrence J. Sejnowski and Wouter-Jan Rappel (2006) Division accuracy in a stochastic model of Min oscillations in *Escheria coli* . Proc. Natl Acad. Sci USA 103(2) 347-352. 18
- [106] Frank J. Trueba (1982) On the precision and accuracy achieved by *Escheria coli* cells at fission about their middle. Arch. Microbiol. 131, 55-59. 18
- [107] Aline Jaffé, Richard D; Ari and Sota Hiraga (1988) Minicell-Forming Mutants of *Escheria coli* : production of minicells and anucleate rods. Journal of Bacteriology 170(7), 3094-3101. 36, 69

- [108] Egbert Mulder, Mohamed El'Bouhali, Evelien Pas and Conrad L. Woldring (1990) The *Escheria coli minB* mutation resembles *gyrB* in defective nucleoid segregation and decreased negative supercoiling of plasmids. *Mol. Gen. Genet.* 221, 87-93. 36, 69
- [109] Joseph C.Chen and Jon Beckwith (2001) FtsQ, FtsL and FtsI require FtsK, but not FtsN, for co-localization with FtsZ during *Escheria coli* cell division. *Molecular Microbiology* 42(2),395-413. 49, 91
- [110] Qin Sun and William Margolin (1998) FtsZ dynamics during the division cycle of live *Escheria coli* cells. *Journal of Bacterology* 180,2050-2056. 49
- [111] Karsten Kruse, Martin Howard and William Margolin (2007) An experimentalist's guide to computational modelling of the Min system. *Molecular Microbiology* 63(5), 1279-1284. 67, 73
- [112] Virginia L. Miller and John J. Mekalanos (1988) A novel suicide vector and its use in construction of insertion mutation: Osmoregulation of outer membrane proteins and virulence determinants in *Vibrio cholerae* requires *toxR*. *Journal of Bacteriology* 170(6), 2575-2583. 91
- [113] Martin Thanbichler, Antonio A. Iniesta and Lucy Shapiro (2007) A comprehensive set of plasmids for vanillate- and xylose-inducible gene expression in *Caulobacter crescentus* . *Nucleic Acids Research* 35(20), e137. 91
- [114] Mischa Schmidt, Martin Creutziger, Peter Lenz (2012) Influence of molecular noise on the growth of single cells and bacterial populations. *PLoS ONE* 7(1)e29932. 59
- [115] Luitpold Fried, Juergen Lassak, Kirsten Jung (2012) A comprehensive toolbox for the rapid construction of lacZ fusion reporters. *Journal of Microbiological Methods* 91,537-543. 91
- [116] J Sambrook and E F Fritsch and T Maniatis (1989) *Molecular cloning: a laboratory manual*. Cold Spring Harbor Laboratory, Cold Spring Harbor, N. Y. 82, 120

Acknowledgements

Most of all I would like to thank my supervisor, Prof. Dr. Peter Lenz, to always support me during the last several years. I worked on very interesting projects, which was sometimes challenging and competitive. Thankfully, Peter always helped me with advice and discussions about the research. He showed me the direction to continue the project and helped me improve my work in details as well. His creativeness, patience and the trust he put on me also encouraged me to persist in the work and face to the challenge. Not only in the research, but also he gave me a lot constructive suggestions on my presentations and writing. When I look backward to my PhD study, I cannot imagine how I could even start the first step of this study without him. I really appreciate his help and support to my PhD study.

I also want to thank Prof. Dr. Lotte Sjøgaard-Andersen and Prof. Dr. Martin Thanbichler. They offered me the possibilities to do the experiments. All the suggestions on the experiments they gave me saved me a lot of time and made the project productive. As a physicist, I feel all the discussions with them are very irradiative and important. Prof. Dr. Hans-Ulrich Mösch also helped with the constructive questions during my talks in Synmikro seminar, I thank him as well.

I also would like to thank Prof. Dr. Wolfgang Eihäuser-Treyer, who spends time on reading my thesis and gives review about it.

Furthermore, I would like to thank all the colleagues in the LSA lab and in the offices of the AG Komplexe Systeme, Especially Dr. Daniela Keilberg and Dr. Edina Hot, who taught me a lot about the technique in molecular biology experiment and microscope using. Their suggestion about the presentations helped me a lot on making talks more understandable to biologists. And also, I want to thank Niyati Vachharajani, Dr. Iryna Bulyha and Dr. Kryssia

Aguiluz-Söngen for their help and suggestions for the experiments. I also want to thank Dr. Barbara Di Ventura for the help she gave me on the experiment. In the theoretical part, I especially want to thank Patrick Bitter, he put a lot of effort on helping me improve my thesis writing, I appreciate every minute he spent on it. I also want to thank others in (or used to be) the group: Dr. Mischa Schmidt, Marcus-A. Assmann, Martin Creutziger, Michael Grau, Konstanze Bandmann, Lisa Beran and Kristof. Beck. They helped me in different ways on programming and data analysis. Furthermore, I would like to thank Mr. Horst Henseling and Mr. Reinhard Böcher, they designed and made the stage heater for me, which is quite important for the experiment.

At the last but not least, I would like to thank my family and friends. My wife was one of the reasons I came to Germany, and her understanding and support, as always, is the most important reason I can persist on fighting on work and in life. I also want to thank my parents, their trust and support in life without any doubt encouraged me to face to the difficulties in my work. Thanks to my daughters, I become happy because of anything they do. And I also want to thank all my friends, all the happy time we spent together helped me concentrated on my work and got everything done in the end.

Thanks, to all the impressive moments I experienced during last several years!

Lebenslauf

Persönliche Daten

Name	Shuxin Jia
Geburtsdatum	22.09.1981 in Jinan, Shandong, China
Nationalität	Chinese
Familienstand	verheiratet

Ausbildung

10.2008-	PhD(Dr. ret. nat) Philips University Marburg, Germany “ Effect of the Min system on timing of bacterial cell division” Supervisor: Prof. Dr. Peter Lenz
09.2004-09.2008	Master of Nature Science Theoretical Physics The Institute of Theoretical Physics, Chinese Academy of Sciences (ITP-CAS) Beijing, China “ The regulation of CRP to the transcription of Lac promoter” Supervisor: Prof. Dr. Hualin Shi
09.2000-07.2004	Bachelor of Physics Shandong University Shandong, China Bachelor thesis: “Development of density functional theory(DFT)” Supervisor: Prof. Dr. Yueyuan Xia

List of Errata

There are just slips which could make some confusion.

p.19, replace

$$”\ln \frac{L-d}{L_0} = \frac{\ln 2}{T}(t_d - t_0).”$$

by

$$”\ln \frac{L_d}{L_0} = \frac{\ln 2}{T}(t_d - t_0).”$$

p.20, replace

$$”\ln \frac{\ln L - \ln L_0}{\ln L_d - \ln L_0} = \frac{t - t - 0}{t_d - t_0},”$$

by

$$”\frac{\ln L - \ln L_0}{\ln L_d - \ln L_0} = \frac{t - t_0}{t_d - t_0},”$$

p.20, replace

$$”l_{resc} = \ln \frac{\ln L - \ln L_0}{\ln L_d - \ln L_0}.”$$

by

$$”l_{resc} = \frac{\ln L - \ln L_0}{\ln L_d - \ln L_0}.”$$

p.31 Table 2.2, line 4 column 4, replace "39" by "29.9".

p.31 Table 2.2, line 5 column 4, replace "36" by "15".

p.82 A.2.1, replace "cells were grown in LB liquid suspension or on plates containing LB supplemented with 1.5% agar at 37 °C with added antibiotics if appropriate (Sambrook and Russell 2001). Liquid cultures were incubated shaking with 220 rpm at 37 °C . The cultures prepared for microscope experiment were grown in M9, incubated shaking with 170 rpm at 30°C ." by "*E.coli* cells were grown in LB liquid suspension or on plates containing LB supplemented with 1.5% agar at 37 °C . When appropriate, antibiotics were added at the concentrations showed in A.4. Liquid cultures were incubated shaking with 220 rpm at 37 °C . The cultures prepared for microscope experiment were grown in M9 [116], incubated shaking with 170 rpm at 30°C . "

p.91 Table A.8, line 8 to line 10, colum 2, replace all "*MinD*" or "*MinE*" by "*minD*" or "*minE*".

p.91 Table A.8, line 14, colum 2, replace "*mobRP4+ori-R6K sacB*" by "*mobRP4⁺ori⁻R6K sacB*".

p.93 line 7, replace "smaller" by "larger".

p.113 add a new reference "J Sambrook and E F Fritsch and T Maniatis (1989) Molecular cloning: a laboratory manual.Cold Spring Harbor Laboratory, Cold Spring Harbor, N. Y."